

GPS Based Position Control and Waypoint
Navigation of a Quad Tilt-Wing UAV

by
Cevdet Haçer

Submitted to the Graduate School of Sabanci University
in partial fulfillment of the requirements for the degree of
Master of Science

Sabanci University

August 2010

GPS Based Position Control and Waypoint Navigation of a
Quad Tilt-Wing UAV

APPROVED BY:

Assoc. Prof. Dr. Mustafa Ünel
(Thesis Advisor)

.....

Assist. Prof. Dr. Kürşat Şendur

.....

Assist. Prof. Dr. Mehmet Yıldız

.....

Assist. Prof. Dr. Hakan Erdoğan

.....

Assist. Prof. Dr. Kayhan Gülez

.....

DATE OF APPROVAL:

.....

© Cevdet Haer 2010

All Rights Reserved

GPS Based Position Control and Waypoint Navigation of a Quad Tilt-Wing UAV

Cevdet Hañer

ME, Master's Thesis, 2010

Thesis Supervisor: Assoc. Prof. Mustafa Ünel

Keywords: UAV, Quad-Rotor, Tilt-Wing, Position Control, Hover,
Waypoint Navigation, Kalman Filter, GPS, Hierarchical Control

Abstract

Unmanned aerial vehicles (UAV) are becoming increasingly capable nowadays and the civilian applications and the military tasks that can be carried out by these vehicles are far more critical than before. There have been remarkable advances in the design and development of UAVs. They are equipped with various sensors which make them capable of accomplishing missions in unconstrained environments which are dangerous or effortful for manned aircrafts. Recently, significant interest in unmanned aerial vehicles has directed researchers towards navigation problem of flying vehicles.

This thesis work focuses on GPS based position control and waypoint navigation of a quad tilt-wing unmanned aerial vehicle (SUAVI: Sabanci University Unmanned Aerial Vehicle). The vehicle is capable of vertical take-off and landing (VTOL). It can also fly horizontally due to its tilt-wing structure. Mechanical and aerodynamic designs are first outlined. A nonlinear mathematical model expressed in a hybrid frame is then obtained using Newton-Euler formulation which also includes aerodynamics effects such as wind and gusts. Extended Kalman filtering (EKF) using raw IMU measurements is employed to obtain reliable orientation estimates which is crucial for attitude stabilization of the aerial vehicle.

A high-level acceleration controller which utilizes GPS data produces roll and pitch references for the low-level attitude controllers for hovering and trajectory tracking of the aerial vehicle. The nonlinear dynamic equations of the vehicle are linearized around nominal operating points in hovering conditions and gravity compensated PID controllers are designed for position and attitude control. Simulations and several real flight experiments demonstrate success of the developed position control algorithms.

Döner-Kanat Mekanizmalı Bir İnsansız Hava Aracının GPS Tabanlı Pozisyon Kontrolü ve Güzargah İzlemesi

Cevdet Hançer

ME, Master Tezi, 2010

Tez Danışmanı: Doç. Dr. Mustafa Ünel

Anahtar Kelimeler: İHA, Dört-Rotor, Döner-Kanat, Pozisyon Kontrolü,
Havada Asılı Kalma, Güzergah İzleme, Kalman Filtresi, GPS, Hiyerarşik
Kontrol

Özet

Günümüzde kabiliyetleri önemli ölçüde artan İnsansız Hava Araçlarının (İHA) sivil uygulamalarda ve askeri görevlerde kullanılması daha da önem arz eden bir hal almıştır. Farklı sensörlerle donatılarak insanlar için tehlikeli ve zorlu çevresel koşullardaki görevlerde kullanılan bu araçların tasarımları ve gelişmelerinde dikkate değer ilerlemeler sağlanmaktadır. Son zamanlarda, bu araçlara olan ilginin ve ihtiyacın önemli ölçüde artması araştırma gruplarını bu alanda çalışmaya kanalize etmiştir.

Bu tez çalışmasında döner kanat mekanizmasına sahip bir insansız hava aracı SUAVI'nin (Sabancı University Unmanned Aerial Vehicle) GPS tabanlı pozisyon kontrolü ve güzergah noktalarını takibi yer almaktadır. Hava aracı dikine kalkış iniş yapabilecek ve döner kanat mekanizması sayesinde yatay uçabilecek şekilde tasarlanmıştır. İlk olarak, mekanik ve aerodinamik tasarımı ana hatlarıyla açıklanmıştır. Aracın doğrusal olmayan matematiksel modeli melez bir koordinat sistemi kullanılarak elde edilmiştir. Newton-Euler metoduyla elde edilen model rüzgar ve hava akımı gibi aerodinamik etkileri de içermektedir. Hava araçlarının yönelim kontrolünde oldukça kritik olan güvenilir oryantasyon ölçümlerini elde edebilmek amacıyla IMU ölçümlerini kullanan genişletilmiş Kalman filtresi tasarlanmıştır.

Hava aracının havada asılı kalma ve güzergah takibi senaryolarında, bir üst seviye denetleyici GPS verilerine dayanarak alt seviye denetleyicilere yuvarlanma ve yunuslama açısı referanslarını yaratmak amacıyla kurgulanmıştır. Aracın doğrusal olmayan dinamik denklemleri havada asılı kalma koşulları

için belirli çalıřma noktaları etrafında doğrusallařtırılmıř, pozisyon ve yönelim kontrolü için yer çekimini kompanse eden PID kontrolör kullanılmıřtır. Benzetim ve deney sonuçları pozisyon kontrol sisteminin başarısını göstermektedir.

Acknowledgements

I would like to express my sincere gratitude and appreciation to my thesis advisor Assoc. Prof. Dr. Mustafa Ünel for his invaluable guidance, support, personal encouragements and bright insights throughout this research. I would also like to thank him for giving me the chance to carry out my MS thesis work in a stimulating project environment.

I would like to thank Assist. Prof. Dr. Kürşat Şendur, Assist. Prof. Hakan Erdoğan, Assist. Prof. Dr. Mehmet Yıldız and Assist. Prof. Dr. Kayhan Gülez for their feedbacks and spending their valuable time to serve as my jurors.

I would like to acknowledge the financial support provided by TÜBİTAK (The Scientific and Technological Research Council of Turkey) through BİDEB scholarship.

I would sincerely like to thank SUAVI project members Kaan Taha Öner, Efe Sırımoğlu, Ertuğrul Çetinsoy, Serhat Dikyar for their pleasant team-work, helpful solutions and competence in this project.

I would like to thank Duruhan Özçelik, Tugba Lelebici, Metin Yılmaz, Melda Şener, Utku Seven, Hakan Ertaş, Eray Baran and all mechatronics laboratory members.

I would also like to thank my friends Uğur Sağıroğlu, Kemal Güler and Emre Topaloğlu for the great time that we spent together.

Finally, I would like to thank my family for all their love, patience and the support in all my choices. They have always encouraged me to pursue my dreams and follow my heart. Through all challenges, they have been there for me.

Contents

1	Introduction	1
1.1	Motivation	17
1.2	Thesis Organization and Contributions	18
1.3	Notes	20
1.4	Nomenclature	22
2	Design of SUAVI	27
2.1	Mechanical Design	27
2.2	Aerodynamic Design	32
2.3	Wind Tunnel Tests	36
3	Mathematical Model of SUAVI	42
3.1	Hybrid Frame	43
3.2	Newton-Euler Formulation	46
3.3	Disturbance Modeling	55
4	GPS Based Position Control and Waypoint Navigation	58
4.1	Low-Level Control: Attitude and Altitude Control Using PID Controllers	62
4.1.1	Development of Switching Logic	62
4.1.2	Averaging Filters	65
4.1.3	Kalman Filtering	67
4.1.4	Altitude and Attitude Control Using PID	70
4.2	Disturbance Observer	73
4.3	GPS Module	76
4.3.1	Data Acquisition with GPS	78

4.4	GPS Based Position Control Laws	80
5	Simulations and Experiments	85
5.1	Simulation Results	85
5.1.1	GPS Based Robust Hover	94
5.1.2	GPS Based Trajectory Tracking	99
5.2	Experimental Results	107
5.2.1	GPS Based Robust Hover	107
6	Concluding Remarks and Future Works	112

List of Figures

2.1	The CAD drawing and prototyping of body structure with chassis and pieces	29
2.2	The CAD drawing (a) and prototyping (b) of the aluminium ring	29
2.3	The wing tilting structure zoomed in	30
2.4	Assembly of landing gear	31
2.5	Carbon spars (a), aluminium elbow connection part (b), T motor connection element (c)	32
2.6	CAD drawings of parts of the aerial vehicle and prototyping	33
2.7	CAD drawings of SUAVI	33
2.8	Prototype SUAVI	34
2.9	Air flow with downwash of the front wing on the rear wing	35
2.10	Spanwise flow speed on the wings with winglets	35
2.11	CAD drawings of half body model	36
2.12	Half body model with one wing is in the wind tunnel	37
2.13	Half body model with two wings is in the wind tunnel	38
2.14	Front and rear angle of attacks for nominal flight	40
2.15	Front and rear motor PWM percentages for nominal flight	40
2.16	Amount of current for nominal flight	41
3.1	Aerial Vehicle is in vertical (a) and horizontal (b) flight modes	42
3.2	Coordinate frames of the aerial vehicle	45
3.3	External forces and torques acting on the vehicle	47
3.4	Effective angle of attack α_i	49
4.1	Hierarchical Control System of SUAVI	59
4.2	Overall flight control system	61

4.3	Flight modes and related low-level controllers	63
4.4	Forces appears on the wing in transition mode	64
4.5	The filtered and raw sonar measurements in real flight exper- iment	67
4.6	Estimation of roll angle with Kalman filter in flight experiment	71
4.7	Estimation of pitch angle with Kalman filter in flight experiment	71
4.8	Block diagram of the closed loop disturbance observer	76
4.9	User interface program that provides GPS position data	78
4.10	The data taken from GPS receiver hold on a stationary point .	79
4.11	GPS position data in waypoint navigation	80
4.12	Visualization of GPS receiver position data around Sabanci University	81
5.1	Graphical User Interface (Vehicle is ready to flight)	86
5.2	Graphical User Interface (Flight)	87
5.3	Visualization Interface	89
5.4	Surveillance (vehicle is at the starting position)	90
5.5	Surveillance (vehicle is on the way of desired location)	91
5.6	The waypoints of the aerial vehicle during surveillance mission (blue: reference, red: vehicle)	91
5.7	Surveillance task: Waypoint navigation performance	92
5.8	Surveillance task: Attitude tracking performance	92
5.9	Surveillance task: Control efforts	93
5.10	Surveillance task: Airspeed of the vehicle	93
5.11	Hovering performance with disturbance observer	96
5.12	Attitude performance with disturbance observer	96
5.13	Motor thrust forces with disturbance observer	97

5.14	Wind forces acting on the vehicle	97
5.15	Hovering performance with disturbance observer (motion in the horizontal plane)	98
5.16	Estimated total disturbance acting on the vehicle	98
5.17	Hovering performance without disturbance observer	99
5.18	Attitude performance without disturbance observer	100
5.19	Hovering performance without disturbance observer (motion in the horizontal plane)	100
5.20	Elliptical helix shaped trajectory tracking performance	102
5.21	Attitude tracking performance	103
5.22	Position tracking performance	103
5.23	Cross track error	104
5.24	Along track speed	104
5.25	Thrust forces created by rotors	105
5.26	Wind forces acting as disturbance	105
5.27	Disturbance Estimation	106
5.28	Square shaped trajectory tracking performance	106
5.29	Outdoor hover test with SUAVI in helicopter field	108
5.30	Outdoor hover test with SUAVI in university campus	109
5.31	Outdoor hover test with SUAVI in university campus	110
5.32	Outdoor hover test with SUAVI in amphitheater	111

List of Tables

1.1	Different Types of Unmanned Aerial Vehicles	2
1.2	Some of UAVs in the history	6
1.3	Tilt-Wing & Tilt-Rotor UAV projects	8
2.1	Weight Measurements	32
2.2	Motor PWM percentage, angle of attack and the current consumption for nominal flight	39
3.1	Modeling Parameters	56
5.1	Implementation Parameters for Robust Hovering Control . . .	94
5.2	Implementation Parameters for Waypoint Navigation	101

Chapter I






1 Introduction

Unmanned aerial vehicles (UAV) have been the subject of a growing research interest during the last thirty years. They are becoming increasingly capable nowadays and the complex mission tasks that are carried out by UAVs are far more critical than before. UAVs are indispensable for various applications where human intervention is impossible, risky or expensive. Low manufacturing and operational costs of the systems leads to increase in demand for these vehicles in the commercial industry. A market investigation held in 2009 [1] reports that 22 industrial and over 40 research groups are currently working on UAVs.

AIAA Committee of Standards defines UAV to be an aircraft which is designed or modified, not to carry a human pilot and is operated through an electronic input initiated through the Flight Controller or by an onboard autonomous flight management control system that does not require flight controller intervention. The name UAV covers all vehicles capable of programmable flight patterns and operated without human intervention [2]. There are various types of UAVs that have different configuration. Fixed-wing UAVs have the advantage of long-range capability due to the use of energy efficiently, but they lack maneuverability required for many tasks. On the other hand, helicopters or quadrotors have the capability to take off

and land in limited space, better maneuverability when compared to conventional fixed-wing UAVs and easily hover over targets. However, the higher rate of energy consumption and the difficulties in control of these vehicles are disadvantages [3]. Besides these commonly used aerial vehicles, the tilt-rotor or tilt-wing aerial vehicles combining the advantages of horizontal and vertical flight have been gaining popularity recently. This hybrid configuration includes advantages and eliminates the disadvantages of previously mentioned types. Examples of different unmanned aerial vehicle configurations are given in Table 1.1.

Table 1.1: Different Types of Unmanned Aerial Vehicles

Configuration		Name of Project
Quadrotor		Draganflyer [4]
Helicopter		Fire Scout [5]
Fixed-wing UAV		Desert Hawk [6]
Tilt-rotor		Smart UAV [7]
Tilt-wing		QTW UAS-FS4 [8]

UAVs can be classified as being for either civilian or military use. The potential of these aircrafts for civilian use is remarkable however the most notable developments falls into military applications until now. The military market revenue was \$2.22 billion whereas the revenues for the civil market were only \$0.08 billion. Despite the fact that the civil UAV market is responsible for only 3% of the total market revenue, after 2000 it is expected to expand rapidly [9].

In [9], civil applications that UAVs are employed can be listed as:

- Exploration of disasters (fire, earthquake, flood, etc.)
- Surveillance over nuclear reactors and hazardous chemicals
- Border interdiction
- Search and rescue
- Wild fire suppression
- Communications relay
- Law enforcement
- Disaster and emergency management
- Industrial applications
- Volcano patrol
- Hurricane observations

Beside civilian uses, military applications of UAVs are:

- Reconnaissance Surveillance and Target Acquisition (RSTA)
- Surveillance for peacetime and combat Synthetic Aperture Radar (SAR)

- Deception operations
- Maritime operations (Naval fire support, over the horizon targeting, anti-ship missile defence, ship classification)
- Electronic Warfare (EW) and SIGINT (SIGnals INTelligence)
- Radio and data relay
- Adjustment of indirect fire and Close Air Support (CAS)
- Battle Damage Assessment (BDA)
- Route and landing reconnaissance support

Such vehicles can also be used in environments where direct or remote human assistance is not feasible. They have even the potential to perform some tasks that are impossible to be performed by other means. The necessary abilities for mentioned applications are to hover above a given fixed point and to maneuver with high agility.

History

According to the work of Nonami [10], the first UAV is constructed by Americans Lawrence and Elmer Sperry in 1916. The designed autopilot uses gyroscope to stabilize the body. In the following years, the gyroscope improvements were incorporated into automatic pilots [11]. Pilotless airplanes in the early twentieth century are used mostly for military purposes such as delivering explosive payloads to a specific target. UAVs gain more significance and attention among researchers after 1950s. The necessity of such vehicles in the Vietnam and Cold War years directs US and Israel to develop more practical and cheaper UAVs. The modern UAV era originated in the early 1970s [12]. An example of UAV of those times is called Firebee [13].

Video cameras are also started to mount on vehicles in these years in order to transmit images to ground station. The progress to construct modern aerial vehicles continues in the following years in parallel to technological enhancements and necessities, and the most famous UAV for military purposes so called Predator [14] is built. The impressive performance of the Predator UAV during the recent Balkan War have also highlighted the importance of UAVs. Besides military improvement, NASA pays attention to UAV research for civil use around 1990s. The aircrafts came out of NASA's ERAST (Environmental Research Aircraft and Sensor Technology) project has the capability of high altitude flight and prolonged flight times by the help of high tech sensors and actuators. Unmanned vehicles are started to be equipped with GPS sensors in order to make them autonomous since late 1990s. The YAMAHA RMAX [15] is one of the pioneers that is capable of autonomous flight. The usage area of YAMAHA unmanned vehicles indicates variety from agricultural field to environmental monitoring. Aerosonde, the Altair and Altus I-II are other examples of UAVs that can be categorized in such missions [10]. The SKYSURVEYOR is used for monitoring power lines by using onboard cameras. After 2000, the capabilities of the aircraft in civil and military use are in high demand due to world circumstances. One of the prototype aircraft called Global Hawk [16] is operated by the U.S. Air Force in 2006. Global Hawk prototypes have been used in Afghanistan and Iraq War. Similarly, Malazgirt Mini Unmanned Helicopter System [17] is the world's first operational mini unmanned helicopter system. This vehicle can be used in geographically harsh environmental conditions by the help of its automatic vertical landing/take off and automatic hovering capability in any desired location. All these UAVs are given in chronological order in Table

1.2.

Table 1.2: Some of UAVs in the history

Name of UAV	Year	Name of UAV	Year
First UAV	1916	Aerosonde	2005
Firebee	1970	Altair	2005
Predator	1990	Altus	2005
SkySurveyor	2001	Global Hawk	2006
Yamaha Rmax	2002	Malazgirt	2007

In the present state of research and development of autonomous UAV, vehicles with altitude sensors, GPS receiver, compass and a control system governs the autonomous flight. At the ground station, operator can input, change or cancel the flight plan.






Airplanes with long flight ranges and helicopters with hovering capabilities have been the major mobile platforms that UAV research groups have been working on until now. Besides the conventional aerial vehicles, one of the increasing trends in UAV research area is vehicles with quad tilt-rotor

and quad tilt-wing mechanisms besides other UAV designs nowadays. Tilt-wing or tilt-rotor UAVs are capable of realizing the vertical take off and landing, and hovering flight that seems to be the helicopter, and high cruising speeds that seems to be fixed wing aircraft by changing angle of wings or rotors with tilting mechanism. Until 2000's, the Tilt-Wing and Tilt-Rotor flying concepts remain only applied to manned aircrafts. Because these new vehicles are open to different design concepts, many research groups build their own tilt-rotor vehicles according to their desired technical properties and objectives.

The Tilt-Rotor and Tilt-Wing aerial vehicles combine the advantages of horizontal and vertical flight. They are in general hard to fly vehicles which require advanced control and actuation technologies for a safe flight. When tilt-wing and tilt-rotor structures are compared, the tilt-wing UAVs have advantage because tilting the entire wing, instead of just the rotor or propeller, provides the benefit of increasing aerodynamic flow over the lifting and control surfaces during transition, and minimizes the lift loss due to downwash in hover [18]. Some of the Tilt-Rotor and Tilt-Wing UAVs are given in Table 1.3.

Unmanned Aerial Vehicles contain infinite potential and competitive development all over the world although the use of vehicles is various among countries. In particular, the US Department of Homeland Security increased its budget for funding UAV research after terrorist attack on September 11, 2001. It is very common to see other examples of increase in the interest. The current worldwide UAV expenditures are estimated at \$4.4 billion and are expected to double over the next 10 years [23]. It is stated in [24] that there are 294 different UAV models for civil and commercial applications.

Table 1.3: Tilt-Wing & Tilt-Rotor UAV projects

Institute/Company Name		Name of UAV	Configuration
Bell Company		Eagle Eye [19]	Tilt-Rotor
Bell Company		V22 [20]	Tilt-Rotor
Arizona State University		HARVee [21]	Tilt-Wing
Korea Aerospace Research Institute		Smart UAV [7]	Tilt-Rotor
Chiba University & G.H. Craft		QTW UAS-FS4 [8]	Tilt-Wing
AVT		Hammerhead	Tilt-Rotor
Sabanci University		SUAVI [22]	Tilt-Wing

Teal group predicts that worldwide UAV market will total over \$62 billion in its just released 2009 UAV market profile. The predicted future trend of UAV autonomy are given in Unmanned Aircraft Systems Roadmap 2005-2030 [25]. Various stages of autonomous control achievement starting from simple remote control to perfect autonomous swarm control are emphasized. It is stated that the key technology for realization of such application is the CPU. The enhancement in the CPU of microprocessors will shape the future of UAV researches.

Navigation

One of the basic tasks for an autonomously flying vehicle is to reach a desired location in an unsupervised manner because precise trajectory tracking is required to perform more complex missions in unconstrained environments. This work of positioning aerial vehicles without human interference is so called navigation. Navigation problem is firstly considered for ground robots. However, the increase in the interest on aerial vehicles directs researches towards navigation of flying vehicles. The transfer of applied methodologies which are suitable for ground robots to aerial vehicles is not straightforward. The major reasons are the complexity of aerial vehicles' dynamics when compared with the ground robots, additional degree of freedom and challenges posed by their 3D movement, and the limited weight, payload and size criteria of aerial vehicles which is directly effective on the sensor choice. The limitation on payload of these small platforms precludes the use of conventional and standard sensors. Therefore, small and available low-cost sensors are attractive for UAVs.

Most of the proposed approaches to navigation problem are designed for

outdoor operation, few techniques focus on indoor environments. In the case of existence of signals from satellite, navigation issue is handled via Global Navigation Satellite Systems (GNSS) such as GPS. In order to overwhelm robotic missions in outdoor environment, position and velocity information are obtained from such devices for navigation. In outdoor, GPS can be utilized for determination of the vehicle's position. In indoor applications, on the other hand, either GPS is not available or the accuracy of the measurements from GPS is not satisfactory. The difficulties that stems from indoor environment are due to limited free space to maneuver and existence of obstacles.

Precise knowledge of aerial vehicle's position is necessary in order to create an autonomous UAV. The performance of the designed controllers are directly affected by the aerodynamics of the vehicle. In [26], Huang et al. emphasize the impact of aerodynamic effects at higher speeds and outdoor conditions in contrast to indoor conditions, and presents a novel feedback linearization controller which successfully compensates these aerodynamic effects. Hoffmann et al. [27] propose a work related to attitude control algorithms. For position hold, they use thrust vectoring with PID structure. The position hold performance in x-y plane is within an error of 40 cm radius whereas altitude control error is within 30 cm, verified by experiments. In the work of Meister et al. [28], a sensor fusion algorithm for stable attitude and position estimation using GPS, IMU and compass modules together, is presented, and the control algorithms for position hold and waypoint tracking are developed. It is reported that the position hold error under a wind disturbance less than 5 m/s is bounded by 3 m. Hoffmann et al. [29] develop an autonomous trajectory tracking algorithm through cluttered environments

for the STARMAC platform and a novel algorithm for dynamic trajectory generation. Both indoor and outdoor flight tests are performed, and an indoor accuracy of 10 cm and an outdoor accuracy of 50 cm are reported. Puls et al. [30] emphasizes that navigation of aerial vehicles between waypoints is undisclosed. The development of 2D GPS based position control system for 4 Rotor helicopters able to keep positions above given destinations as well as to navigate between waypoints while minimizing trajectory errors is presented. Waslander and Wang [31] focus on improvement of STARMAC quadrotor position hold performance by modeling the wind effects, i.e. using Dryden Wind Gust Model, on quadrotor dynamics in order to estimate wind velocities during flight. A DD term in position hold algorithm is claimed to improve the error on tracking from 40 cm to 15 cm whereas the addition of disturbance rejection further improved the tracking performance to 10 cm. The performance of the controller and the disturbance rejection is evaluated only in simulations. In [32], the main focus is on waypoint navigation, trajectory tracking, hovering and autonomous take-off and landing. An inexpensive Guidance Navigation and Control system is developed using low cost sensors. The aim was to obtain a reliable model-based nonlinear controller. The controller algorithms are tested with experiments and results indicates satisfactory tracking performance. Grzonka et al. [33] emphasizes the significance of the indoor navigation of aerial vehicles. They propose a navigation system for indoor flying vehicles by using state estimation modules such as laser sensors, IMU and Linux-based Gumstix for localization, altitude and attitude estimation. In [34], the design of a four-rotor Autonomous Flying Vehicle (AFV) equipped with an indoor global positioning system. A decomposed estimation approach is used to combine the IMU and the indoor GPS

information effectively and to determine the vehicle's attitude. Hover flight and trajectory tracking were successfully demonstrated using the presented estimation scheme in combination with a linear quadratic regulator (LQR). Herisse and his colleagues [35] focuses on the terrain following and ground collision avoidance problem, given a forward velocity reference. The proposed flight controller is nonlinear depending on Lyapunov stability analysis. The vehicle is equipped with the sensors of IMU, camera and a forward velocity measurement device such as an indoor GPS. In the proposed algorithm the translational optical flow data is combined with the measurements from IMU. The algorithm is verified with simulations and experiments. Shimuzu et al. [36] propose techniques for precise point positioning (PPP) of a helicopter. They use GPS helicopter flight data in post-processing mode and show that point positioning accuracy at about decimeter level both horizontally and vertically has been achieved. In [37], design and test results of a Micro-Electro-Mechanical (MEMS) based navigation system for micro air vehicle. The raw IMU measurements are blended in a Kalman filter with measurements from GPS, barometric altimeter and a magnetometer in order to handle problematic sensor datas. The proposed technique is verified with the test results. Yun and his colleagues [38] uses Kalman filter together with a complementary filter to regenerate smooth and accurate signals coming from GPS system. Otherwise, such a problem degrades the overall performance of the automatic flight control system of UAV. The simulation and implementation results indicates that proposed scheme is very effective and yield a good improvement on the performance.

In the literature there are also several works related to vision based navigation. For example, Soundararaj et al. [39] proposes purely vision based

navigation technique using only an on-board light weight camera. The approach is based on fast nearest neighbor classification for 3D localization and optical flow for velocity estimation. The output of the estimation algorithm is used in proportional and derivative controller in order to control the helicopter. The satisfactory performance of this approach in hovering and following the user defined trajectories is validated by flight tests. In the work of Azrad et al. [40], an object tracking system using an autonomous Micro Air Vehicle (MAV) is described. The vision-based control system relies on a color and feature based vision algorithm, and a nonlinear controller. The vision algorithm relies on information from a single onboard camera. Experimental results obtained from outdoor flight tests showed that the vision-control system enabled the MAV to track and hover above the target as long as the battery is available. Kendoul and his colleagues [41] present a visual navigation system depending on pose estimation method. For more robustness, accuracy and overcoming non desired rotation effects, the visual estimates are fused with IMU and pressure sensor altimeter for flight control, accurate landing and target tracking. Experimental results of the presented technique indicates that long range navigation by preventing accumulation of odometric errors is satisfactory enough to estimate motion and position of the vehicle. In the work of Yu [42], an experimental study in hovering control of an unmanned helicopter with a 3D vision system instead of GPS is described. The position of the vehicle is estimated by vision technique with stereo camera onboard and then fused with acceleration measurement from IMU by Kalman filter for velocity estimation. The performance of the proposed methodology is observed to be equivalent to that when GPS is used. The vehicle is able to hover within 0.4 meter radius circle. Kanade et al. [43]

present a structure including motion approach for visual navigation. The idea is to recover the ego-motion of autonomous micro aerial vehicle. In the BEAR project, Shakernia and his colleagues [44] use multiple view geometry to land an autonomous helicopter on a moving deck. The results of the proposed methodology are quite satisfactory. Similarly, Saripalli et al. [45] proposes a vision based strategy that allows helicopter to land on a slowly moving previously known helipad.

Control

The design of reliable control systems for UAVs is another crucial step in development of such autonomous aerial vehicles. In order to develop the flight control systems for autonomous underactuated aerial vehicles, accurate dynamic models for their flight envelop are needed. The main difficulties for designing stable feedback controller stem from nonlinearities and couplings. Design, modeling and control of autonomous aerial vehicles have become very challenging research area since 90s, however there is no work yet that is made on the design of generic aerodynamic model valid for all autonomous flying vehicles.

Weng and his colleagues [46] present the control of a Quad-Rotor VTOL to be controlled by a pilot using radio frequency. Due to the naturally unstable behavior of the flying robot, PID control system is implemented with the aid of accelerometer, compass sensor and gyro sensors to stabilize the flying robot. Hably and Merchand [47] have recently proposed a global asymptotic stabilizing controller under bounded inputs. In [48], a minimalist control strategy for fixed wing micro UAVs that provides airspeed, altitude and heading turn rate control by only using two pressure sensors and a single

axis rate gyro. In [49], Earl et al. develop an attitude estimation technique by using a decomposition approach. Another study is carried out to use an output feedback controller with estimators and observers in [50]. Nicol et al. [51] presents a new adaptive neural network control for attitude stabilization of a quadrotor considering unknown modeling parameters and wind disturbance. The controller is based on a cascaded CMAC (Cerebellar Model Articulation Controller) neural network structure. This new method is compared to the deadzone and improvements in terms of achieving a desired attitude are verified with simulations. Cheviron et al. [52] presents a generic nonlinear model of reduced scale UAVs in order to be simple enough to design a controller. Different vertical take-off and landing UAV architectures such as quadricopter, ducted fan and classical helicopter are presented in their works and generic model focusing on the key physical efforts acting on the dynamics is proposed. Backstepping control of Madani and Benallegue [53] is another example of recent non-linear control methods applied on quadrotors. In the work of Waslander and his colleagues [54], a comparison of two non-linear controllers based on integral sliding mode and reinforcement learning are presented.

It is significant to note that the performance of the designed controller is directly affected by aerodynamics of the vehicles. Huang and colleagues [55] emphasizes the impact of aerodynamic effects at higher speeds and outdoor conditions in contrast to indoor conditions. A novel feedback linearization controller which successfully compensates these aerodynamic effects is presented. In the work of Muraoka [56], aerodynamic characteristics of the quad tilt-wing UAV to fly over a wide flight envelope derived from wind tunnel data are summarized. Moreover, a primary flight control system allowing continu-

ous control through all flight phases enables a pilot to perform vertical take-off, accelerating transition, cruise, decelerating transition and hover landing with sufficient flying qualities. In [57], attitude stabilization of a quadrotor helicopter under sinusoidal wind disturbances is presented. According to the simulation results, the fuzzy controller scheme is stable, computationally efficient and theoretically proven to be robust to disturbances.

Many well known mathematical models and control architectures have been developed for fixed wing airplanes, helicopters, quadrotors and tilt-rotor vehicles. However, modeling and control of Quad Tilt-Wing (QTW) aerial vehicles still remains as a challenging problem. Because of with this wing configuration, the vehicle's airframe transforms into a quadrotor structure if the wings are at the vertical position and into an airplane structure if the wings are at the horizontal position. There is also a transition phase of the wings from vertical to horizontal position and vice versa which constitute the major challenge for research groups. The modeling and robust control of these aerial vehicles has to take all flight modes into consideration. There are few sources related to modeling and control of tilt-wing vehicles in the literature. In [58], a dynamic model for a tilt-wing aerial vehicle by identification method is proposed. Transition between vertical and horizontal flight modes of the QTW aerial vehicle is highly unstable, an effective control strategy using conventional control techniques are highly inefficient. Therefore, Omar et al. [59] focus on a fuzzy logic flight controller for transition between vertical and horizontal flight modes of a tailsitter VTOL aerial vehicle. In simulations, their UAV was able to perform the transition manoeuvre in a short time (3 sec.) within the range of tolerable attitudes and without losing the altitude in a great manner before getting in horizontal flight. Kang et

al. [60] studies on transition between horizontal and vertical flight modes of a small scale tilt-rotor UAV similar to the V-22. After several tethered flight tests, a conversion corridor which maps the forward flight speed to the tilt angle is obtained. During this conversion, the pitch of the vehicle is controlled by a PID controller.

1.1 Motivation

There is an increasing demand for autonomous unmanned aerial vehicles among research groups. They are becoming increasingly capable nowadays such that the application areas of UAVs are far reaching. Both civilian and military complex mission tasks such as surveillance, reconnaissance, traffic monitoring, border security are carried out by them. The main reason of interest is that these vehicles can execute tasks that are either too expensive to be accomplished by human operated vehicles or too dangerous for human life.

There are various types of UAVs that have different design configuration. Fixed-wing UAVs have the advantage of being able to fly at high speeds for long duration with simpler control structure, but they lack maneuverability required for many tasks such as takeoff-landing and hovering. On the other hand, helicopters or quadrotors have the capability to take off and land vertically with agile maneuvering capability when compared to conventional fixed-wing UAVs. However, the higher rate of energy consumption, high mechanical complexity, low speed, short flight range and the difficulties in control structure design of these vehicles are disadvantages. Besides these commonly used aerial vehicles, the tilt-rotor or tilt-wing aerial vehicles combining the advantages of horizontal and vertical flight have been gaining

popularity recently. Tilt-wing or tilt-rotor UAVs are capable of realizing the vertical take off and landing, and hovering flight that seems to be the helicopter, and high cruising speeds that seems to be fixed wing aircraft. This hybrid configuration includes advantages and eliminates the disadvantages of previously mentioned configurations.

When tilt-wing and tilt-rotor structures are compared, the tilt-wing UAVs have advantageous because tilting the entire wing, instead of just the rotor or propeller, provides the benefit of increasing aerodynamic flow over the lifting and control surfaces during transition, and minimizes the lift loss due to downwash in hover. However, they are in general require advanced control architectures and actuation technologies for a safe flight.

1.2 Thesis Organization and Contributions

In Chapter II, the mechanical and aerodynamic designs of SUAVI (Sabancı University Unmanned Aerial VehIcle) are outlined. Mechanical parts are overviewed and ANSYS simulations are presented. Flight characteristics of the aerial vehicle is determined via wind tunnel tests.

In Chapter III, a full mathematical model for tilt-wing SUAVI is obtained including aerodynamics effects such as wind and gusts. The model is expressed in a hybrid frame and derived using Newton-Euler formulation.

In Chapter IV, a high-level controller (supervisor) that is responsible for orchestrating switching of the low-level controllers into the system for attitude stabilization is presented. Extended Kalman filtering (EKF) is employed to obtain reliable orientation estimates. A GPS based acceleration controller is utilized to produce roll and pitch references for low-level attitude controllers. A disturbance observer is also employed to estimate and

compensate for the total disturbance acting on the system.

In Chapter V, simulation and experimental results related to GPS based hovering and waypoint navigation are discussed. The performance of the proposed position controller is verified by both simulations and real flight tests.

In Chapter VI, concluding remarks and possible future directions are presented.

Contribution of the thesis can be summarized as follows:

- A nonlinear mathematical model which also includes aerodynamic effects for tilt-wing SUAVI is obtained using Newton-Euler formulation.
- A GPS based robust position controller for a tilt-wing quadrotor is designed as a high-level controller. Aerial vehicle performs hovering and waypoint navigation tasks under external wind and aerodynamic disturbances successfully. Low-level controllers that are responsible for attitude stabilization are developed to work under the supervision of high-level controller.
- Extended Kalman filtering (EKF) is utilized for accurate orientation (roll, pitch and yaw) estimates. Moreover, noisy sensor measurements are filtered by analog and digital filters such as weighted averaging and low pass filters.
- Flight characteristics of the tilt-wing aerial vehicle under different aerodynamic circumstances is acquired from the tests performed in the wind tunnel. Some of the measurements obtained in the wind tunnel tests are verified with the literature, and some of them are new contributions to the literature.

- A disturbance observer which estimates and compensates for the total disturbance acting on the system is developed and implemented.
- Several hovering and waypoint navigation simulations and real flight experiments have been successfully performed under different weather conditions.

1.3 Notes

SUAVI is being developed in the context of a TÜBİTAK (The Scientific & Technological Research Council of Turkey) funded research project under the grant 107M179 (Mechanical Design, Prototyping and Flight Control of an Unmanned Autonomous Aerial Vehicle).

Published journal and conference papers from this thesis are:

Journal Articles

- “Mathematical Modeling and Vertical Flight Control of a Tilt-Wing UAV”, K. T. Öner, E. Çetinsoy, E. Sırımoğlu, **C. Hançer**, M. Ünel, M. F. Aksit, K. Gülez, İ. Kandemir, *Turkish Journal of Electrical Engineering and Computer Sciences*, (forthcoming), 2010.
- “Design and Development of a Tilt-Wing UAV”, E. Çetinsoy, E. Sırımoğlu, K. T. Öner, **C. Hançer**, M. Ünel, M. F. Aksit, İ. Kandemir, K. Gülez, *Turkish Journal of Electrical Engineering and Computer Sciences*, (forthcoming), 2010.

Conference Proceedings

- “Robust Position Control of a Tilt-Wing Quadrotor”, **C. Hançer**, K. T. Öner , E. Sırımoğlu, E. Çetinsoy, M. Ünel, *IEEE 49th Conference on Decision and Control*, Atlanta, 15-17 December 2010.
- “Robust Hovering Control of a Quad Tilt-Wing UAV”, **C. Hançer**, K. T. Oner, E. Sirimoglu, E. Cetinsoy, M. Unel, *IEEE 36th International Conference on Industrial Electronics (IECON'10)*, Phoenix, AZ, USA, Nov.7-10, 2010.
- “LQR and SMC Stabilization of a New Unmanned Aerial Vehicle”, K. T. Öner, E. Çetinsoy, E. Sırımoğlu, **C. Hançer**, T. Ayken, M. Ünel, *Proceedings of International Conference on Intelligent Control, Robotics, and Automation (ICICRA 2009)*, Venice, Italy, October 28-30, 2009.

National Conference Proceedings

- “Döner Kanatlı Quadrotorun Havada Asılı Kalmasını Sağlayan Gürbüz Pozisyon Denetleyici Tasarımı”, **C. Hançer**, K. T. Öner , E. Sırımoğlu, E. Çetinsoy, M. Ünel, *TOK'10: Otomatik Kontrol Ulusal Toplantısı*, İstanbul, 21-23 Eylül 2010.
- “Yeni Bir İnsansız Hava Aracının (SUAVI) Prototip Üretimi ve Algılayıcı-Eyleyici Entegrasyonu”, E. Çetinsoy, K. T. Öner , E. Sırımoğlu, T. Ayken, **C. Hançer**, M. Ünel, M. F. Akşit, İ. Kandemir, K. Gülez *TOK'09: Otomatik Kontrol Ulusal Toplantısı*, İstanbul, 2009.

1.4 Nomenclature

Symbol	Description
a	total acceleration of the aerial vehicle
a_i	amplitude of the sinusoids in wind model
a_x	x component of the reference acceleration vector
a_y	y component of the reference acceleration vector
a_z	acceleration of the aerial vehicle along z axis
a_{xy}	reference acceleration vector in x-y plane
A	area of the wing
A_k	state transition matrix
b_g	bias in gyros
c_D	drag coefficient
c_L	lift coefficient
$C(\zeta)$	Coriolis-centripetal matrix
$D(\zeta, \xi)$	external disturbance vector
\dot{e}_{at}	along track error rate
e_{ct}	cross track error
\dot{e}_{ct}	derivative of cross track error
e_x	position error of the aerial vehicle along x axis
\dot{e}_x	derivative of position error along x axis
e_y	position error of the aerial vehicle along y axis
\dot{e}_y	derivative of position error along y axis
E	rotational velocity transformation matrix
$E(\xi)w^2$	system actuator vector
F_d	forces due to external disturbances
F_D	drag forces
F_g	gravity force
F_L	lift forces
F_t	total external force acting on the aerial vehicle
F_{th}	thrust force created by rotors
F_w	aerodynamic forces generated by wings

Symbol	Description
G	gravity matrix
H_k	observation matrix
I_b	inertia matrix of the aerial vehicle in body fixed frame
I_{xx}	moment of inertia around x_b in body frame
I_{yy}	moment of inertia around y_b in body frame
I_{zz}	moment of inertia around z_b in body frame
J	Jacobian transformation between generalized vectors
J_{prop}	inertia of the propellers about their rotation axis
K_k	Kalman gain
K_{atp}	proportional gain for along track controller
K_{ati}	integral gain for along track controller
K_{ctp}	proportional gain for cross track controller
K_{ctd}	derivative gain for cross track controller
K_{cti}	integral gain for cross track controller
$K_{x,p}$	proportional gain for controller along x axis
$K_{x,d}$	derivative gain for controller along x axis
$K_{x,i}$	integral gain for controller along x axis
$K_{y,p}$	proportional gain for controller along y axis
$K_{y,d}$	derivative gain for controller along y axis
$K_{y,i}$	integral gain for controller along y axis
l_l	rotor distance to center of gravity along x_b in body frame
l_s	rotor distance to center of gravity along y_b in body frame
L_h	horizontal gust length scale
L_v	vertical gust length scale
m	mass of the aerial vehicle
M	inertia matrix
M_d	torques due to external disturbances
M_{gyro}	gyroscopic torques
M_{nom}	nominal inertia matrix

Symbol	Description
M_t	total torque acting on the aerial vehicle
M_{th}	rotor torques
M_w	aerodynamic torques due to lift/drag forces
\tilde{M}	difference between actual and nominal inertia matrices
n_i	unit normal vector perpendicular to path P
O_b	origin of body fixed frame
O_w	origin of inertial (world) frame
$O(\zeta)w$	gyroscopic matrix
p	angular velocity of the aerial vehicle along x_b in body frame
P	reference path generated by waypoints
P_w	position of the aerial vehicle in inertial (world) frame
\dot{P}_w	linear velocity of the aerial vehicle in inertial (world) frame
$P_{k k-1}$	a-priori error covariance matrix
$P_{k k}$	posterior error covariance matrix
q	angular velocity of the aerial vehicle along y_b in body frame
Q	process covariance matrix
r	angular velocity of the aerial vehicle along z_b in body frame
R	measurement covariance matrix
R_x	elementary rotation around x axis
R_y	elementary rotation around y axis
R_z	elementary rotation around z axis
R_{wb}	orientation of body frame with respect to world frame
R_{bw}	orientation of world frame with respect to earth frame
S_t	filtered sonar measurement at time t
t_i	unit tangent vector along path P
T	sampling time
u_i	virtual control inputs
u^H	high-level input signal
u^L	low-level input signal

Symbol	Description
v_w	time dependent estimate of wind vector
v_w^0	static wind vector
v_x	linear velocity along x_b in body fixed frame
v_y	linear velocity along y_b in body fixed frame
v_z	linear velocity along z_b in body fixed frame
v_α	airstream velocity
V_w	linear velocity of the aerial vehicle in inertial (world) frame
V_b	linear velocity of the aerial vehicle in body fixed frame
w_i	propellers rotational speed
x_b	x axis of body fixed frame
x^d	desired reference position
x_i^d	waypoints of the path P
x_k	state of the system
$\hat{x}_{k k-1}$	priori state estimate
$\hat{x}_{k k}$	posteriori state estimate
x_n	unit vector along x_w in inertial (world) frame
$x(t)$	instantaneous position of aerial vehicle provided by GPS
x_w	x axis of inertial (world) frame
X	position of the aerial vehicle along x_w in inertial (world) frame
\dot{X}	linear velocity of the aerial vehicle along x_w in inertial (world) frame
y_b	y axis of body fixed frame
y^H	high-level output signal
y^L	low-level output signal
y_n	unit vector along y_w in inertial (world) frame
y_w	y axis of inertial (world) frame
Y	position of the aerial vehicle along y_w in inertial (world) frame
\dot{Y}	linear velocity of the aerial vehicle along y_w in inertial (world) frame
Y_{t-1}	raw sonar measurement at time (t-1)
z_b	z axis of body fixed frame
z^d	desired reference altitude

Symbol	Description
z_w	z axis of inertial (world) frame
Z	position of the aerial vehicle along z_w in inertial (world) frame
\dot{Z}	linear velocity of the aerial vehicle along z_w in inertial (world) frame
α_w	attitude of the aerial vehicle in inertial (world) frame
α_i	effective angle of attack
$\dot{\alpha}_w$	time derivative of attitude in inertial (world) frame
β	weighting parameter
Ω_b	angular velocity of the aerial vehicle in body fixed frame
Ω_i	randomly selected frequency in wind model
Ω_w	time derivative of attitude in inertial (world) frame
ϕ	roll angle, angular position around x_w
ϕ_{ref}	reference roll angle
θ	pitch angle, angular position around y_w
θ_{ref}	reference pitch angle
ψ	yaw angle, angular position around z_w
$\dot{\phi}$	time derivative of angular position around x_w
$\dot{\theta}$	time derivative of angular position around y_w
$\dot{\psi}$	time derivative of angular position around z_w
θ_i	angle of attack for each wing
ρ	air density
λ_i	torque/force ratio
ζ	generalized velocity vector of the aerial vehicle
ξ	position and orientation of the aerial vehicle in inertial (world) frame
φ_i	phase shift in wind model
$\Phi_h(\Omega)$	power spectral density for horizontal winds
$\Phi_v(\Omega)$	power spectral density for vertical winds
σ_h	horizontal turbulence intensity
σ_v	vertical turbulence intensity
η_k	process noise
ν_k	measurement noise
τ_{dist}	total disturbance
$\hat{\tau}_{dist}$	estimated disturbance

Chapter 2

2 Design of SUAVI

The design of Sabanci University Unmanned Aerial Vehicle SUAVI is shaped based on the tasks it will perform. It is designed as a compact electric powered air vehicle for both outdoor and indoor applications such as observation of indoor and outdoor spaces of large buildings and storages, surveillance, monitoring and exploration of disasters like fire, earthquake, flood and other events. It has four tilting wings with the motors mounted on the wings. The wings are horizontal during horizontal flight and vertical during hovering and vertical takeoff-landing. It is planned that this aerial vehicle will perform vertical flight for approximately half an hour and horizontal flight for around one hour in order to perform desired missions effectively. Accordingly, the main design specifications of the air vehicle are as follows: 1 m wingspan, 1 m total length and approximately 4.5 kg weight. Moreover, SUAVI is expected to fly with speed up to 60 km/h in horizontal flight mode.

2.1 Mechanical Design

One of the main goals in the design of aerial vehicle is to obtain the most light-weight structure that is capable of withstanding the possible loadings in vertical, horizontal and transition flight modes. For lightness and endurance,

SUAVI is produced from carbon composite material. Sandwich structure on the entire body is preferred to improve the durability of composite materials. In this sandwich structure, light-weight core material is surrounded by carbon fiber cloth on both sides. Forces that the air vehicle will experience are estimated in simulation environment and mechanical analysis are completed.

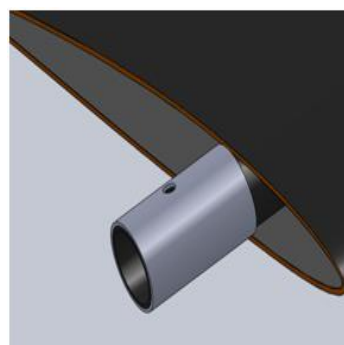
In order to reach a rigid and light-weight body structure and prevent from extra vibrations stemming from actuators that will affect the measurement performance of sensors, a carbon fiber tube is used as a chassis to connect front and back wing connections ruggedly. The body structure is designed to be protection shell instead of being carrier platform. The motivation to do so is the isolation of electronic systems located inside of body from outside and protection of wing roots' aerodynamic features. This protection shell is constructed from four pieces: nose, rear, middle top, middle bottom (see Fig. 2.1). This structure provides to reach electronics and mechanical systems of the vehicle in an quicker and easy way.

For the assembly of wings to the body and change of wing angles, the bearing and wing tilting structure are designed and prototyped. One of the problem is the variation in the outer diameters of carbon fiber tubes. This variation might lead to undesired spaces in the connection parts. The precision of wing angle adjustment is very crucial for control of aerial vehicle in transition phase. Therefore, aluminium rings that have fixed outer diameter are located to end of the carbon fiber tubes from where they are attached to body. The tilting structure is constructed from a hallow arm that is beard from two ends and tilted by servo (see Fig. 2.2). As a result, there is no space between carbon fiber tubes and hallow arm.

The diameter of the carbon fiber tube is chosen to be big enough to



Figure 2.1: The CAD drawing and prototyping of body structure with chassis and pieces



(a)



(b)

Figure 2.2: The CAD drawing (a) and prototyping (b) of the aluminium ring

touch both top and bottom surface of the wing. This contributes to increase in endurance of the wing markedly. As seen in Fig. 2.3, bearings are located on aluminium box profiles that are lightened by extra holes on it. Only one servo for right and left wing is employed for tilting process in order to guarantee that each wing has the same angle of attack.



Figure 2.3: The wing tilting structure zoomed in

One of the significant point in the design of SUAVI is the integration process of batteries and landing gear. If batteries are located inside of the body, the vehicle becomes very sensitive to disturbances coming through roll axis because the inertia of the vehicle about this axis is very small. Moreover, the wings have to carry all the payload coming from the body. The roots of the wings are subject to high bending moments. In the light of these observations, the batteries are located inside the wings. Similar to determination of battery location, the landing gears and their location are determined by taking same criteria into consideration. If landing gear is assembled to the body directly, it results in extra drag force when aerial vehicle flies horizontally with higher speeds. Therefore, carbon fiber tubes that come out of wings

are used as a landing gear. This structure is advantageous during horizontal flight since it tilts together with the wings and does not result in drag force (see Fig. 2.4).



Figure 2.4: Assembly of landing gear

During the integration of landing gear to wings, aluminium elbow connection part is designed to connect enduring carbon spars and landing gear in order to prevent wing hulls from higher loads. Motors are also assembled to this item by a T element that enables quicker replacement (see Fig. 2.5). The cables that combines the equipments located inside the wing and the flight controllers are passed through the carrier carbon fiber tubes and transferred to body. This type of transfer avoid the deterioration of the cables in time. The location of batteries and landing gear into wings prevent the variation of strength points resulting from landing and lift forces. As a result, the transfer of the bending moment from one location to another is reduced. In the final design, the body is a platform that carries the electronics, tilts the wings and holds the wings in a rigid manner as seen in Fig 2.6. The weight

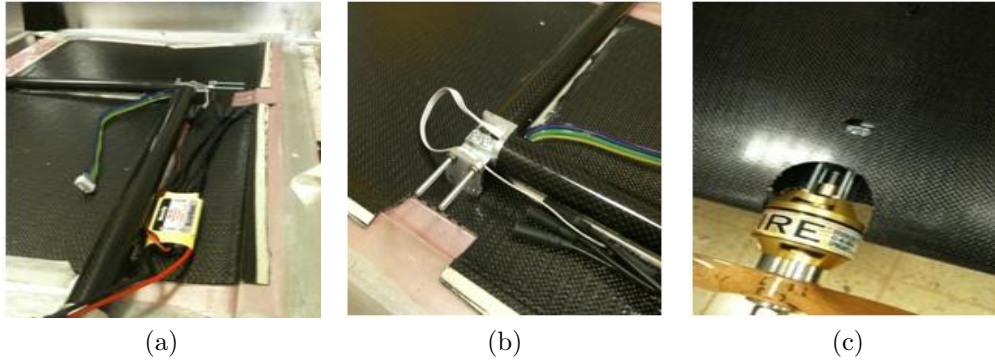


Figure 2.5: Carbon spars (a), aluminium elbow connection part (b), T motor connection element (c)

measurement data of the parts of SUAVI is given in Table 2.1. The CAD drawings and final prototype SUAVI are seen in Fig. 2.7 and Fig. 2.8. Total weight of the aerial vehicle is measured as 4660 gr.

Table 2.1: Weight Measurements

Name of Part	Weight (gr)
Parts inside the wing	$64.9 \times 4 = 259.6$
Landing Gear	71.6
Servo connection	9.2
Servo	$64.8 \times 2 = 129.6$
Wing - body connection	$142.8 \times 2 = 285.6$
Batteries	$146.1 \times 12 = 1753.2$
Total	2508.8

2.2 Aerodynamic Design

In the aerodynamic design of SUAVI, both aerodynamic efficiency and mechanical features are of interest. The criteria on wing profile decision

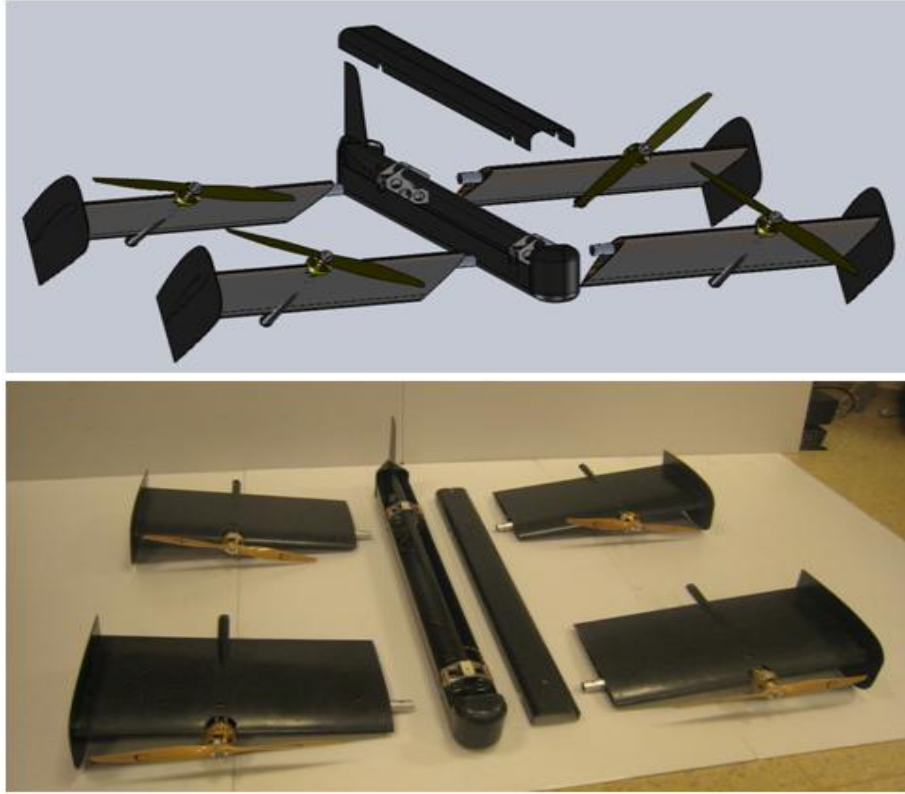


Figure 2.6: CAD drawings of parts of the aerial vehicle and prototyping

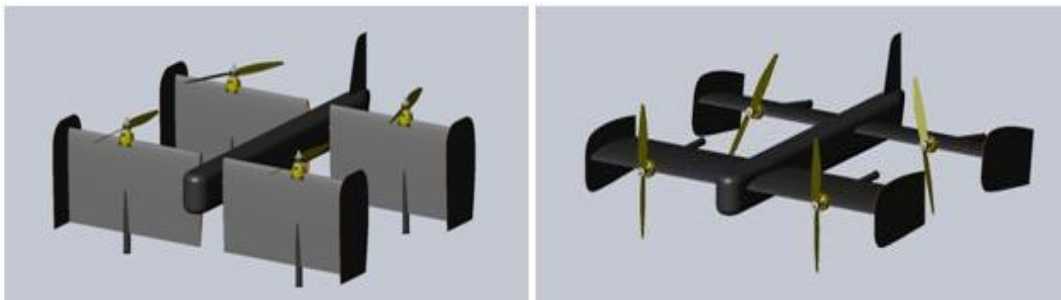


Figure 2.7: CAD drawings of SUAVI

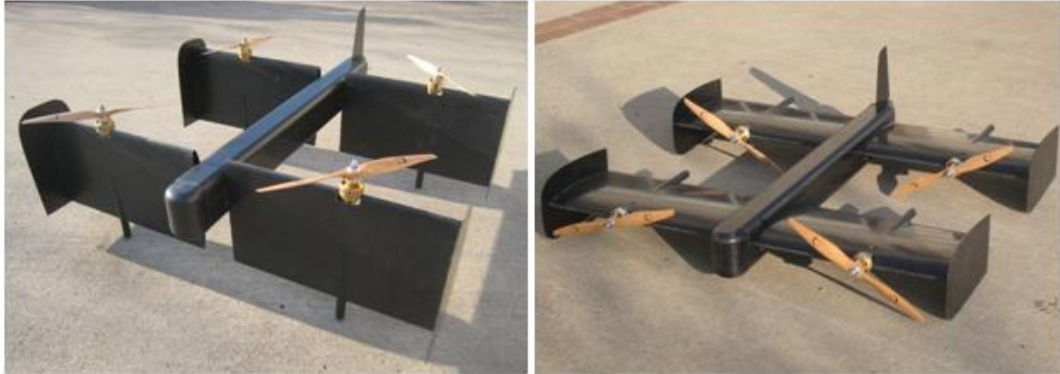


Figure 2.8: Prototype SUAVI

are that the angle-of-attack is $2\text{-}3^\circ$ with respect to the body at maximum speed and the drag is kept minimum on the entire speed range. Through the utilization of wing profile analysis programs like NASA Foilsim[®] II and JavaFoil[®], NACA2410 wing profile is decided to be appropriate with 25 cm chord length. The details of this analysis can be found in [61]. An important element in the design is that the lift generated by the rear wings is decreased due to the downwash generated by the front wings, since the rear wings behave as if they have less angle of attack (see Fig. 2.9). In aerodynamic simulations it is observed that the rear wings have to be placed more than one chord length higher than the front wings to prevent this effect.

However, to make the design and production less complicated, the front and rear wings are located at the same vertical level and the rear wings are decided to be used with higher angle of attack. This additional angle of attack ranges from 0 to 15° depending on the flight speed. In order to cease the drag generating trailing vortices at the wing tips, large winglets are installed on the wings (see Fig. 2.10). These winglets operate by stopping the spanwise flows both on the upper and lower surfaces of the wings. The size of these winglets are near to 15 cm in vertical direction.

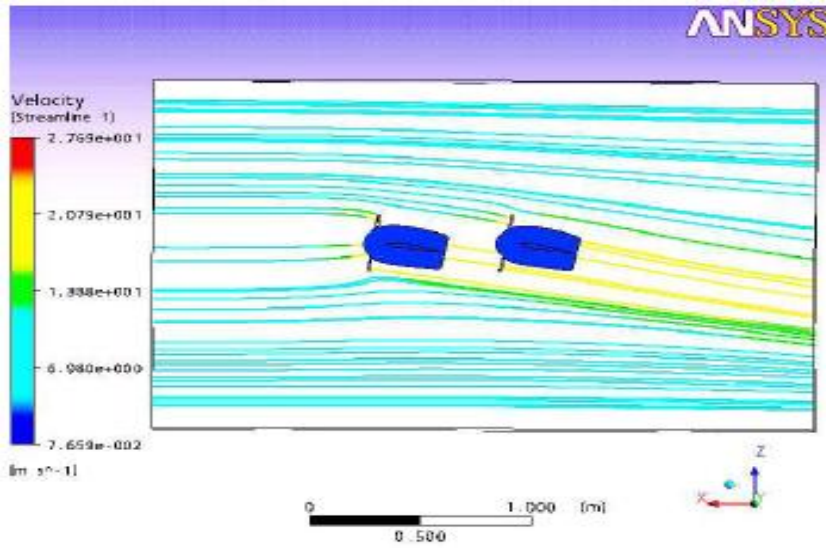


Figure 2.9: Air flow with downwash of the front wing on the rear wing

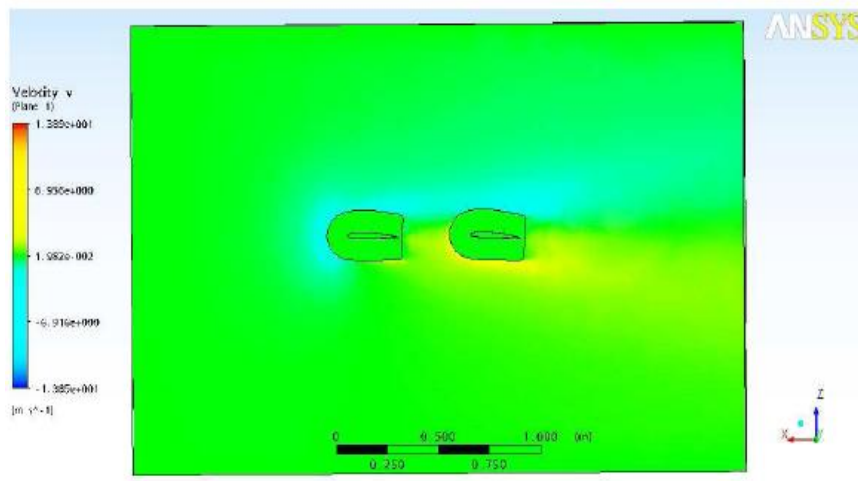


Figure 2.10: Spanwise flow speed on the wings with winglets

2.3 Wind Tunnel Tests

Wind tunnel tests have a very crucial role to obtain aerodynamics characteristics of the aerial vehicle for different angle of attack and motor PWM configurations. In order to observe the effects of front wings and motors on the rear wings and motors, and to design flight control system depending on this model, wind tunnel tests of SUAVI are performed by prototyped half body model 2.11. A very sensitive 6 DOF load cell is employed to measure the forces and moments appearing on the vehicle.

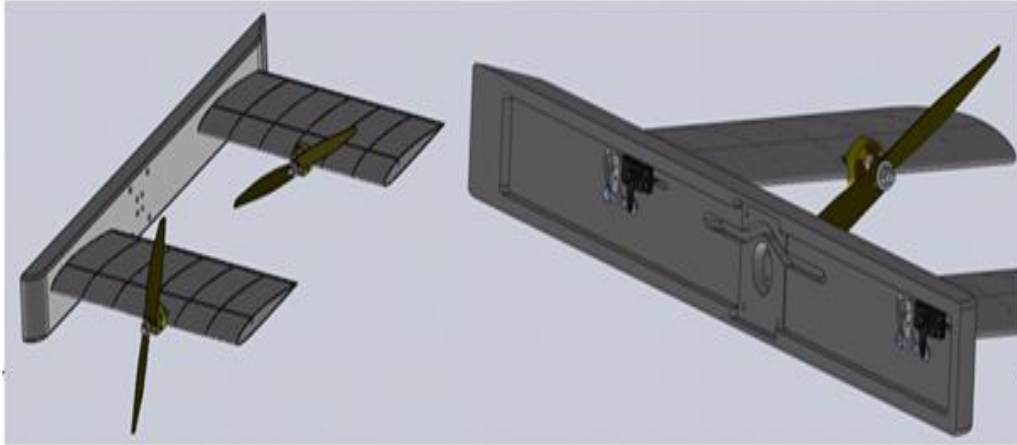


Figure 2.11: CAD drawings of half body model

Wind tunnel tests can be categorized under two topics. First, lift and drag coefficients are measured by using only one wing without any motor interaction as seen in Fig 2.12. The motivation behind the first type of test were to have an idea about the endurance of the wing, to test the capability of servos to hold wings on the desired angle of attack. Secondly, the measurements of lift, drag and pitch moments are carried out by using half body model equipped with two wings and actuators (see Fig 2.13). The outputs are the final design of the winglets, the combinations of motor inputs and

wing angles that will result in robust flight for different velocity and angle of attack. Moreover, the amount of current consumed is also noted for different voltage values in order to keep the flight performance even if there appears a situation where the voltage value decreases.



Figure 2.12: Half body model with one wing is in the wind tunnel

In order to observe the power consumption of the aerial vehicle flying at the desired velocity, angle of attacks and motor PWMs are arranged in such a way that drag force is 0 N, pitch moment is 0 Nm, lift force is 22 N. This amount of lift force seems to be meaningful since the weight of the half body model is approximately 2.25 kg. As a result of the tests, the angle of attacks, motor PWM percentages and required current for nominal flight of the aerial vehicle having different velocities are tabulated in Table 2.2 and depicted graphically in Fig. 2.14, 2.15, 2.16. As seen in Fig. 2.14, the angle of attacks of front and rear wings are very close to each other until 2 m/s air speed. In the case of higher air speed, they diverge and have a difference



Figure 2.13: Half body model with two wings is in the wind tunnel

value up to 17° . This difference results from vortex and air flow generated by front wing on the rear wing. In motor PWM percentage graph (see Fig. 2.15), the patterns of the front and rear motor PWM values are very similar to the wings until 6 m/s air speed, are almost same in the case of higher air speeds. PWM necessities have the minimum values in the interval of 11-14 m/s air speed. However, due to increase in the drag forces, necessary PWM values have a tendency to increase even if the angle of attacks reduce in the other air speed values. The current graph (see Fig. 2.16) seems to be averaging of motor PWM values. The lowest consumption is observed in the interval of 12-13 m/s air speed where the angle of attacks are almost in stall situation. Except this interval, the amount of current consumption increases because motors have to resist drag forces and provide necessary lift forces in lower and higher air speeds.

Table 2.2: Motor PWM percentage, angle of attack and the current consumption for nominal flight

Air speed (m/s)	Front motor PWM (%)	Rear motor PWM (%)	Front wing angle	Rear wing angle	Current (A)
0	62.5	62.5	90	90	32
1	62.5	62.5	88	88	32.4
2	62.5	62.5	86	86	32.4
3	54.3	59	76	86	30.8
4	46.9	53.5	68	82	27
5	41	46.1	54	71	22.8
6	41.8	41.8	41	51	21
7	41.8	41.8	31.5	45	20.2
8	41.8	41.8	29	39	20
9	38.3	38.3	24	30	16.7
10	36.7	36.7	16	25	14.6
11	34	34	14.5	20.5	12.3
12	34.8	34.8	11	15.5	11.9
13	33.6	33.6	10	14.5	10.5
14	38.7	38.7	8	12	12.5
15	42.2	42.2	7	9	14.1
16	45.7	45.7	5.5	8	15.2
17	49.6	49.6	4.5	6	17.5

The result of these tests can be summarized as follows:

- Robust flight characteristics of the aerial vehicle under different circumstances such as air speed, angle of attack and level of battery is obtained.
- The endurance of the wing and the capability of servos to hold wings on the desired angle of attack precisely are verified.
- The design of ideal winglet that results in desired characteristics is finalized.
- Some of the measurements obtained in wind tunnel tests are verified

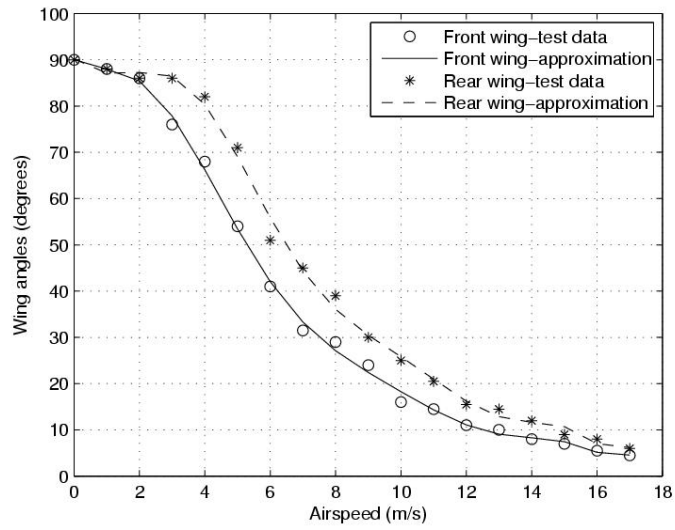


Figure 2.14: Front and rear angle of attacks for nominal flight

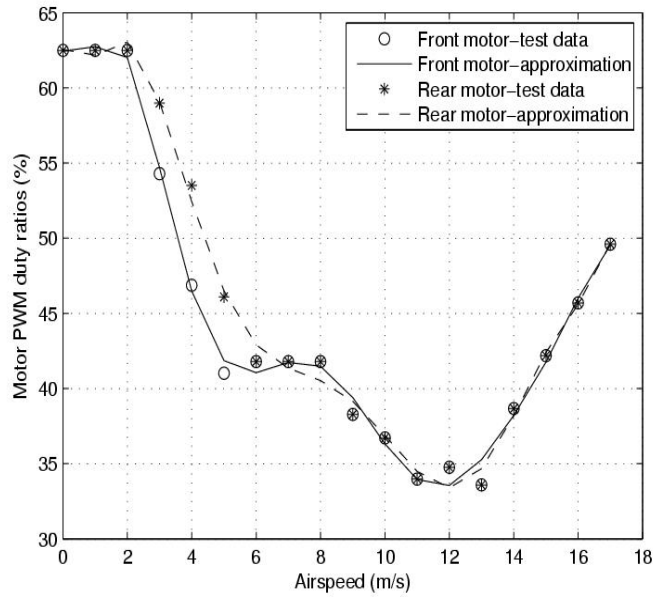


Figure 2.15: Front and rear motor PWM percentages for nominal flight

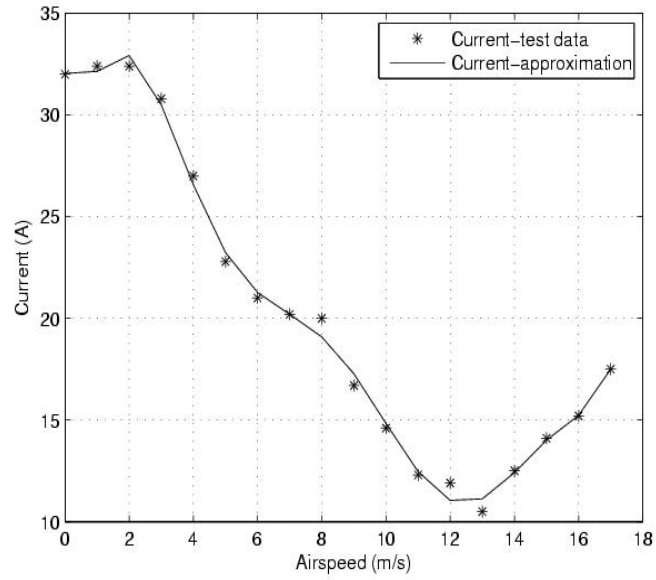


Figure 2.16: Amount of current for nominal flight

with the ones in the literature, some of them are new contributions to the literature.

Chapter 3

3 Mathematical Model of SUAVI

In order to control a complicated system like SUAVI, it will be useful to develop a good mathematical model. Both high-level and low-level control architectures of SUAVI will then depend on this mathematical model. If the system is modeled and identified well, it may be relatively easy to control it. Therefore, all steps of the modeling have to be thought carefully.

SUAVI is equipped with four wings that are mounted at the front and at the back of the vehicle, and can be rotated from vertical to horizontal positions. Fig. 3.1 below shows the aerial vehicle in vertical and horizontal flight modes.

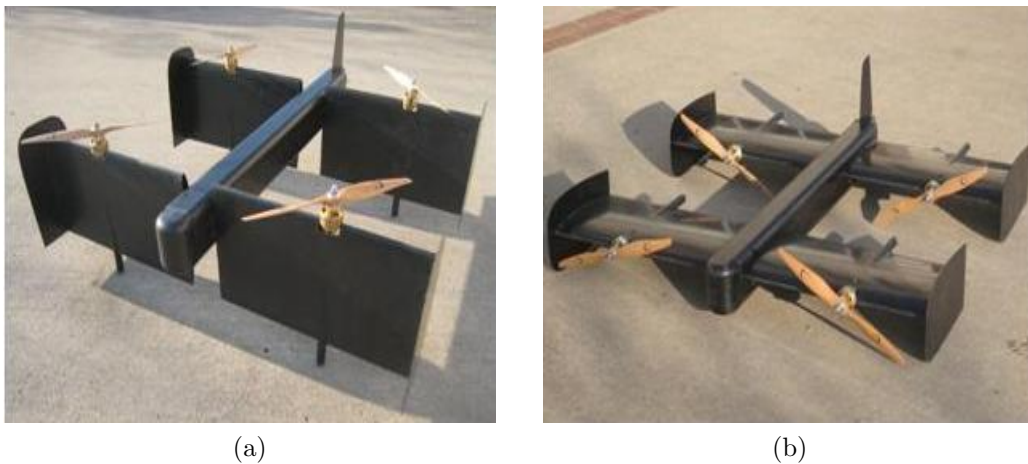


Figure 3.1: Aerial Vehicle is in vertical (a) and horizontal (b) flight modes

With these wing configurations, the vehicle's airframe transforms into a quadrotor structure if the wings are at the vertical position and into an airplane structure if the wings are at the horizontal position. Two wings at the front can be rotated independently to behave as the ailerons while two wings at the back are rotated together to behave as the elevator. This way the control surfaces of a regular plane in horizontal flight mode are mimicked with minimum number of actuators.

The dynamic modeling of a quad tilt-wing aerial vehicle is a challenging engineering problem. Nonlinear mathematical model of SUAVI consists of horizontal flight dynamics, vertical flight dynamics and the transition phase that incorporates both horizontal and vertical flight dynamics. Newton-Euler formulation is used to obtain full mathematical model of a tilt-wing UAV including wind effects using Dryden Wind Model.

The following assumptions are made while obtaining mathematical model [62]:

- The vehicle has 6 DOF and is a rigid body.
- The center of mass and the origin of body fixed frame are coincident.
- The drag force of the fuselage is neglected.
- The relative airspeed on the body frame is only due to vehicle's flight speed.

3.1 Hybrid Frame

In deriving dynamical models for unmanned aerial vehicles, it is usually preferred to express positional dynamics with respect to a fixed world coor-

dinate frame and the rotational dynamics with respect to a body fixed frame attached to the vehicle. Hence, a hybrid frame [63] is resulted.

The two reference frames given in Fig. 3.2 are used for mathematical modeling of the aerial vehicle:

- Earth fixed inertial reference frame (world frame) $W : (O_w, x_w, y_w, z_w)$.
- Body fixed reference frame $B : (O_b, x_b, y_b, z_b)$

The subscripts w and b used in these equations express the vector and matrix quantities in world and body frames, respectively. x_w points toward the North, y_w points toward the East, z_w points downwards with respect to the earth and O_w is the axis origin according to earth fixed inertial reference frame. Similarly, x_b points towards the aerial vehicle's front, y_b points toward the vehicle's right, z_b points downwards and O_b is the axis origin. O_b is chosen to coincide with the center of mass of the aerial vehicle as stated before.

The position and linear velocity of the vehicle's center of mass in world frame are described as,

$$P_w = [X, Y, Z]^T \quad (1)$$

$$V_w = \dot{P}_w = [\dot{X}, \dot{Y}, \dot{Z}]^T \quad (2)$$

The attitude of the vehicle in world frame is given as,

$$\alpha_w = [\phi, \theta, \psi]^T \quad (3)$$

where the time derivative of attitude angles in world frame is given as,

$$\Omega_w = \dot{\alpha}_w = [\dot{\phi}, \dot{\theta}, \dot{\psi}]^T \quad (4)$$

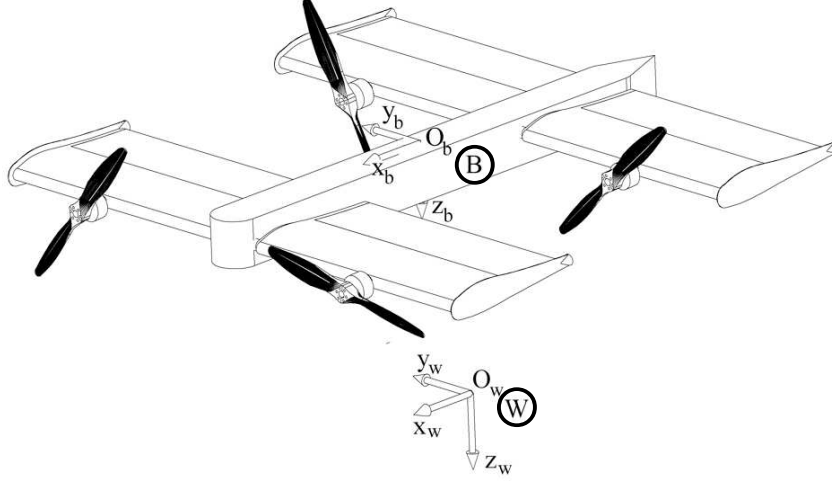


Figure 3.2: Coordinate frames of the aerial vehicle

In these equations ϕ , θ and ψ are named roll, pitch and yaw angles respectively. The orientation of the body frame with respect to earth frame is defined by the following rotation matrix:

$$R_{wb}(\phi, \theta, \psi) = R_z(\psi)R_y(\theta)R_x(\phi) = \begin{bmatrix} c_\psi c_\theta & s_\phi s_\theta c_\psi - c_\phi s_\psi & c_\phi s_\theta c_\psi + s_\phi s_\psi \\ c_\theta s_\psi & s_\phi s_\theta s_\psi + c_\phi c_\psi & c_\phi s_\theta s_\psi - s_\phi c_\psi \\ -s_\theta & s_\phi c_\theta & c_\phi c_\theta \end{bmatrix} \quad (5)$$

where s_β and c_β are abbreviations for $\sin(\beta)$ and $\cos(\beta)$ respectively. The transformation of linear velocities between world and body frames is given as,

$$V_b = \begin{bmatrix} v_x \\ v_y \\ v_z \end{bmatrix} = R_{wb}^T(\phi, \theta, \psi) \cdot V_w = R_{bw}(\phi, \theta, \psi) \cdot V_w \quad (6)$$

The transformation between body angular velocities and time derivative of Euler angles is given as,

$$\Omega_b = \begin{bmatrix} p \\ q \\ r \end{bmatrix} = E(\phi, \theta) \underbrace{\begin{bmatrix} \dot{\phi} \\ \dot{\theta} \\ \dot{\psi} \end{bmatrix}}_{\Omega_w} \quad (7)$$

where the E is the rotational velocity transformation matrix [63] and defined as

$$E(\phi, \theta) = \begin{bmatrix} 1 & 0 & -s_\theta \\ 0 & c_\phi & s_\phi c_\theta \\ 0 & -s_\phi & c_\phi c_\theta \end{bmatrix} \quad (8)$$

The transformation matrix between the rate of change of orientation angles $(\dot{\phi}, \dot{\theta}, \dot{\psi})$ and the body angular velocities (p, q, r) can be considered as identity matrix only if the perturbations during hover flight are small.

3.2 Newton-Euler Formulation

There are several techniques that can be used to derive the equations of a rigid body with 6 DOF. The Newton-Euler formulation has been adopted to derive full mathematical model of the vehicle.

Utilizing a hybrid frame and considering the aerial vehicle as a rigid body, the dynamics of an unmanned aerial vehicle can be written as

$$\begin{bmatrix} mI_{3 \times 3} & 0_{3 \times 3} \\ 0_{3 \times 3} & I_b \end{bmatrix} \begin{bmatrix} \dot{V}_w \\ \dot{\Omega}_b \end{bmatrix} + \begin{bmatrix} 0 \\ \Omega_b \times (I_b \Omega_b) \end{bmatrix} = \begin{bmatrix} F_t \\ M_t \end{bmatrix} \quad (9)$$

Here, m is the mass and I_b is the inertia matrix of the vehicle expressed

in its body coordinate frame. $I_{3 \times 3}$ and $0_{3 \times 3}$ matrices are 3×3 identity and zero matrices respectively. Since the aerial vehicle is modeled as a 6 DOF rigid body, note that the left hand side of Eqn. (9) is standard for many aerial vehicles. Total force and moment terms, F_t and M_t , will be different for different platforms. It should be remarked that for a tilt-wing quadrotor these terms will be functions of the thrusts produced by the rotors and cosine or sine of the rotation angles of the wings. The external forces and torques acting on the vehicle are given in Fig.3.3.

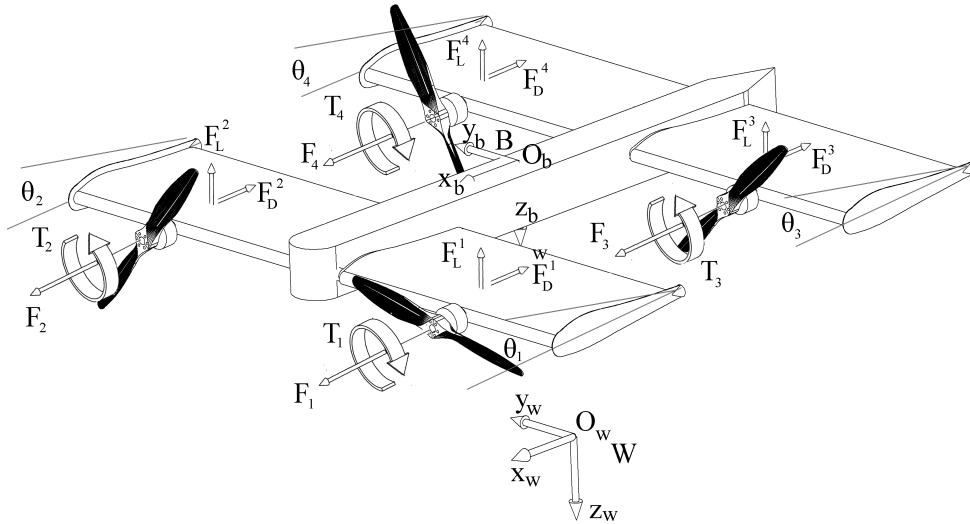


Figure 3.3: External forces and torques acting on the vehicle

The total external force F_t acting on the vehicle's center of gravity is the sum of the thrust forces F_{th} created by the rotors, the lift and drag forces generated by the wings F_w , F_g due to gravity and F_d due to external disturbances (e.g. wind, gusts). These forces that are expressed in the body frame must be transformed to the earth frame by the rotation matrix since

the total external force F_t is expressed in the world frame. So, we have

$$F_t = R_{wb}(F_{th} + F_w + F_g + F_d) \quad (10)$$

where

$$F_{th} = \begin{bmatrix} c_{\theta_1} & c_{\theta_2} & c_{\theta_3} & c_{\theta_4} \\ 0 & 0 & 0 & 0 \\ -s_{\theta_1} & -s_{\theta_2} & -s_{\theta_3} & -s_{\theta_4} \end{bmatrix} \begin{bmatrix} k\omega_1^2 \\ k\omega_2^2 \\ k\omega_3^2 \\ k\omega_4^2 \end{bmatrix}$$

$$F_w = \begin{bmatrix} (F_D^1(\theta_1, v_x, v_z) + F_D^2(\theta_2, v_x, v_z) + F_D^3(\theta_3, v_x, v_z) + F_D^4(\theta_4, v_x, v_z)) \\ 0 \\ (F_L^1(\theta_1, v_x, v_z) + F_L^2(\theta_2, v_x, v_z) + F_L^3(\theta_3, v_x, v_z) + F_L^4(\theta_4, v_x, v_z)) \end{bmatrix}$$

and

$$F_g = \begin{bmatrix} -s_{\theta} \\ s_{\phi}c_{\theta} \\ c_{\phi}c_{\theta} \end{bmatrix} mg$$

In these equations, θ_i represents wing angles. Note that the propeller thrusts $F_{(1,2,3,4)}$ are modeled as

$$F_i = k\omega_i^2 \quad (11)$$

where ω_i is the propeller's rotational speed [64].

For design simplicity, two wings at the back and two wings at the front are rotated together, i.e. their angle of attacks are the same for all time ($\theta_1 = \theta_2, \theta_3 = \theta_4$). Note that the lift forces $F_L^i(\theta_i, v_x, v_z)$ and the drag forces $F_D^i(\theta_i, v_x, v_z)$ are not just functions of linear velocities (v_x and v_z) like on a fixed-wing type of an airplane, but also functions of angle of attack θ_i for

each wing, namely

$$\begin{bmatrix} F_D^i \\ 0 \\ F_L^i \end{bmatrix} = R(\theta_i) \begin{bmatrix} -\frac{1}{2}c_D(\alpha_i)\rho Av_\alpha^2 \\ 0 \\ -\frac{1}{2}c_L(\alpha_i)\rho Av_\alpha^2 \end{bmatrix} \quad (12)$$

where

$$v_\alpha = \sqrt{v_x^2 + v_z^2}$$

$$\alpha_i = \theta_i - (-\text{atan2}(v_z, v_x))$$

In these expressions, ρ is the air density, A is the wing area, v_α is the airstream velocity and α_i is the effective angle of attack as shown in Fig. 3.4. Note that due to the geometry of the wing, a rotation around y axis, i.e. $R(\theta_i)$, is needed in Eqn. (12).

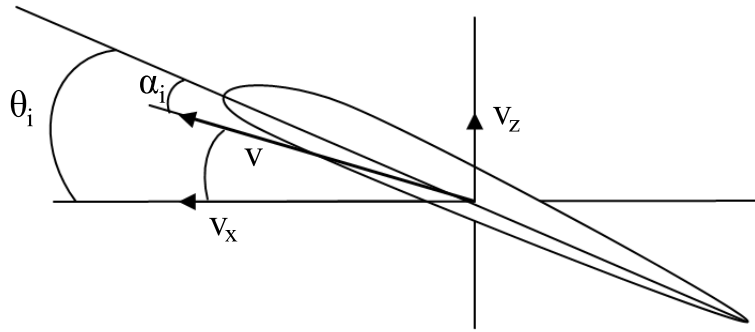


Figure 3.4: Effective angle of attack α_i

The lift coefficient $c_L(\alpha_i)$ and drag coefficient $c_D(\alpha_i)$ are modeled according to the data points obtained from Javafoil and airfoil models from [65], [66]. (see [62] for details)

The total torque M_t acting on the vehicle's center of gravity is the sum of

the torques M_{th} created by the rotors, M_w created by the drag/lift forces of the wings, M_{gyro} created by the gyroscopic effects of the propellers and M_d due to external disturbances, namely

$$M_t = M_{th} + M_w + M_{gyro} + M_d \quad (13)$$

where

$$M_{th} = \begin{bmatrix} l_s s_{\theta_1} - c_{\theta_1} \lambda_1 & -l_s s_{\theta_2} - c_{\theta_2} \lambda_2 & l_s s_{\theta_3} - c_{\theta_3} \lambda_3 & -l_s s_{\theta_4} - c_{\theta_4} \lambda_4 \\ l_l s_{\theta_1} & l_l s_{\theta_2} & -l_l s_{\theta_3} & -l_l s_{\theta_4} \\ l_s c_{\theta_1} + s_{\theta_1} \lambda_1 & -l_s c_{\theta_2} + s_{\theta_2} \lambda_2 & l_s c_{\theta_3} + s_{\theta_3} \lambda_3 & -l_s c_{\theta_4} + s_{\theta_4} \lambda_4 \end{bmatrix} \begin{bmatrix} k\omega_1^2 \\ k\omega_2^2 \\ k\omega_3^2 \\ k\omega_4^2 \end{bmatrix},$$

$$M_w = \begin{bmatrix} l_s(F_L^1(\theta_1, v_x, v_z) - F_L^2(\theta_2, v_x, v_z) + F_L^3(\theta_3, v_x, v_z) - F_L^4(\theta_4, v_x, v_z)) \\ l_l(F_L^1(\theta_1, v_x, v_z) + F_L^2(\theta_2, v_x, v_z) - F_L^3(\theta_3, v_x, v_z) - F_L^4(\theta_4, v_x, v_z)) \\ l_s(-F_D^1(\theta_1, v_x, v_z) + F_D^2(\theta_2, v_x, v_z) - F_D^3(\theta_3, v_x, v_z) + F_D^4(\theta_4, v_x, v_z)) \end{bmatrix}$$

and

$$M_{gyro} = \sum_{i=1}^4 J_{prop} [\eta_i \Omega_b \times \begin{bmatrix} c_{\theta_i} \\ 0 \\ -s_{\theta_i} \end{bmatrix} \omega_i]$$

In the above equations, parameters l_s and l_l denote distances between the rotors and the center of mass of the vehicle, J_{prop} is the inertia of the propellers about their rotation axes and $\eta_{(1,2,3,4)} = 1, -1, -1, 1$. The propeller torques $T_{(1,2,3,4)}$ are modeled as

$$T_i = \lambda_i k \omega_i^2 \quad (14)$$

where $\lambda_{1,2,3,4}$ are torque/force ratios. For clockwise rotating propellers, λ_2, λ_3 are negative whereas λ_1, λ_4 are positive for counterclockwise rotating propellers. It turns out that λ for such kind of propeller sets are measured as 1-5% in the literature [63].

Note that the sum of torques created by the rotors result in a roll moment along the x axis in horizontal flight mode ($\theta_{1,2,3,4} = 0$) and in a yaw moment along the z axis in vertical flight mode ($\theta_{1,2,3,4} = \pi/2$).

Using vector-matrix notation above equations can be rewritten in a more compact form as

$$M\dot{\zeta} + C(\zeta)\zeta = G + O(\zeta)\omega + E(\xi)\omega^2 + W(\zeta) \quad (15)$$

where ζ denotes the vehicle's generalized velocity vector and is defined as

$$\zeta = [\dot{X}, \dot{Y}, \dot{Z}, p, q, r]^T \quad (16)$$

The vector ξ which appears in Eqn. (15), describes the position and the orientation of the vehicle with respect to the world frame, and is defined as

$$\xi = [X, Y, Z, \phi, \theta, \psi]^T \quad (17)$$

The relation between ζ and ξ can easily be derived as

$$\dot{\xi} = J\zeta \quad (18)$$

$$\begin{bmatrix} \dot{X} \\ \dot{Y} \\ \dot{Z} \\ \dot{\phi} \\ \dot{\theta} \\ \dot{\psi} \end{bmatrix} = \begin{bmatrix} 1 & 0 & 0 & 0 & 0 & 0 \\ 0 & 1 & 0 & 0 & 0 & 0 \\ 0 & 0 & 1 & 0 & 0 & 0 \\ 0 & 0 & 0 & 1 & s_\phi t_\theta & c_\phi t_\theta \\ 0 & 0 & 0 & 0 & c_\phi & -s_\phi \\ 0 & 0 & 0 & 0 & s_\phi/c_\theta & c_\phi/c_\theta \end{bmatrix} \begin{bmatrix} \dot{X} \\ \dot{Y} \\ \dot{Z} \\ p \\ q \\ r \end{bmatrix} \quad (19)$$

where $c_{(\cdot)}$, $s_{(\cdot)}$ and $t_{(\cdot)}$ are abbreviations for $\cos(\cdot)$, $\sin(\cdot)$ and $\tan(\cdot)$ respectively. The inertia matrix, M , the Coriolis-centripetal matrix, $C(\zeta)$, the gravity term, G , and the gyroscopic term, $O(\zeta)\omega$, all expressed in the hybrid frame, are defined as

$$M = \begin{bmatrix} mI_{3 \times 3} & 0_{3 \times 3} \\ 0_{3 \times 3} & \text{diag}(I_{xx}, I_{yy}, I_{zz}) \end{bmatrix} \quad (20)$$

$$C(\zeta) = \begin{bmatrix} 0 & 0 & 0 & 0 & 0 & 0 \\ 0 & 0 & 0 & 0 & 0 & 0 \\ 0 & 0 & 0 & 0 & 0 & 0 \\ 0 & 0 & 0 & 0 & I_{zz}r & -I_{yy}q \\ 0 & 0 & 0 & -I_{zz}r & 0 & I_{xx}p \\ 0 & 0 & 0 & I_{yy}q & -I_{xx}p & 0 \end{bmatrix} \quad (21)$$

$$G = [0, 0, mg, 0, 0, 0]^T \quad (22)$$

$$O(\zeta)\omega = J_{prop} \left(\begin{array}{c} 0_{3 \times 1} \\ \sum_{i=1}^4 [\eta_i \Omega_b \times \begin{bmatrix} c_{\theta_i} \\ 0 \\ -s_{\theta_i} \end{bmatrix} \omega_i] \end{array} \right) \quad (23)$$

where I_{xx} , I_{yy} and I_{zz} are vehicle's moments of inertia about x , y , z axes of its body frame, $0_{3 \times 1}$ is a 3×1 zero vector. $u_{(1,2,3,4)}$ are the virtual control inputs.

System actuator vector, $E(\xi)\omega^2$, is defined as

$$E(\xi)\omega^2 = \begin{bmatrix} -([s_\phi s_\psi + c_\psi s_\theta c_\phi]s_{\theta_i} + [c_\theta c_\psi]c_{\theta_i})u_1 \\ -([c_\psi s_\phi + s_\psi s_\theta c_\phi]s_{\theta_i} + [c_\theta s_\psi]c_{\theta_i})u_1 \\ -([c_\theta c_\phi]s_{\theta_i} - s_\theta c_{\theta_i})u_1 \\ u_2 \\ u_3 \\ u_4 \end{bmatrix} \quad (24)$$

$u_{1,2,3,4}$ terms used in Eqn. (24) are explicitly written below:

$$u_1 = b(\omega_1^2 + \omega_2^2 + \omega_3^2 + \omega_4^2) \quad (25)$$

$$u_2 = l_s b((\omega_1^2 + \omega_3^2) - (\omega_2^2 + \omega_4^2)) \quad (26)$$

$$u_3 = l_l b((\omega_1^2 + \omega_2^2) - (\omega_3^2 + \omega_4^2)) \quad (27)$$

$$u_4 = d(-\omega_1^2 + \omega_2^2 - \omega_3^2 + \omega_4^2) \quad (28)$$

Parameters b and d are lift and drag coefficients.

Lift and drag forces produced by the wings and the resulting moments due to these forces for different wing angles are defined as

$$W(\zeta) = \begin{bmatrix} R_{wb} \begin{bmatrix} F_D^1 + F_D^2 + F_D^3 + F_D^4 \\ 0 \\ F_L^1 + F_L^2 + F_L^3 + F_L^4 \end{bmatrix} \\ l_s(F_L^1 - F_L^2 + F_L^3 - F_L^4) \\ l_l(F_L^1 + F_L^2 - F_L^3 - F_L^4) \\ l_s(-F_D^1 + F_D^2 - F_D^3 + F_D^4) \end{bmatrix} \quad (29)$$

where R_{wb} is the rotation matrix between world and body coordinate axis, $F_D^i = F_D^i(\theta_i, v_x, v_z)$ and $F_L^i = F_L^i(\theta_i, v_x, v_z)$ are the lift and drag forces produced at the wings.

Note that the tilt-wing UAV model above boils down to a quadrotor model when $(\theta_{1,2,3,4} = \pi/2)$. The inertia matrix M , the Coriolis-centripetal matrix $C(\zeta)$ and the gravity vector G remain without change since they do not depend on wing angles. However, some of the elements in the gyroscopic term $O(\zeta)w$, system actuator vector $E(\xi)w^2$ and the aerodynamic force vector $W(\zeta)$ drop since they are functions of wing angles. There is no lift force produced by the wings anymore since they are in the vertical position. The resulting dynamic model written for the quadrotor mode of our tilt-wing aerial vehicle is verified with the models existing in the literature ([63]).

$$O(\zeta)\omega = J_{prop} \left(\begin{array}{c} 0_{3 \times 1} \\ \sum_{i=1}^4 [\eta_i \Omega_b \times \begin{bmatrix} 0 \\ 0 \\ -1 \end{bmatrix} \omega_i] \end{array} \right) = J_{prop} \begin{bmatrix} 0 & 0 & 0 & 0 \\ 0 & 0 & 0 & 0 \\ 0 & 0 & 0 & 0 \\ -q & q & -q & q \\ p & -p & p & -p \\ 0 & 0 & 0 & 0 \end{bmatrix} \begin{bmatrix} w_1 \\ w_2 \\ w_3 \\ w_4 \end{bmatrix}$$

$$E(\xi)\omega^2 = \begin{bmatrix} -(s_\phi s_\psi + c_\psi s_\theta c_\phi)u_1 \\ -(c_\psi s_\phi + s_\psi s_\theta c_\phi)u_1 \\ -(c_\theta c_\phi)u_1 \\ u_2 \\ u_3 \\ u_4 \end{bmatrix}, \quad W(\zeta) = \begin{bmatrix} R_{wb} \begin{bmatrix} F_D^1 + F_D^2 + F_D^3 + F_D^4 \\ 0 \\ 0 \\ 0 \\ 0 \end{bmatrix} \\ l_s(-F_D^1 + F_D^2 - F_D^3 + F_D^4) \end{bmatrix}$$

Position and attitude dynamics of the aerial vehicle in quadrotor mode represented in a system of equations are given as follows:

$$\begin{aligned} \ddot{X} &= -(s_\phi s_\psi + c_\psi s_\theta c_\phi)u_1 \\ \ddot{Y} &= -(c_\psi s_\phi + s_\psi s_\theta c_\phi)u_1 \\ \ddot{Z} &= -(c_\theta c_\phi)\frac{u_1}{m} + g \\ \ddot{\phi} &= \frac{u_2}{I_{xx}} + \frac{I_{yy} - I_{zz}}{I_{xx}}qr - \frac{J_{prop}}{I_{xx}}q\omega_p \\ \ddot{\theta} &= \frac{u_3}{I_{yy}} + \frac{I_{zz} - I_{xx}}{I_{yy}}pr + \frac{J_{prop}}{I_{yy}}p\omega_p \\ \ddot{\psi} &= \frac{u_4}{I_{zz}} + \frac{I_{xx} - I_{yy}}{I_{zz}}pq + \frac{J_{prop}}{I_{zz}}r\omega_p \end{aligned} \quad (30)$$

The parameters of the vehicle used in mathematical modeling are given in Table 3.1 below.

3.3 Disturbance Modeling

The effect of wind on aerial vehicle flight control can be significant and can lead to instabilities. In order to improve the positioning performance of the quadrotor, wind effects can be modeled and the generalized wind forces can

Table 3.1: Modeling Parameters

Symbol	Description	Dimensions/Magnitude
m	mass	4 kg
l_s	rotor distance to COG along y axis	0.25 m
l_l	rotor distance to COG along x axis	0.25 m
I_{xx}	moment of inertia along x axis	0.195 kgm^2
I_{yy}	moment of inertia along y axis	0.135 kgm^2
I_{zz}	moment of inertia along z axis	0.135 kgm^2
$\lambda_{1,4}$	torque/force ratio	0.01 Nm/N
$\lambda_{2,3}$	torque/force ratio	-0.01 Nm/N

be estimated. The wind estimate is used to reject the external disturbances created by the wind and gust effects.

The main framework of wind modeling represented in [31] depends on the Dryden wind-gust model. This model is defined as a summation of sinusoidal excitations:

$$v_\omega(t) = v_\omega^0 + \sum_{i=1}^n a_i \sin(\Omega_i t + \varphi_i) \quad (31)$$

where $v_\omega(t)$ is a time dependent estimate of the wind vector given time t , randomly selected frequencies Ω_i in the range of 0.1 to 1.5 rad/s and phase shifts φ_i . n is the number of sinusoids, a_i is the amplitude of sinusoids and v_ω^0 is the static wind vector. The magnitudes a_i are defined as $a_i = \sqrt{\Delta\Omega_i \Phi(\Omega_i)}$ where $\Delta\Omega_i$ are frequency intervals between different frequencies and $\Phi(\Omega_i)$ are the power spectral densities. The power spectral density for vertical and horizontal winds are different and can be determined from the following equations:

$$\Phi_h(\Omega) = \sigma_h^2 \frac{2L_h}{\pi} \frac{1}{1 + (L_h\Omega)^2} \quad (32)$$

$$\Phi_v(\Omega) = \sigma_v^2 \frac{2L_v}{\pi} \frac{1 + 3(L_v\Omega)^2}{(1 + (L_v\Omega)^2)^2} \quad (33)$$

Here σ_h and σ_v are horizontal and vertical turbulence intensities respectively. L_h and L_v are horizontal and vertical gust length scales. It is stated that these relations are valid for altitudes below 1000 feet [31]. The relations between L_h and L_v , and σ_h and σ_v are altitude dependent as can be seen from the following equations:

$$\frac{L_h}{L_v} = \frac{1}{(0.177 + 0.000823Z)^{1.2}} \quad (34)$$

$$\frac{\sigma_h}{\sigma_v} = \frac{1}{(0.177 + 0.000823Z)^{0.4}} \quad (35)$$

Using velocities predicted by this wind model, generalized forces are calculated by multiplying wind velocities by related aerodynamic drag coefficients. These generalized forces are integrated into the dynamic model given in Eqn. (15) as external disturbances $D(\zeta, \xi)$. After incorporating the external disturbances, the final form of the dynamic model of the quadrotor vehicle given in Eqn. (36) becomes as follows:

$$M\dot{\zeta} + C(\zeta)\zeta = G + O(\zeta)\omega + E(\xi)\omega^2 + W(\zeta) + D(\zeta, \xi) \quad (36)$$

Chapter III

4 GPS Based Position Control and Waypoint Navigation

Complexity is a very common problem in control systems and the necessity of appropriate decomposition techniques to analyze these problems in a systematic approach is well known. Hierarchical control can be considered as a decomposition of complex missions into subtasks and combination of individual solutions in a hierarchical structure to cope with them successfully. Complexities commonly arise from design of hybrid control systems since continuous and discrete levels are the points at issue [67].

For the control of SUAVI, a hierarchical control system is inevitable since it is a complex multiple-input multiple-output (MIMO) system and is affected by internal and external uncertainties during flight experiments. Hierarchical control system is designed which consists of a high-level controller for hovering and trajectory tracking and low-level controllers for attitude stabilization. As seen in Fig. 4.1, a control architecture having two steps is framed [68]. Low-level control system is behaved as middle layer that communicates with aerial vehicle via low-level (physical) signals (u^L and y^L) and with high-level controller (supervisor) via high-level (not physical) signals (u^H and y^H). This middle layer is responsible for verification of low-level control mechanisms that are triggered by high-level inputs (u^H) and to gather low-level

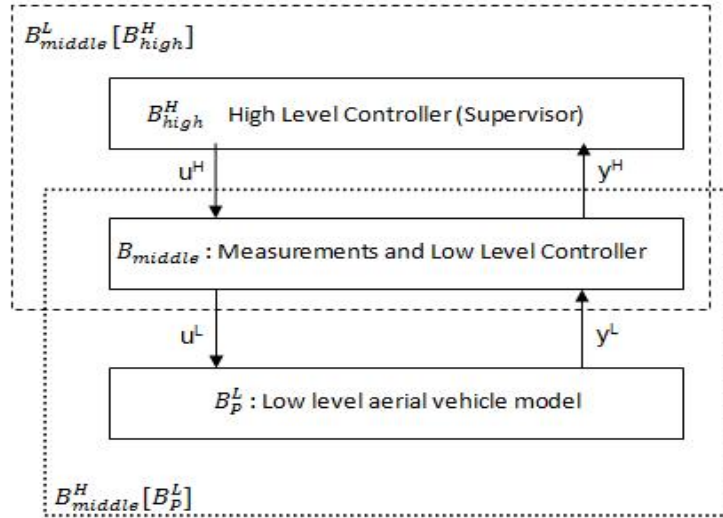


Figure 4.1: Hierarchical Control System of SUAVI

measurement datas (y^L) in order to send high-level information to high-level controller. Aforementioned gathering process can be realized in both signal and time space. This is why the frequencies of high and low-level signals will be different. For instance, the time axis for high-level signals might be slower than the one for low-level signals.

The purpose of hierarchical control synthesis is to develop a control architecture having two steps ($B_{middle}[B_{high}^H]$) that satisfies the following properties [68]:

- Integrated controller ($B_{middle}[B_{high}^H]$) has to force the behavior of the aerial vehicle into desired manner.
- Integrated controller ($B_{middle}[B_{high}^H]$) has to be an feasible controller for the model of aerial vehicle.
- High-level controller (B_{high}^H) has to be an feasible controller for aerial vehicle that is controlled by low-level controllers.

In this context, *feasible* refers to an architecture that controller does not deteriorate the input-output structure and the response of the system to the reference in the past has to be expanded towards future. In order to realize these conditions, the middle layer has to be capable of gathering the measurements from low-level in both time and signal space and switching the low-level controllers to the system in accordance with the orders coming from high-level controller.

It is obvious that the success of task implementation ordered by high-level structure depends on performance of high and low-level controller working together harmoniously. The hardware equipment of the system is constructed by ground station, high-level and low-level controllers and sensors, modules and connection of all mentioned sub volumes with each other. The overall structure of the control system is given in Fig. 4.2 in detail.

As a high-level controller, a Gumstix® microcomputer (see Appendix A for details) is used. This microcomputer is responsible for

- determination of aerial vehicle's flight mode according to data coming from sensors
- the choice of which low-level controller is switched to the system depending on the flight mode of the vehicle in order to generate the attitude references required for the desired mission
- forming the communication link with the ground station
- performing all controls including the security control

This microcomputer is equipped with a GPS receiver for obtaining the position of SUAVI and an onboard camera for various visual servoing applications such as vision based landing. Gumstix® microcomputer is preferred as the

supervisory controller due to its ability to handle complex computations using its DSP processor and Arm Cortex-A8 in a very light-weight and compact structure.

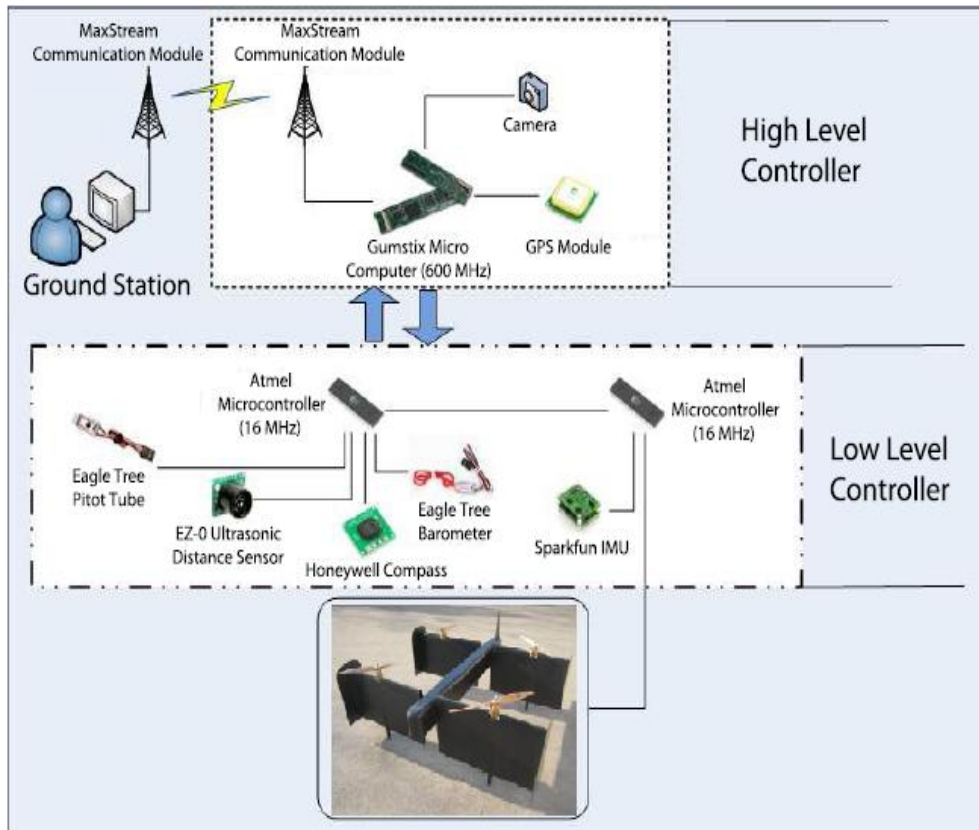


Figure 4.2: Overall flight control system

SUAVI has two different flight configuration: vertical take off-landing (VTOL) and horizontal flight. The transition between flight modes is not instantaneous since the change of wings from vertical to horizontal position is handled by servos and the speeds of servos are physically limited. Consequently, aerial vehicle has to be in one of the three flights modes in anytime:

- Vertical teke-off or landing

- Transition phase
- Horizontal flight

According to different surveillance scenarios, vehicle performs either vertical take off and landing mode or vertical take off, transition from vertical to horizontal flight mode, horizontal flight, back transition vertical flight mode and vertical landing. Especially, the latter combination of flight modes is envisioned since continuous surveillance scenarios necessitate this kind of flight operation.

4.1 Low-Level Control: Attitude and Altitude Control Using PID Controllers

The main goal of the low-level controller is to keep the aircraft at the position and orientation demanded by the high-level controller. To achieve this task, it generates the actuator signals by fusing the flight data obtained from several sensors such as altimeter, sonar, ultrasonic distance sensor, GPS receiver, compass, inertial measurement unit (IMU) and pitot tube.

4.1.1 Development of Switching Logic

As mentioned in the previous part, the vehicle has three different flight modes. For each one of these flight modes, various low-level controllers are designed (see Fig. 4.3). According to momentary flight mode of the vehicle, the low-level controller group is put into the service by the high-level controller (supervisor). Note that number of low-level controllers for each flight modes are different from each other. For the transition between flight modes,

switching among different controller groups is performed. This switching operation determines whether inputs variables such as servo, motor or angle of attack are used or not. The aerial vehicle always prefers vertical flight mode

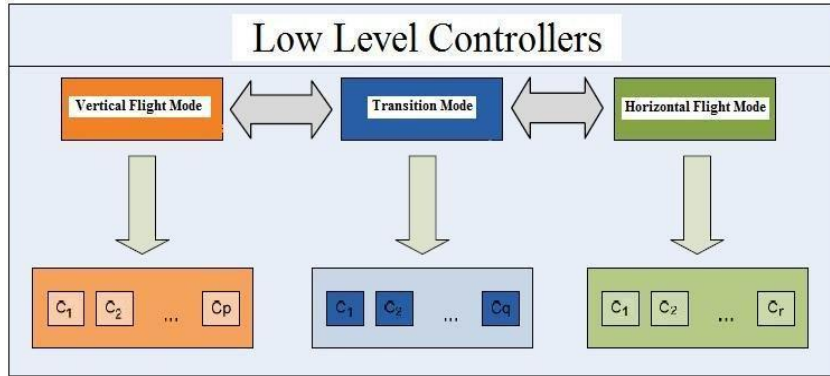


Figure 4.3: Flight modes and related low-level controllers

for take off and landing. In this case, the low-level controllers responsible for vertical flight mode are switched to the system. There are several low-level controllers (C_1, C_2, \dots, C_p) that are responsible for attitude (angular position and velocity) control of the vehicle. It is also possible that some of the feedback signals coming from sensors are not used depending on the configuration of the vehicle. For instance, when aerial vehicle is closer to the ground, the altitude controller uses the data coming from sonar sensor. However, by the time altitude of the aerial vehicle exceeds 5-6 meters, vehicle prefers to use data coming from GPS or altimeter since this amount of altitude is not in working range of the sonar sensor.

While the aerial vehicle is in vertical flight mode, the supervisor is capable of sending command for transition to horizontal flight mode. In such a case, low-level controllers (C_1, C_2, \dots, C_q) that are responsible for transition mode is switched to the system (see Fig. 4.3). The transition of wings from vertical to horizontal position is performed by servos. There are two servos

commissioned for this operation: one of which is for front wings, the other one is for rear wings. Besides low-level controllers for attitude stabilization, there are 2 additional low-level controllers for servo control.

The transition from vertical to horizontal flight mode is performed by changing the angle of attacks of the front and rear wings in a synchronized way. As seen in Fig. 4.4, altitude control input is the sum of thrust force (F_i) and aerodynamic lift force (F_L). The velocity of the aerial vehicle caused by the change in wing angles and the thrusts produced by motors provide a stable horizontal flight. When aerial vehicle is in transition mode, the thrust forces in vertical axis ($F_i \sin(\theta)$) decrease. High-level controller determines the amount of current that motors require to prevent vehicle from losing altitude. As can be seen, not only servo control but also altitude control have to be in charge in transition mode. All these switching issues and control of low-level controllers are operated by high-level controller. When

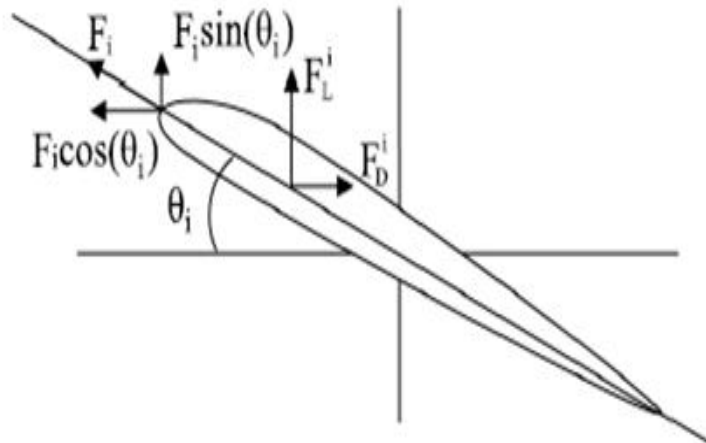


Figure 4.4: Forces appears on the wing in transition mode

aerial vehicle finalizes the transition and is in horizontal flight mode, the

high-level controller switch the low-level controllers (C_1, C_2, \dots, C_r) that are responsible for horizontal flight to the system at this time. Similar to vertical flight modes, these low-level controllers are responsible for attitudes and their velocities. The decision about the amount of current for motors is carried out by high-level controller since this amount decreases due to effect of lift forces generated by wings. Moreover, high-level controller is also responsible for the communication of aerial vehicle with ground station during horizontal flight. When mission is completed, the back transition to vertical mode is ordered from high-level controller and then vehicle slowly lands.

For the sensor-actuator integration of SUAVI, four Atmega16 microcontrollers form the low-level controllers. Atmega16 has analog-digital conversion and real-time data processing capabilities. An important reason for the choice of this chip has been that it facilitates coding of complex mathematical operations through the C language. These microcontrollers are utilized to handle high-frequency periodic tasks such as obtaining attitude data from IMU and generating actuator signals for following position reference, and obtaining aperiodic data from other sensors to be used in the control.

The key point in controlling such an aerial vehicle is to obtain reliable orientation and altitude measurements. However, the signals coming from sensors are not so reliable at all. Some of them are highly noisy, some of them indicates undesired drifts. Therefore, analog and digital filters are used to obtain reliable measurements.

4.1.2 Averaging Filters

Maxbotix Ultrasonic Range Finder is utilized for altitude control of the aerial vehicle. EZ4 model of this sensor (see Appendix A for details) which

provides very accurate readings of 0 to 255 inches (0 to 6.45m) in 1 inch increments is preferred due to dependable measurement performance when compared to others. EZ4 which provides narrower beam angles are not affected by motor blows and obstacles on the ground. The sensor is directly connected to ADC channel of microcontroller since the measurement is analog voltage proportional to altitude. Therefore, there is no need for a communication protocol.

In flight experiments, sensor measurements are observed to be very noisy due to motor vibrations and air flows. This kind of noisy output of sensor is not a reliable altitude measurement for altitude control of such an aerial vehicle. Therefore, Exponentially Weighted Moving Average (EWMA) filter is implemented as a digital filter in the microprocessor, namely

$$S_t = \beta Y_t + (1 - \beta)S_{t-1} \quad (37)$$

Here, β is a weight parameter ($0 \leq \beta \leq 1$). S_t and Y_t refers to the filtered and raw sonar measurements at time t , respectively. The filtered sonar measurement S_t is a weighted average of the new sonar measurement (Y_t) and the filtered sonar measurement (S_{t-1}) obtained at time $(t - 1)$.

As seen in Fig. 4.5, the sensor measurement sometimes results in jumps and oscillates in high frequency. The filter increases the weighting $(1 - \beta)$ of previously filtered value when the difference between two consecutive sonar measurements is large and gives much more importance to previous filtered data while still not discarding new measurement entirely. When the difference is not large, the weight of new measurement (β) is increased. If the difference between two consecutive sonar measurements is denoted by ΔY

(i.e. $\Delta Y = Y_t - Y_{t-1}$), then the following formula is used for the adaptive calculation of β :

$$\beta = \frac{|\Delta Y|}{|\Delta Y|^{\delta_1} + (|\Delta Y|^{\delta_2} + \epsilon)^{-1}} \quad (38)$$

where δ_1 , δ_2 and ϵ are selected as $\delta_1 = 1.4$, $\delta_2 = 0.2$ and $\epsilon = 0.1$. This selection implies a maximum for β which is $\beta_{max} = 0.5814$. By utilizing this filter, sonar data becomes smooth enough to be used in altitude control (see Fig. 4.5).

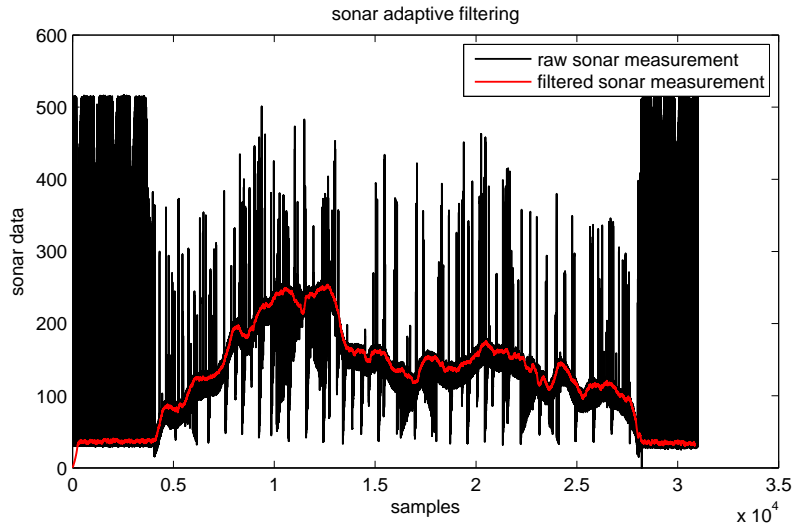


Figure 4.5: The filtered and raw sonar measurements in real flight experiment

4.1.3 Kalman Filtering

The key point in controlling an aerial vehicle is to obtain reliable orientation measurements. To take reliable inertial measurements, Sparkfun 6-DOF IMU (see Appendix A for details) is used, which is a compact electronic circuit containing 3-axis gyro, 3-axis accelerometer, 3-axis magnetometer and a high-performance microcomputer. One should note that, using only gyro

integrations to obtain angular position estimation would cause a significant gyro drift. In the literature, there are several methods that rely on using accelerometers as three-axis gravity sensors [69], [70], [71].

One method to eliminate the drift in gyro measurements is to apply Kalman filter [72]. The assumption that gives rise to implementation of a Kalman filter is negligible coupling between roll and pitch dynamics when vehicle is hovering. Since model of the aerial vehicle is nonlinear, extended Kalman filtering (EKF) is utilized for orientation estimation. In EKF, the state transition and observation models need not to be linear functions of the state but may instead be nonlinear functions of state and inputs. Therefore, the following non-linear dynamic model is used as a system model for the design of the filter.

$$x_k = f(x_{k-1}, u_{k-1}) + \eta_{k-1} \quad (39)$$

$$z_k = h(x_k) + \nu_k \quad (40)$$

Here, η_k and ν_k are process and measurement noises respectively. Let Q and R denote process and measurement covariance matrices, respectively.

In light of Eqn. (7), it follows that

$$\dot{\alpha}_w = \Omega_w = E^{-1}(\phi, \theta) \cdot \Omega_b \quad (41)$$

or,

$$\begin{bmatrix} \dot{\phi} \\ \dot{\theta} \\ \dot{\psi} \end{bmatrix} = \begin{bmatrix} 1 & s_\phi t_\theta & c_\phi t_\theta \\ 0 & c_\phi & -s_\phi \\ 0 & s_\phi/c_\theta & c_\phi/c_\theta \end{bmatrix} \begin{bmatrix} p \\ q \\ r \end{bmatrix} \quad (42)$$

Discretizing Eqn. (42) using approximate derivative, we obtain

$$\alpha_{w_k} = \alpha_{w_{k-1}} + TE^{-1}(\alpha_{w_{k-1}})\Omega_{b_{k-1}} \quad (43)$$

State evolution will then be governed by

$$x_k = \begin{bmatrix} \alpha_w \\ b_g \end{bmatrix}_k = \begin{bmatrix} \alpha_{w_{k-1}} + TE^{-1}(\alpha_{w_{k-1}})\Omega_{b_{k-1}} \\ b_{g_{k-1}} + v_{g_{k-1}} \end{bmatrix} \quad (44)$$

where $b_g \in \mathbb{R}^3$ denotes the bias in gyros and T refers to the sampling time. Kalman filter corrects bias term at each cycle by comparing the estimation of angle with the measurements coming from the accelerometers. The filter has two steps: prediction and correction. The prediction part is given as

$$\hat{x}_{k|k-1} = f(\hat{x}_{k-1|k-1}, u_{k-1}) \quad (45)$$

Four celebrated equations of the Kalman Filter are:

$$P_{k|k-1} = A_{k-1}P_{k-1|k-1}A_{k-1}^T + Q_{k-1} \quad (46)$$

$$K_k = P_{k|k-1}H_k^T(H_kP_{k|k-1}H_k^T + R_k)^{-1} \quad (47)$$

$$\hat{x}_{k|k} = \hat{x}_{k|k-1} + K_k(z_k - h(\hat{x}_{k|k-1})) \quad (48)$$

$$P_{k|k} = (I - K_kH_k)P_{k|k-1} \quad (49)$$

where A and H matrices are defined as

$$A_{k-1} = \frac{\partial f}{\partial x} \Big|_{\hat{x}_{k-1|k-1}, u_{k-1}} \quad (50)$$

$$H_k = \frac{\partial h}{\partial x} \Big|_{\hat{x}_{k|k-1}} \quad (51)$$

$P_{k|k-1}$ in Eqn. (46) is known as a-priori error covariance matrix and is used in Eqn. (47) to compute Kalman gain (K_k). The optimal state vector $\hat{x}_{k|k}$ is calculated as the sum of predicted state vector $\hat{x}_{k|k-1}$ and the correction term $K_k(z_k - h(\hat{x}_{k|k-1}))$ which is computed by measurements coming from the accelerometers and the compass. $P_{k|k}$ in Eqn. (49) refers to posterior error covariance matrix and is used to update $P_{k|k-1}$ in Eqn. (46). Note that the filter needs initial conditions of \hat{x}_0 and $P_{0|0}$.

The elements of Q and R matrices in Kalman filter can be tuned experimentally. This may enhance the performance of the filter.

$$Q = \begin{bmatrix} 0.0001 & 0 \\ 0 & 0.000001 \end{bmatrix}, \quad R = \begin{bmatrix} 0.2 & 0 \\ 0 & 0.2 \end{bmatrix} \quad (52)$$

EKF is implemented in the onboard microprocessors of the vehicle. The correct estimation of the roll and pitch angles are achieved and the drifts are eliminated.

Accelerometer measurements which are filtered by a low pass filter in order to get rid of high frequency noise and angular velocities coming from gyros are fused in EKF. The drift in the integral of gyro reading is eliminated as seen in Fig. 4.6 and 4.7. Note that the results are not affected by the vibrations resulted from motors.

4.1.4 Altitude and Attitude Control Using PID

Once reliable orientation measurements are obtained, reference values for (ϕ) and (θ) calculated by high-level controller can be used in the design of the

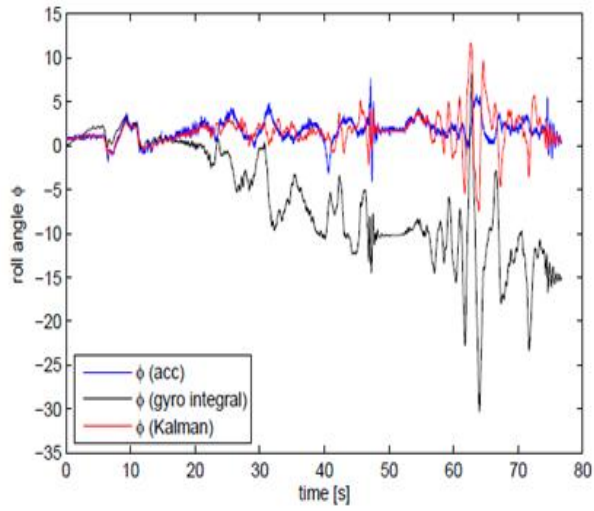


Figure 4.6: Estimation of roll angle with Kalman filter in flight experiment

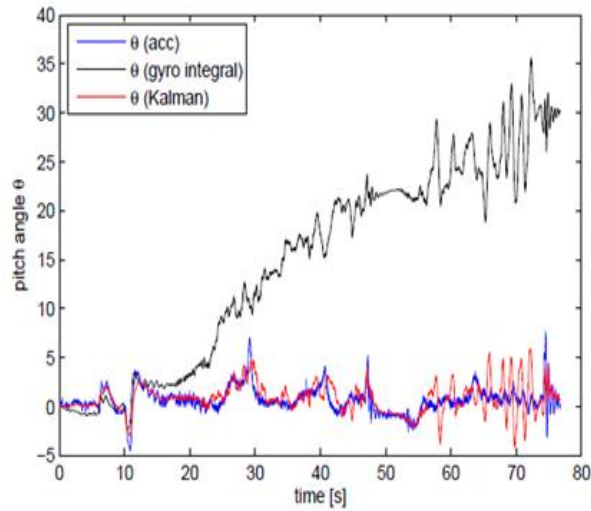


Figure 4.7: Estimation of pitch angle with Kalman filter in flight experiment

orientation controllers in this section. For this purpose, let's recall that the quadrotor's altitude (Z) and attitude (ϕ , θ and ψ) dynamics expressed in the world frame can be given by the following equations:

$$\begin{aligned}
\ddot{Z} &= -(c_\theta c_\phi) \frac{u_1}{m} + g \\
\ddot{\phi} &= \frac{u_2}{I_{xx}} + \frac{I_{yy} - I_{zz}}{I_{xx}} qr - \frac{J_{prop}}{I_{xx}} q \omega_p \\
\ddot{\theta} &= \frac{u_3}{I_{yy}} + \frac{I_{zz} - I_{xx}}{I_{yy}} pr + \frac{J_{prop}}{I_{yy}} p \omega_p \\
\ddot{\psi} &= \frac{u_4}{I_{zz}} + \frac{I_{xx} - I_{yy}}{I_{zz}} pq + \frac{J_{prop}}{I_{zz}} r \omega_p
\end{aligned} \tag{53}$$

Total propeller speed ω_p is defined by the formula

$$\omega_p = \omega_1 - \omega_2 - \omega_3 + \omega_4$$

For controller design, altitude and attitude dynamics can be linearized around hover conditions, i.e. $\phi \approx 0$, $\theta \approx 0$ and $\psi \approx 0$, where angular accelerations in body and world frames can be assumed to be approximately equal, i.e. $\dot{p} \approx \ddot{\phi}$, $\dot{q} \approx \ddot{\theta}$, $\dot{r} \approx \ddot{\psi}$. Resulting linearized altitude and attitude dynamics can be expressed in world frame as

$$\begin{aligned}
\ddot{Z} &= -(c_\theta c_\phi) \frac{u_1}{m} + g \\
\ddot{\phi} &= \frac{u_2}{I_{xx}} \\
\ddot{\theta} &= \frac{u_3}{I_{yy}} \\
\ddot{\psi} &= \frac{u_4}{I_{zz}}
\end{aligned} \tag{54}$$

Altitude and attitude controllers are then designed by the following expressions:

$$\begin{aligned}
u_1 &= K_{p,z}e_z + K_{d,z}\dot{e}_z + K_{i,z} \int e_z - \frac{mg}{c_\theta c_\phi} \\
u_2 &= K_{p,\phi}e_\phi + K_{d,\phi}\dot{e}_\phi + K_{i,\phi} \int e_\phi \\
u_3 &= K_{p,\theta}e_\theta + K_{d,\theta}\dot{e}_\theta + K_{i,\theta} \int e_\theta \\
u_4 &= K_{p,\psi}e_\psi + K_{d,\psi}\dot{e}_\psi + K_{i,\psi} \int e_\psi
\end{aligned} \tag{55}$$

where $e_q = q^d - q$ for $q = Z, \phi, \theta, \psi$. Note that the altitude controller given by the first equation in (55) is a gravity compensated PID controller. Similarly, other three orientation controllers are also PID controllers. In these controllers $K_{p,q} > 0$, $K_{d,q} > 0$ and $K_{i,q} > 0$ are proportional, derivative and integral control gains, respectively.

4.2 Disturbance Observer

In this section, a disturbance observer [73], which is frequently used in motion control systems, is designed to estimate the total disturbance acting on the system. In addition to the external disturbances, nonlinear terms and parametric uncertainties are also included in the total disturbance.

Note that the inertia matrix of the aerial vehicle can be written as,

$$M = M_{nom} + \tilde{M}$$

Here, M_{nom} refers to the nominal inertia matrix which is a diagonal matrix defined as $M_{nom} = \text{diag}(m, m, m, I_{xx}, I_{yy}, I_{zz})$ in terms of nominal system

parameters and (\tilde{M}) is the difference between actual and nominal inertia matrices.

Eqn. (36) can be rewritten in terms of the nominal inertia matrix as

$$M_{nom}\dot{\zeta} = f + \tau_{dist} \quad (56)$$

where f and τ_{dist} are the actuator input and the total disturbance, respectively, and are defined as

$$f = E(\xi)\omega^2$$

$$\tau_{dist} = -\tilde{M}\dot{\zeta} - C(\zeta)\zeta + G + O(\zeta)\Omega + W(\zeta) + D(\zeta, \xi) \quad (57)$$

Note that τ_{dist} contains, in addition to the external disturbances like wind and gust, the nonlinear terms and the parametric uncertainties in the dynamics.

Note that Equation (56) implies 6 first order differential equations of the form

$$M_{nom_i}\dot{\zeta}_i = f_i + \tau_{dist_i}, \quad i = 1, \dots, 6 \quad (58)$$

Taking the Laplace transform and solving for τ_{dist_i} imply

$$M_{nom_i}s\zeta_i(s) = f_i(s) + \tau_{dist_i}(s) \quad (59)$$

and

$$\tau_{dist_i}(s) = M_{nom_i}s\zeta_i(s) - f_i(s) \quad (60)$$

Right hand side of Eqn. (60) can not be realized in practice since due to the $s\zeta_i(s)$ term future values of ζ are needed. However, both sides of the

equation can be multiplied by $G(s) = \frac{g}{s+g}$ (transfer function of a low-pass filter) to obtain

$$G(s)\tau_{dist_i}(s) = M_{nom_i}sG(s)\zeta_i(s) - G(s)f_i(s) \quad (61)$$

Note that, $sG(s)$ can be written as

$$sG(s) = s\frac{g}{s+g} = g\left(1 - \frac{g}{s+g}\right) = g(1 - G(s)) \quad (62)$$

Let's denote the term $G(s)\tau_{dist_i}(s)$ by $\hat{\tau}_{dist_i}(s)$ (estimated disturbance). Thus,

$$\hat{\tau}_{dist_i}(s) = -G(s)f_i(s) - gM_{nom}G(s)\zeta_i(s) + gM_{nom}\zeta_i(s) \quad (63)$$

which is now in a realizable form. Let's subtract the estimated disturbance from the input term in Eqn. (59), i.e. $f_i \leftarrow f_i - \hat{\tau}_{dist_i}$. We thus obtain

$$M_{nom_i}s\zeta_i(s) = f_i(s) + (1 - G(s))\tau_{dist_i}(s) \quad (64)$$

In Eqn. (64), if $G(s) \approx 1$, then the total disturbance on the system is eliminated in the low frequency range and the input-output relation of the system becomes a linear model defined in terms of nominal parameters. Consequently, the full dynamics of the aerial vehicle given in Eqn. (36) is reduced to the following linear dynamics:

$$M_{nom_i}\dot{\zeta}_i = f_i \quad (65)$$

In order to estimate the total disturbance given in Eqn. (57), a closed-loop disturbance observer is implemented using Eqn. (63). The block diagram of

the implemented disturbance observer is depicted in Fig. 4.8.

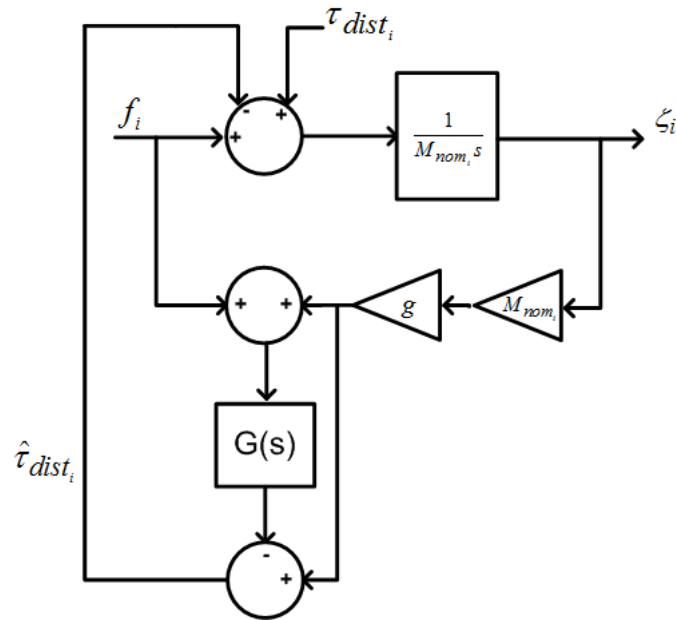


Figure 4.8: Block diagram of the closed loop disturbance observer

4.3 GPS Module

Global Positioning System (GPS) provides reliable location and time information in all weather and at all times and anywhere on or near the Earth when and where there is an unobstructed line of sight to four or more GPS satellites. GPS consists of three parts: the space segment, the control segment, and the user segment [74].

- **The space segment** consists of a nominal constellation of 24 to 32 operating satellites that transmit one-way signals. The current GPS satellite position and time are extracted from these signals.
- **The control segment** consists of worldwide monitor and control stations that maintain the satellites in their proper orbits through occa-

sional command maneuvers, and adjust the satellite clocks. It tracks the GPS satellites, uploads updated navigational data, and maintains health and status of the satellite constellation.

- **The user segment** consists of the GPS receiver equipment. GPS satellites broadcast signals from space, which each GPS receiver uses to calculate its three-dimensional location (latitude, longitude, and altitude) plus the current time.

GPS satellites provide service to civilian and military users. GPS has become a widely used and a useful tool for commerce, scientific uses, tracking and surveillance. Accurate timing of GPS facilitates everyday activities such as banking, mobile phone operations, and even the control of power grids. The outstanding positioning performance of GPS over many years has earned the confidence of users worldwide. It has proven its dependability throughout the world.

The electronic circuit component that provides position information in horizontal plane (X and Y) during outdoor flight experiments of the aerial vehicle SUAVI is GPS. 50 Channel D2523T Helical GPS Receiver (see Appendix A for details) is chosen as a positioning sensor of SUAVI. It has a 4 Hz position update rate which is a significant feature for waypoint navigation of aerial vehicles. This antenna is popular among UAV designers since it has a property of natural rejection of other radio frequencies such as those originating from the modem or video system. Moreover, its improved rejection of signals reflected from the ground is another reason for interest. The manufacturer company recommends this antenna and features it in their reference design. Frequency and polarization are not dependent upon ground plane geometry so this antenna is sold only in the true GPS frequency of 1575Mhz. Possibly the most important aspect of this antenna is its natural RFI filtering.

4.3.1 Data Acquisition with GPS

The GPS receiver of SUAVI, D2523T Helical GPS, provides position information in 1-2 m resolution depending on the whether conditions and the number of satellites is connected. This amount of resolution is enough for the aerial vehicle to accomplish the desired hovering or waypoint navigation tasks.

In Fig. 4.9, user interface program that is used for reading GPS position data is seen. By the help of this program, important data for position control of an aerial vehicle such as the latitude, longitude, altitude and flight speed are obtained both in numeric and visual form. These data are then used to find the position information in horizontal (X, Y) and vertical (Z) planes according to the point that is determined as reference in real time.

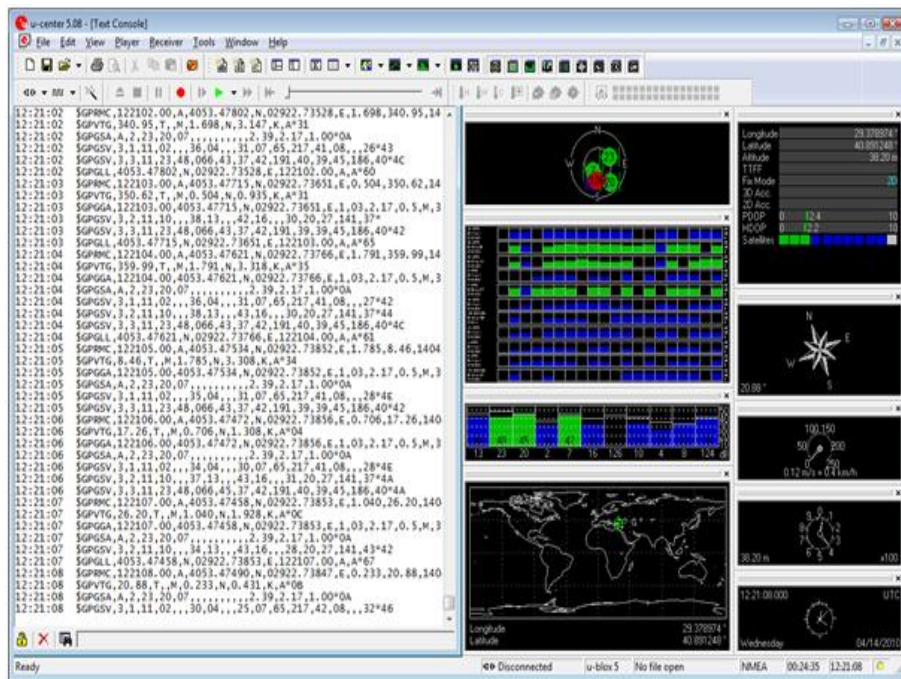


Figure 4.9: User interface program that provides GPS position data

The results of the experiments to test the resolution of GPS receiver are given in Fig. 4.10. In this graph, position data provided by GPS receiver that is hold on a stationary point about 10 minutes as if an aerial vehicle is hovering around a point. When the result of experiment is analyzed by taking the cloudy weather condition into consideration, it is verified that the departure from starting point does not exceed 1-2 meters.

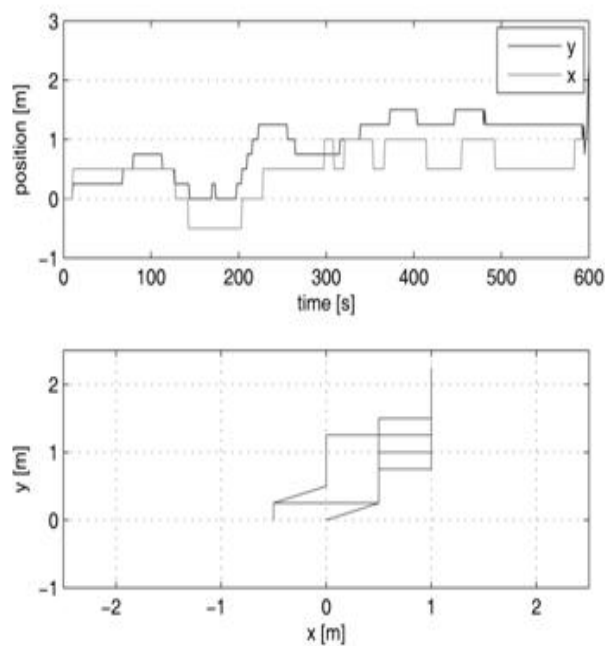


Figure 4.10: The data taken from GPS receiver hold on a stationary point

Another experiment to test the GPS receiver is arranged as if the aerial vehicle is in waypoint navigation task. GPS receiver is taken from starting position to reference position by passing through predetermined waypoints and turned back by using the same way. As seen in Fig. 4.11, the performance of GPS receiver in terms of position data and resolution is quite satisfactory.

In order to visualize the position information taken from GPS receiver,

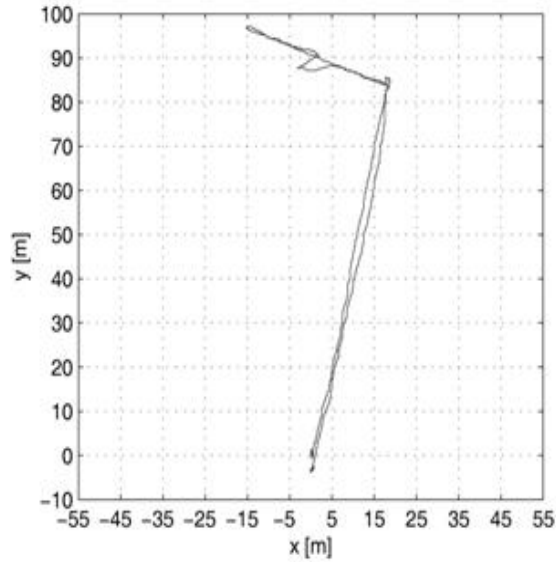


Figure 4.11: GPS position data in waypoint navigation

Google Earth program is utilized. In Fig. 4.12, the results of the experiment that GPS receiver takes a tour around Sabanci University. The position data coming from GPS is processed in real time, and the location of the receiver is seen in ground station visually.

4.4 GPS Based Position Control Laws

GPS based position control laws of a quad tilt-wing UAV for hovering and waypoint navigation is developed following the work presented in [29].

Robust Hovering Control

Suppose the aerial vehicle is in the VTOL (Vertical Take-Off and Landing) mode and the reference position and the desired altitude are defined as \mathbf{x}^d , z^d . It is aimed that the vehicle should not lose the reference position until



Figure 4.12: Visualization of GPS receiver position data around Sabanci University

reaching the desired altitude from the take-off position and then stay in the vicinity of the reference position at the desired altitude.

Let \mathbf{x}_n ve \mathbf{y}_n be the unit vectors along the x and y axes of the world frame, respectively. Let $x(t)$ denote instantaneous position of the vehicle provided by GPS and let e_x and e_y denote vehicle's position errors along x and y axes. It follows that

$$e_x = (\mathbf{x}^d - \mathbf{x}(t)) \cdot \mathbf{x}_n \quad (66)$$

$$\dot{e}_x = -\mathbf{v}(t) \cdot \mathbf{x}_n \quad (67)$$

$$e_y = (\mathbf{x}^d - \mathbf{x}(t)) \cdot \mathbf{y}_n \quad (68)$$

$$\dot{e}_y = -\mathbf{v}(t) \cdot \mathbf{y}_n \quad (69)$$

In order to hover the vehicle at a given position, PID controllers are designed along both x and y axes, namely

$$u_x = K_{x,p}e_x + K_{x,d}\dot{e}_x + K_{x,i} \int_0^t e_x dt \quad (70)$$

$$u_y = K_{y,p}e_y + K_{y,d}\dot{e}_y + K_{y,i} \int_0^t e_y dt \quad (71)$$

Note that these controllers are nothing else than the acceleration controllers along x and y axes. Depending on the heading, ψ , of the vehicle, these accelerations must be transformed using a 2D rotation matrix, $R(\psi)$, as follows:

$$a_{xy} = R(\psi)(u_x \cdot \mathbf{x}_n + u_y \cdot \mathbf{y}_n) \quad (72)$$

By using equation (72), reference attitude angles which allows the vehicle to

hover at a given position can easily be computed using the following formulas [75]:

$$\theta_{ref} = -\arcsin\left(\frac{a_x}{\|a\|}\right) \quad (73)$$

$$\phi_{ref} = \arcsin\left(\frac{a_y}{\|a\| \cos(\theta)}\right) \quad (74)$$

where a is the total acceleration of the vehicle, $a = (a_x, a_y, a_z)$, a_x and a_y are the x and y components of the acceleration vector, a_{xy} , defined by Eqn. (72). The third component of the acceleration vector, a_z , is the acceleration of the vehicle along the z axis and is computed as $a_z = u_1/m$. $\|a\|$ is the Euclidean norm of a and is defined as

$$\|a\| = \sqrt{a_x^2 + a_y^2 + a_z^2} \quad (75)$$

Reference attitude angles computed by (73) and (74) can be filtered through a low-pass filter to be used by the attitude controller for the attitude control of the vehicle.

Waypoint Navigation

In order to develop flight controllers for waypoint navigation, a similar approach to hovering is followed. A path, $P \in \mathbb{N} \times \mathbb{R}^3$ is generated by N waypoints \mathbf{x}_i^d . Let the desired flight speeds of the vehicle between two consecutive waypoints i and $i+1$ be v_i^d . For each path segment P_i , the vehicle travels along the subpath vector that combines \mathbf{x}_i^d and \mathbf{x}_{i+1}^d . A unit tangent vector \mathbf{t}_i and a unit normal vector \mathbf{n}_i along and perpendicular to the subpath vector are defined. Let $x(t)$ be the current position of the vehicle measured from GPS. The cross track error e_{ct} and its derivative, and along track error

rate \dot{e}_{at} are defined as

$$e_{ct} = (\mathbf{x}_i^d - \mathbf{x}(t)) \cdot \mathbf{n}_i \quad (76)$$

$$\dot{e}_{ct} = -\mathbf{v}(t) \cdot \mathbf{n}_i \quad (77)$$

$$\dot{e}_{at} = v_i^d - \mathbf{v}(t) \cdot \mathbf{t}_i \quad (78)$$

A PI controller is designed for the along track direction and a PID controller is designed for the cross track direction; i.e.

$$u_{at} = K_{atp}\dot{e}_{at} + K_{ati} \int_0^t \dot{e}_{at} dt \quad (79)$$

$$u_{ct} = K_{ctp}e_{ct} + K_{ctd}\dot{e}_{ct} + K_{cti} \int_0^t e_{ct} dt \quad (80)$$

Desired acceleration vector in XY plane of the vehicle is constructed from the controller outputs (79) and (80) as,

$$a_{xy} = R(\psi)(u_{ct} \cdot \mathbf{n} + u_{at} \cdot \mathbf{t}) \quad (81)$$

where $R(\psi)$ is a 2D rotation matrix which performs the necessary transformation of the acceleration using the heading (ψ) of the vehicle.

By using Eqn. (73) and Eqn. (74) given in hovering section, the reference attitude configuration of the vehicle that enables the vehicle to travel in the desired trajectory is obtained from the desired acceleration vector calculated in Eqn. (81).

Proposed position control for hovering and waypoint navigation of the aerial vehicle has been verified with several simulations and experiments presented in Chapter IV.

Chapter IV

5 Simulations and Experiments

In this section, several simulation and experimental results will be presented.

5.1 Simulation Results

A Graphical User Interface (GUI) is developed in Matlab environment. The integration of interface with VRealm Builder Environment of Matlab that enables to visualize the 3D motion of aerial vehicle is also accomplished. These two software programs are run in the computer located at the ground station. Real time flight information such as velocity, altitude, heading etc., all control parameters of the system, measurements of sensors, the video captured by the camera mounted on the aerial vehicle and the instantaneous coordinates of vehicle on the map are monitored and tracked (see Fig. 5.1, 5.2). The satellite map that enables operator to monitor the visual location information of the aerial vehicle depending on the GPS data is also added to interface screen. In other words, operator has a cockpit sight of flight information.

Operator has also capability to maneuver the vehicle. He either chooses the predetermined missions such as reconnaissance, surveillance, line inspection and closed area or defines its own mission by entering the details like

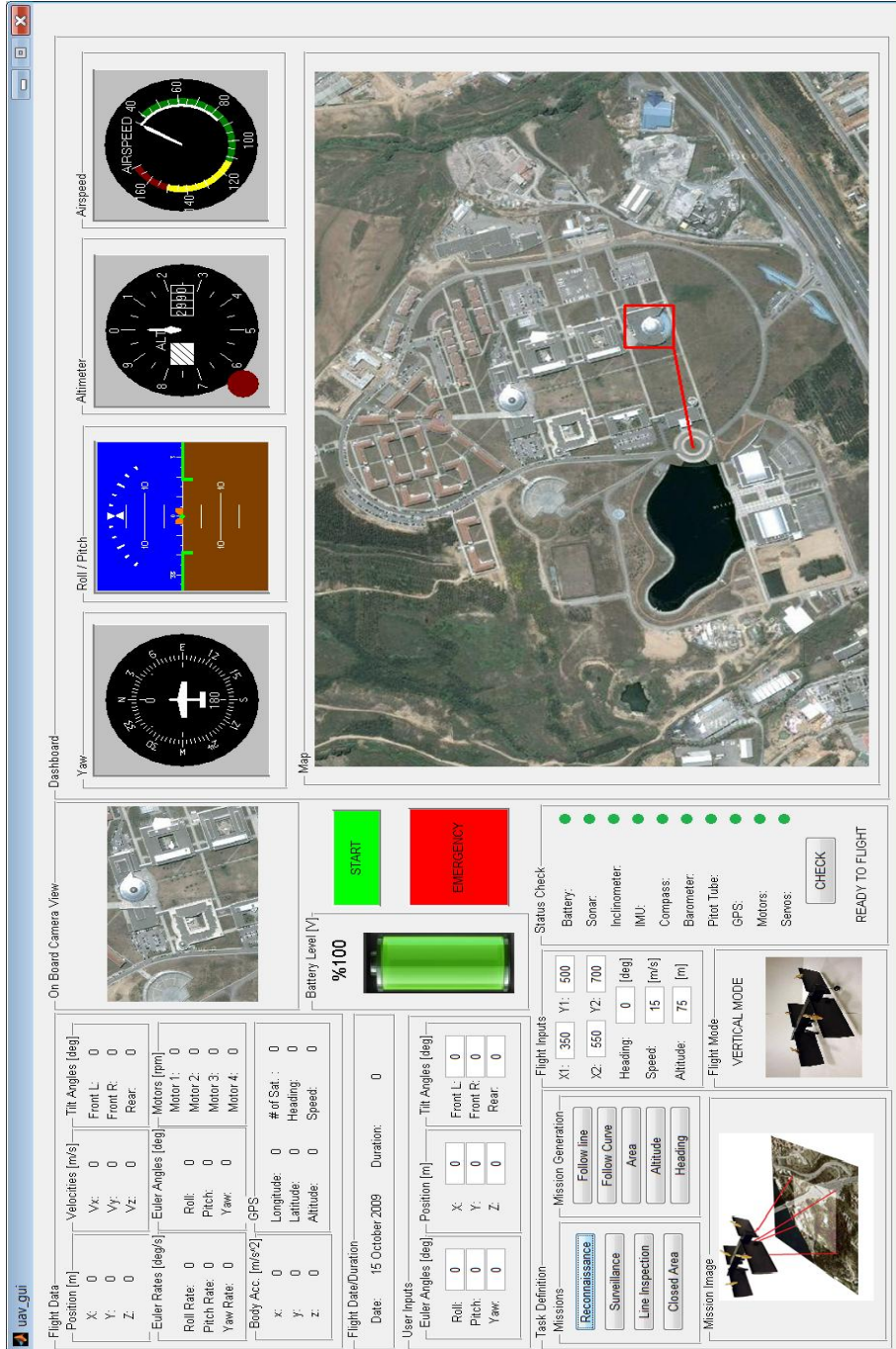


Figure 5.1: Graphical User Interface (Vehicle is ready to flight)

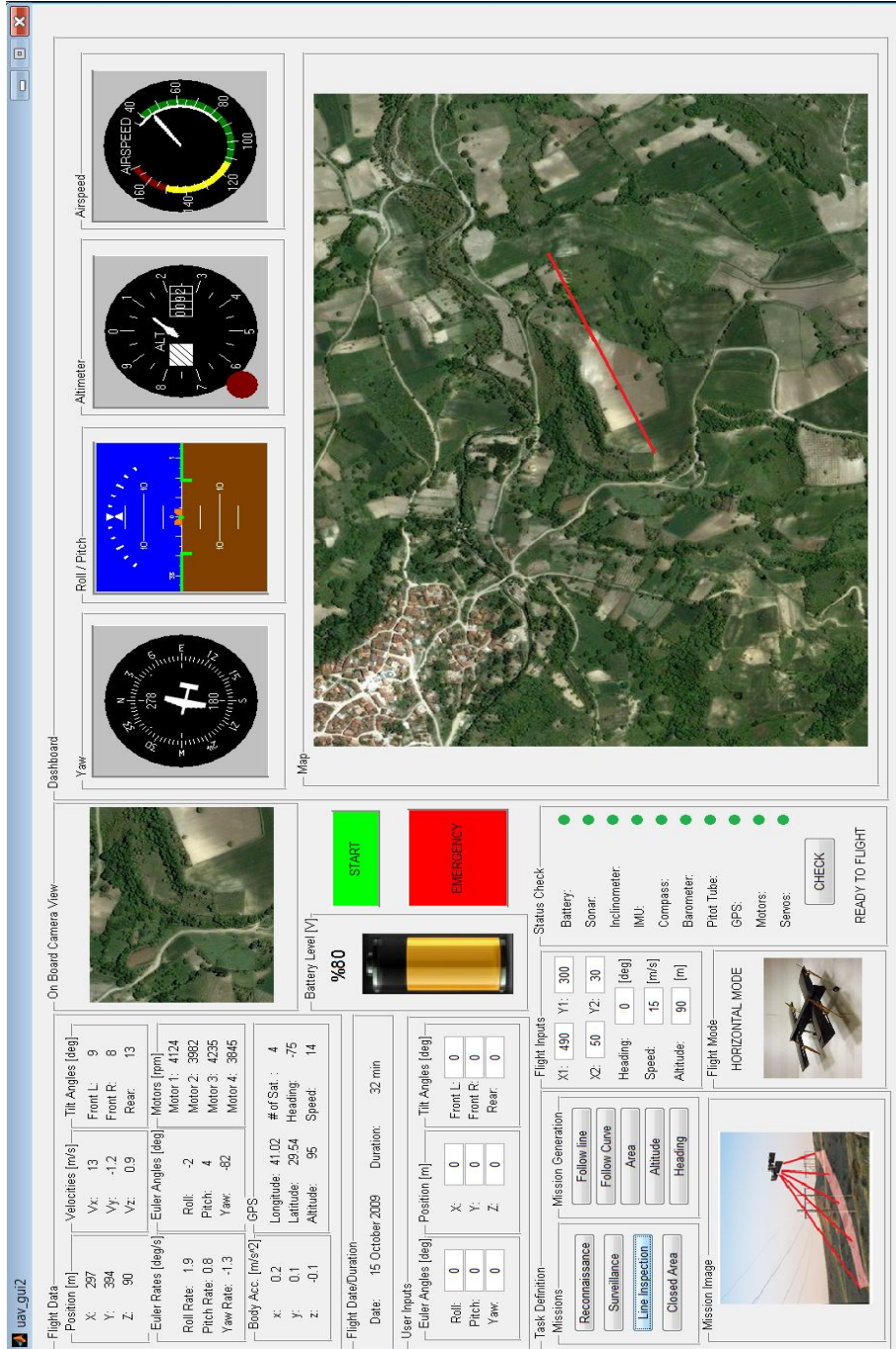


Figure 5.2: Graphical User Interface (Flight)

type of mission, the reference altitude, heading and position. Moreover, it is also possible to send instantaneous commands to aerial vehicle that is performing an autonomous flight.

It is important to be sure about the sensors on the vehicle before flight. An error during flight might lead to catastrophic results. Therefore, a feature that enables operator to complete all the checks before flight is added. When the *check* button is pushed, the voltages of batteries, the measurements of sonar, IMU, compass, barometer, GPS and pitot tubes, servos and motor are controlled. The green buttons on the interface screen indicates that all criteria are satisfied, the vehicle is ready to fly.

When *start* command is sent to the aerial vehicle via user interface, the vertical flight modes are chosen by high-level controller and all low-level controllers responsible for vertical flight are switched to the system. The high-level controller leads the low-level controllers with respect to the mission type during the whole flight. By the help of user interface, operator monitors roll, pitch and yaw angles, position information (X, Y, Z), the velocities and accelerations of vehicle around three axis, the angle of attacks of front and rear wings, the latitude, longitude and attitude measurements taken from GPS, the number of satellites fixed.

Using the CAD drawing of the aerial vehicle a vrmf model is created in VRealm Builder Environment which is integrated with VR Toolbox of Matlab [62]. This visual model is connected to the dynamic model of the aerial vehicle through Simulink and the simulations are visualized in real-time. With the help of this visualization toolbox the vehicle dynamics can easily be observed and the performance evaluations can easily be made. In Fig. 5.3, a building, a hangar, empty land and the 3 dimensional CAD model

of the aerial vehicle are modeled to simulate flight experiments having various scenarios.

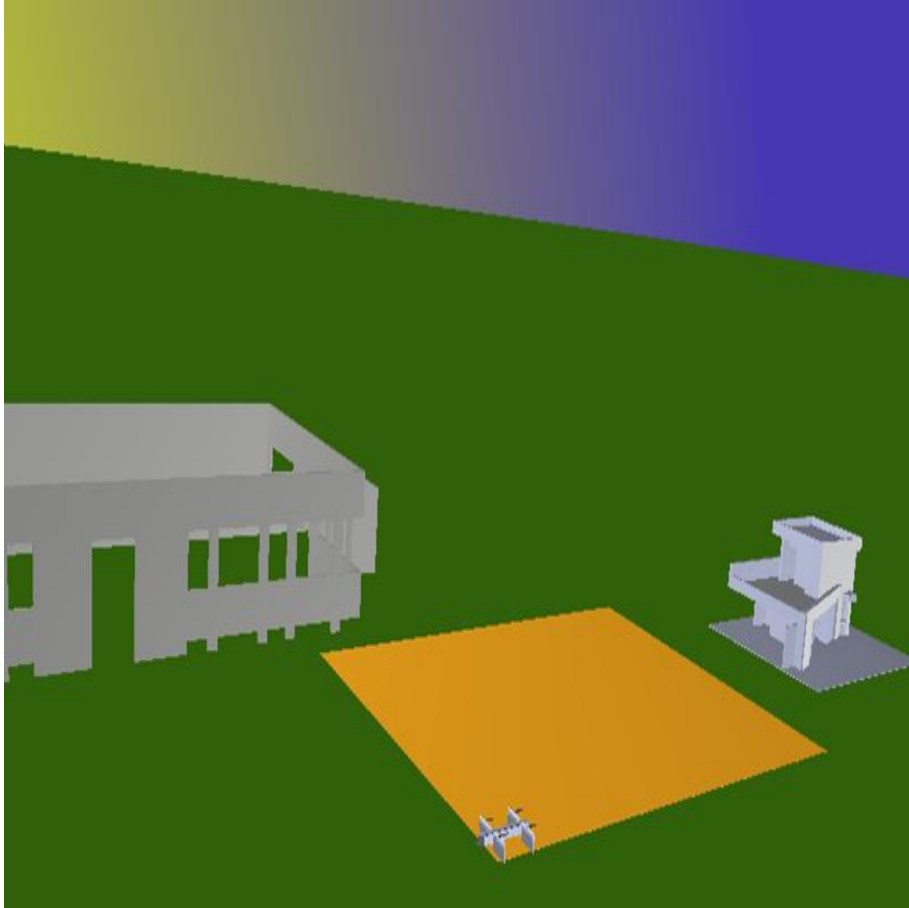


Figure 5.3: Visualization Interface

One of the mission that SUAVI accomplishes is surveillance. A surveillance scenario is simulated in the interfaces and the reference tracking performance of the aerial vehicle is evaluated. The vehicle takes off from the starting position, accomplishes the surveillance mission over the desired area, at the desired altitude and velocity (see Fig. 5.4, 5.5, 5.6). As a result of evaluation of the visual data and simulation results related to surveillance

task, the performance the aerial vehicle is quite satisfactory.

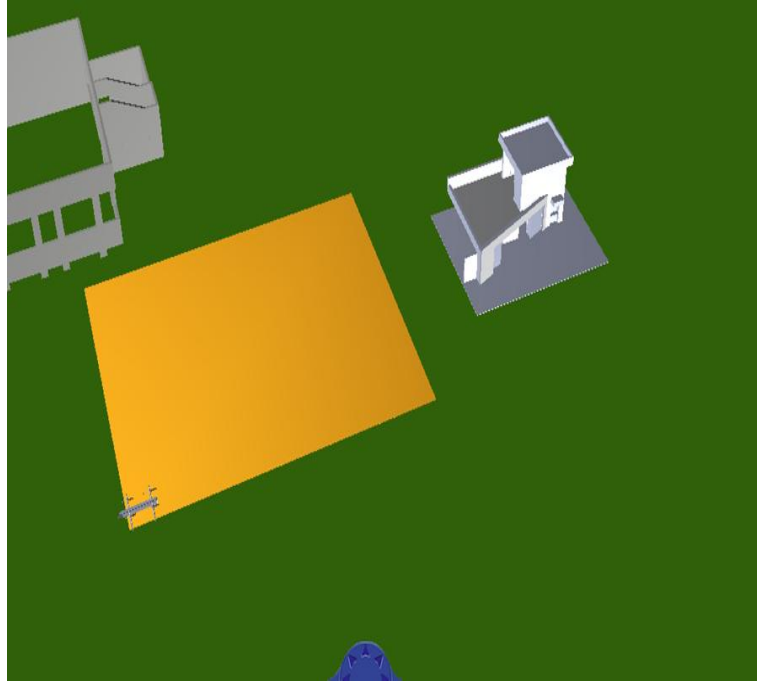


Figure 5.4: Surveillance (vehicle is at the starting position)

As seen in Fig. 5.22, the aerial vehicle tracks the position references (way-points) successfully. The vehicle follows the step trajectory references with small overshoots with a fast response. The variations of attitude parameters are given in Fig. 5.21. Reference values for attitude angles are given as $(0, 0, 0)$ and the attitude controllers of the vehicle achieves this task. The orientation of the vehicle is hold with in ± 20 degree. The control effort of the vehicle is graphed in Fig. 5.9. The figure depicts that forces are within physical limitations ($\simeq 16$ N). The maximum airspeed of the vehicle during this surveillance task is 15 km/h. The variation of the airspeed is given in Fig. 5.10.

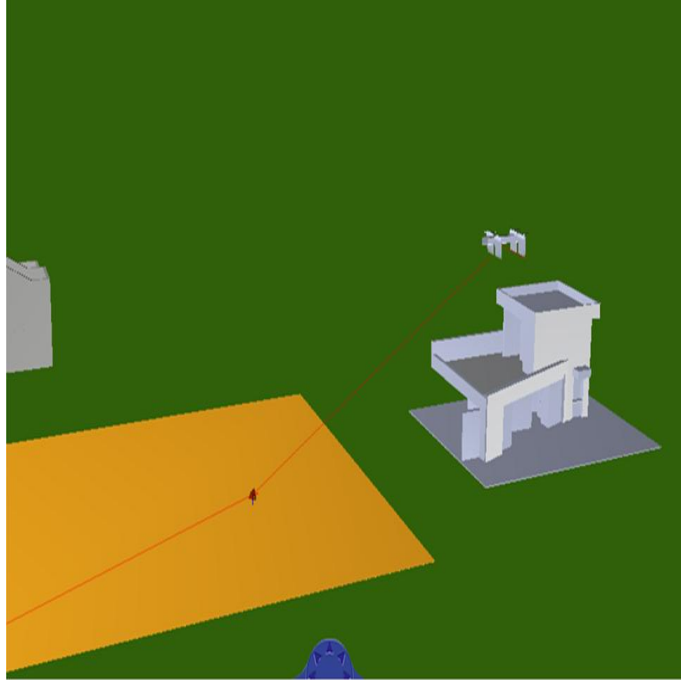


Figure 5.5: Surveillance (vehicle is on the way of desired location)

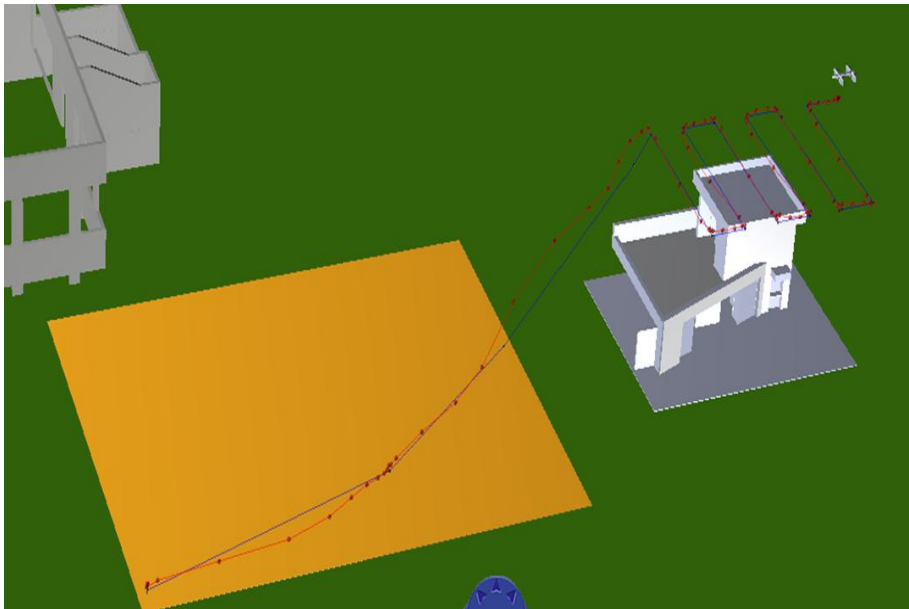


Figure 5.6: The waypoints of the aerial vehicle during surveillance mission (blue: reference, red: vehicle)

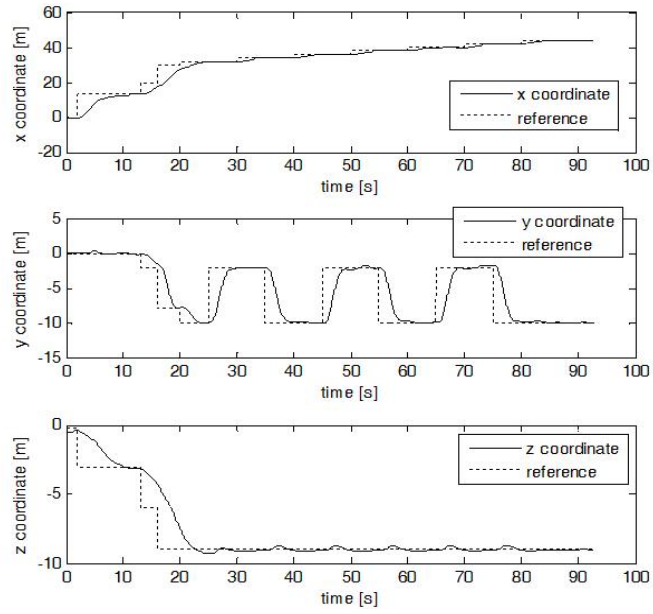


Figure 5.7: Surveillance task: Waypoint navigation performance

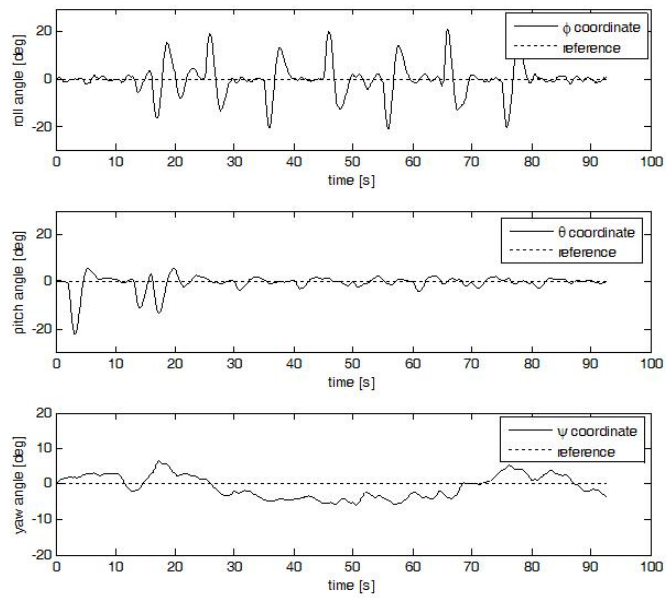


Figure 5.8: Surveillance task: Attitude tracking performance

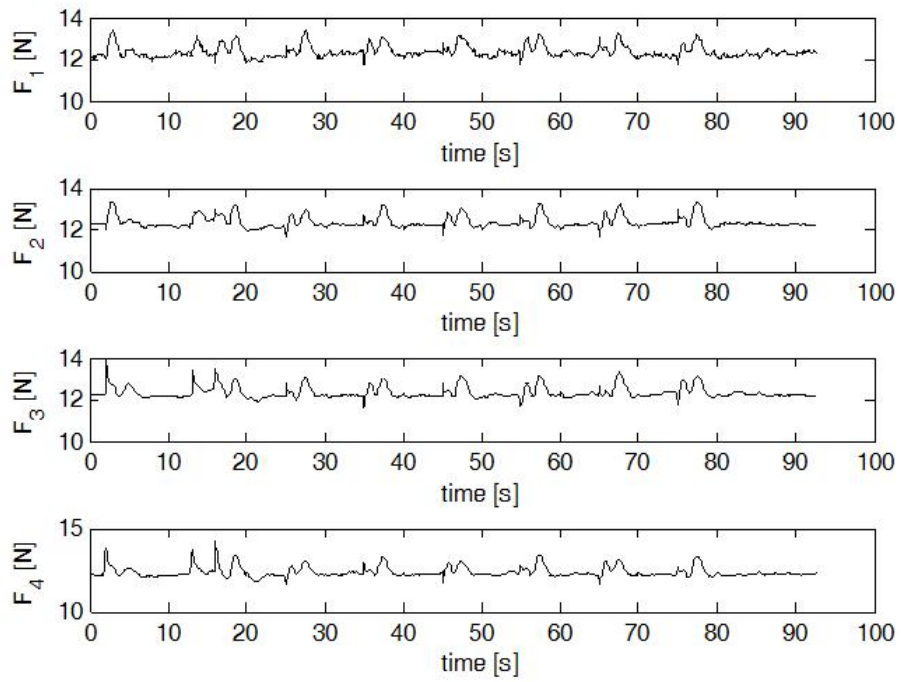


Figure 5.9: Surveillance task: Control efforts

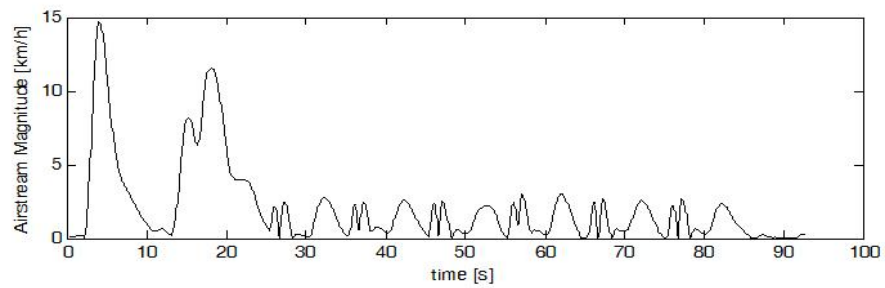


Figure 5.10: Surveillance task: Airstream Magnitude of the vehicle

5.1.1 GPS Based Robust Hover

The performance of the robust hovering control proposed in Chapter 3 is evaluated on the dynamic model of the aerial vehicle introduced in Chapter 2 in MATLAB/Simulink. For robust hovering control, only PID type simple controllers have been employed and their performances have been found very satisfactory.

The implementation parameters are given in Table 5.1.

Table 5.1: Implementation Parameters for Robust Hovering Control

Control	K_p	K_d	K_i
Roll	30	10	0.1
Pitch	30	15	0.1
Yaw	10	4	0.1
Altitude	40	15	0.1
X position	25	40	8
Y position	25	40	8

Figures 5.11 and 5.12 depict the hovering and the attitude tracking performances when a disturbance observer is utilized. The aerial vehicle takes off from the reference position and the hovering controller holds aerial vehicle around the position of take off. Note that position and angle references are tracked with small steady state errors. The position hold performance in x-y plane is within an error of 20 cm radius whereas altitude control error

is less than 10 cm. In addition, the vehicle's attitude angles follow reference attitude values computed by Eqn. (74) and Eqn. (73) very closely with an error not exceeding $\pm 2^\circ$. It is also obvious that during the entire flight, aerial vehicle keeps its heading and follows the reference heading angle, $\psi_{ref} = 0^\circ$, with an error less than 1° . The addition of disturbance rejection further improved the tracking performance. The better performance of the attitude controller in tracking reference values contributes to better results in position hold. The maximum attitude angle that aerial vehicle maneuvers is 5 degree. Thrust forces produced by the motors are seen in Fig. 5.13. The figure depicts that forces are within physical limitations of motors ($\simeq 16$ N). The wind forces generated by the wind model are shown in Fig. 5.14. The effect of wind forces is on the level of 5-6 N. As seen from the graphs, aerial vehicle is able to hover at a given point or in the vicinity of that despite the negative effects of the wind gusts. As can be concluded from the motion of the vehicle in the horizontal plane depicted in Figure 5.15, positioning errors along x and y axes did not exceed 20 cm.

The total disturbance estimated by the disturbance observer is plotted in Figure 5.16. Note that the estimated total disturbance is very similar to the dominating disturbances such as wind gusts acting on the vehicle. Successful estimation of the total disturbance on the system has a dramatic effect on the flight performance since the performance of the designed controllers are directly affected by the aerodynamics effects acting on the vehicle. For example, as can be seen from Figures 5.17 and 5.18 when the disturbance observer is not utilized, wind effects become dominant and position errors along x and y axes are increased a lot and large changes in the attitude of the vehicle are observed. In particular, after 80th sec wind gusts become

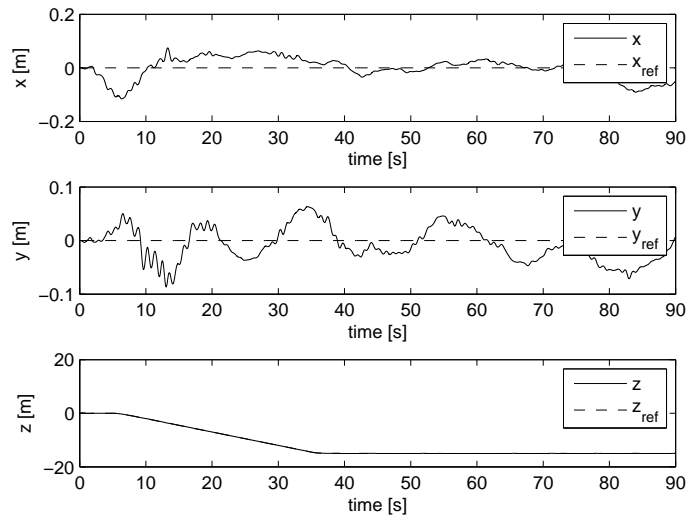


Figure 5.11: Hovering performance with disturbance observer

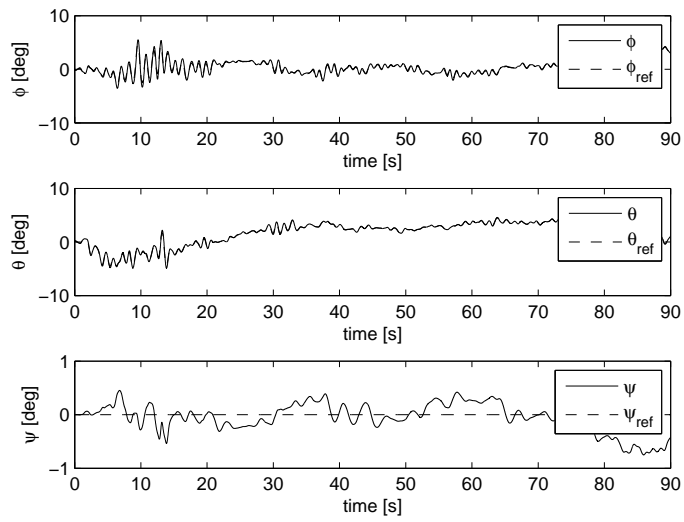


Figure 5.12: Attitude performance with disturbance observer

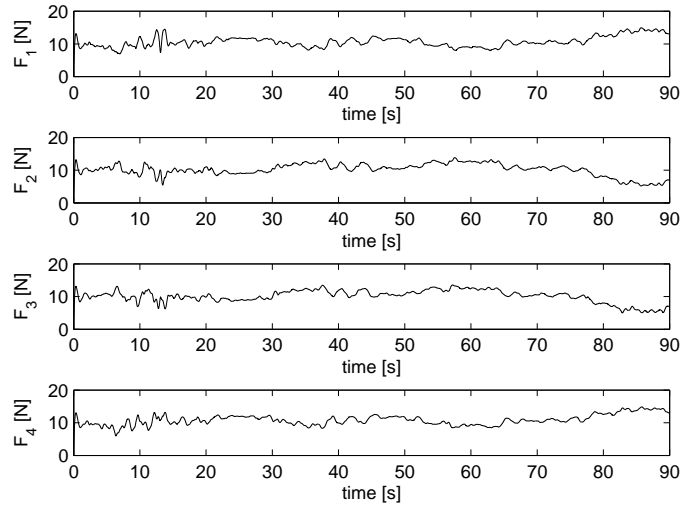


Figure 5.13: Motor thrust forces with disturbance observer

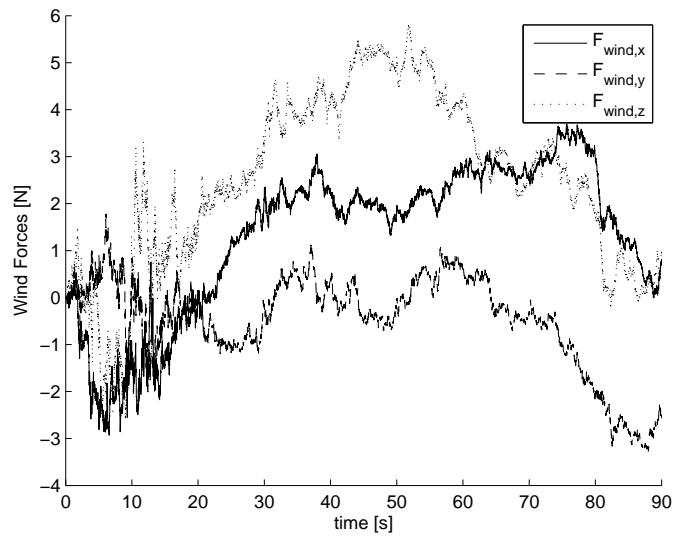


Figure 5.14: Wind forces acting on the vehicle

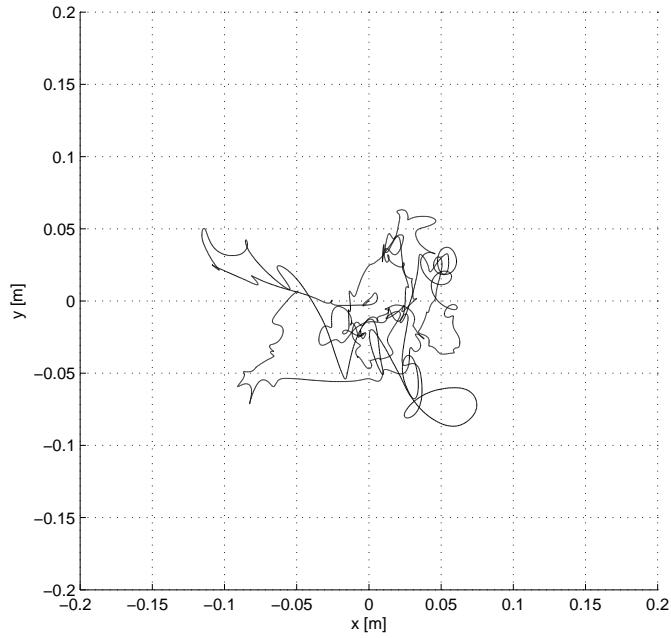


Figure 5.15: Hovering performance with disturbance observer (motion in the horizontal plane)

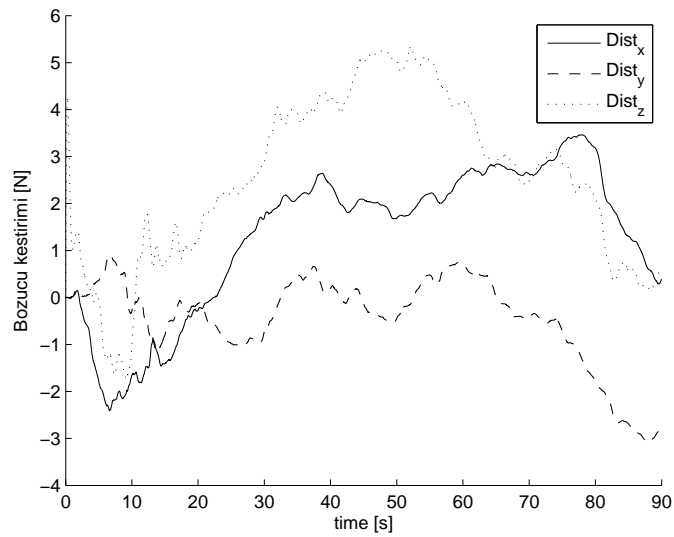


Figure 5.16: Estimated total disturbance acting on the vehicle

quite dominant and dramatically affect stability of the vehicle. Therefore, the vehicle can not hover at a given point or in the vicinity of it. When the motion of the vehicle in the horizontal plane depicted in Figure 5.19 is analyzed it is clear that the vehicle, due to disturbances, can not hover at the given point and moves away.

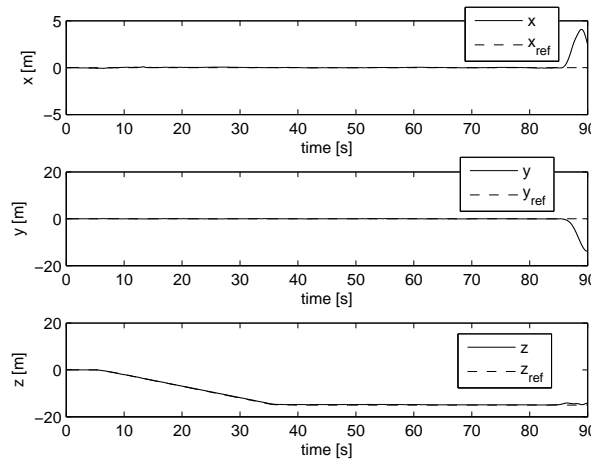


Figure 5.17: Hovering performance without disturbance observer

5.1.2 GPS Based Trajectory Tracking

The performance of the GPS based position control for a tilt-wing quadrotor to track desired trajectories under external wind and aerodynamic disturbances proposed in Chapter 3 is verified in MATLAB/Simulink. Utilization of the disturbance observer implies a linear model with nominal parameters. Since the resulting dynamics are linear, only PID type simple controllers are designed for position and attitude control.

The implementation parameters are given in Table 5.2.

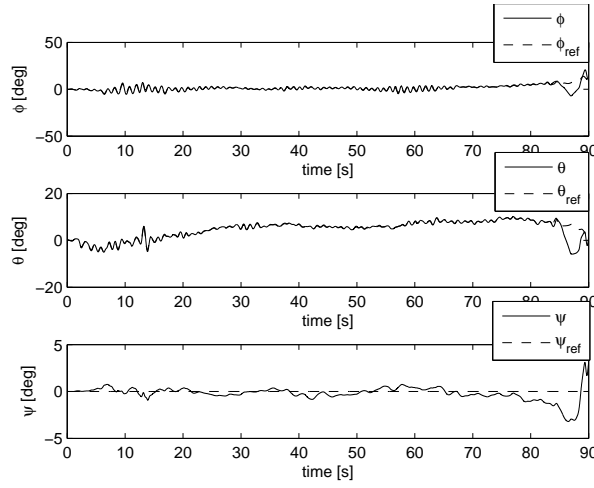


Figure 5.18: Attitude performance without disturbance observer

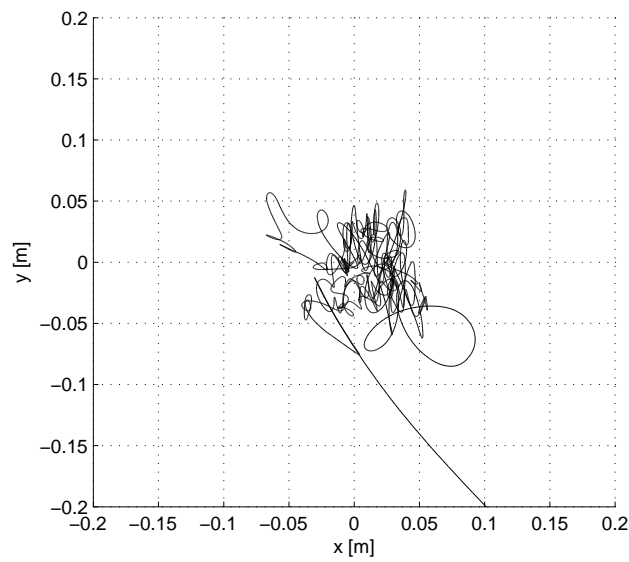


Figure 5.19: Hovering performance without disturbance observer (motion in the horizontal plane)

Table 5.2: Implementation Parameters for Waypoint Navigation

Control	K_p	K_d	K_i
Roll	30	10	0.1
Pitch	30	15	0.1
Yaw	10	4	0.1
Altitude	40	15	0.1
Along track	1	0	0.1
Cross track	25	40	8

Two simulation results will be presented in this section. In the first one, the 3D cartesian reference trajectory is an elliptical helix shown in Figure 5.20 where the actual trajectory followed by the aerial vehicle is also superimposed. Attitude angles and position coordinates are depicted in Figures 5.21 and 5.22 along with references. Note that reference angles and positions are tracked with reasonably small tracking errors. As seen in the figures, aerial vehicle tracks the reference attitude angles (ϕ_{ref} and θ_{ref}), obtained from desired cartesian acceleration vector via Equations (73) and (74), very accurately with an error of less than $\pm 2^\circ$. Moreover, heading of the vehicle is also kept around zero with an error less than $\pm 1^\circ$. To see how the cross track error and the along track speed change over time, they are also plotted (see Figures 5.23 and 5.24). Note that the cross track error at steady state is bounded by 0.5 m. Along track error, on the other hand, somehow oscillates with ± 1.5 m/sec around the reference speed value, which is 4 m/sec. To see if the generated thrusts by the rotors remain within physical limits, which is

16 N, rotor forces are plotted in Figure 5.25. Clearly they are kept within the physical limits. One might wonder what kind of wind forces acted on the system. They are shown in Figure 5.26. The estimation and compensation of the disturbance acting on the aerial vehicle is quite important for trajectory tracking performance. The components of the total disturbance estimated by the disturbance observer are depicted in Figure 5.27. Note that these components are similar to components of the wind and gust forces plotted in Figure 5.26, which are the dominant component of the total disturbance.

In the second simulation, a 2D cartesian trajectory (square) is tracked by the aerial vehicle. Figure 5.28 depicts the result of this simulation. As in the previous simulation, the trajectory tracking performance of the proposed observer based control system is quite satisfactory.

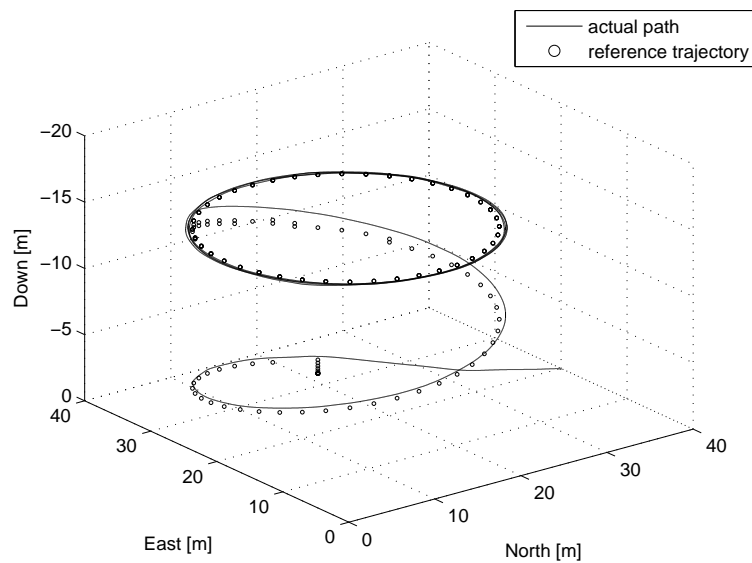


Figure 5.20: Elliptical helix shaped trajectory tracking performance

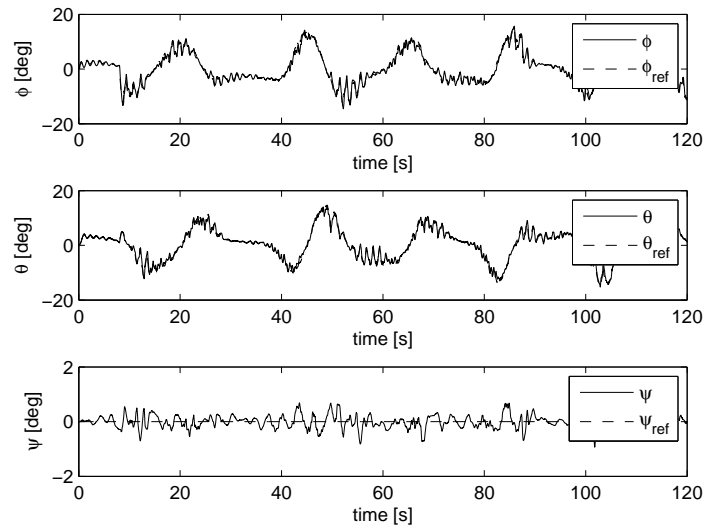


Figure 5.21: Attitude tracking performance

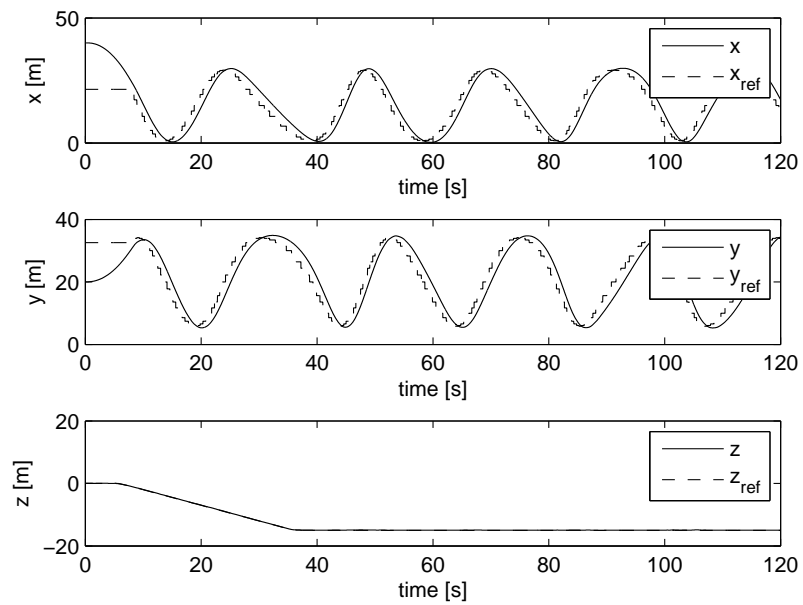


Figure 5.22: Position tracking performance

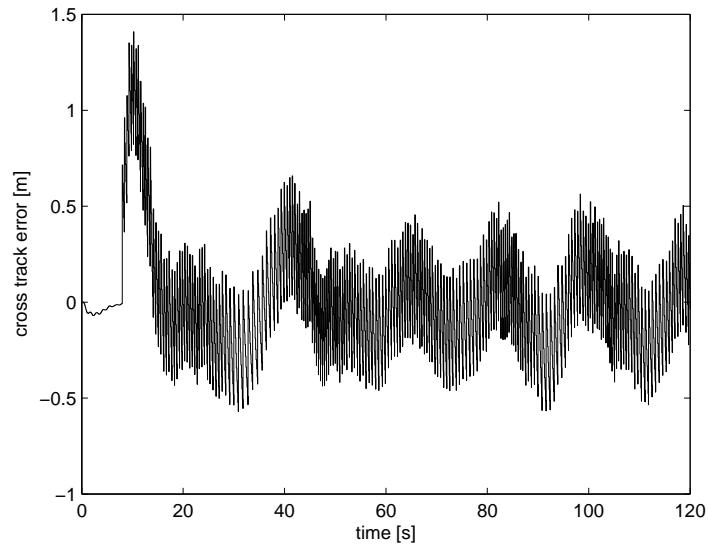


Figure 5.23: Cross track error

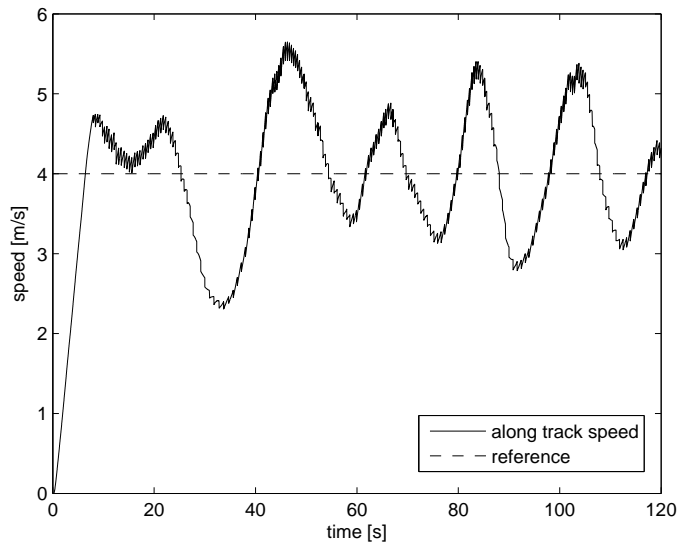


Figure 5.24: Along track speed

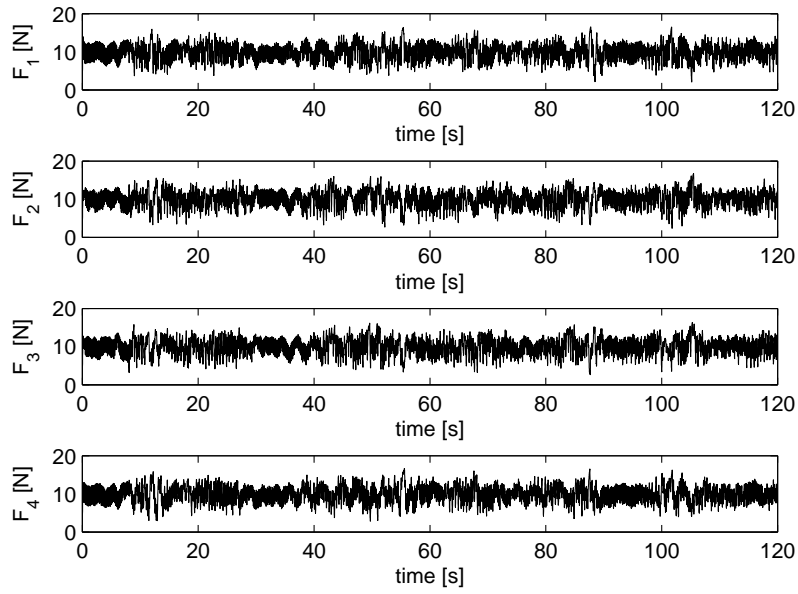


Figure 5.25: Thrust forces created by rotors

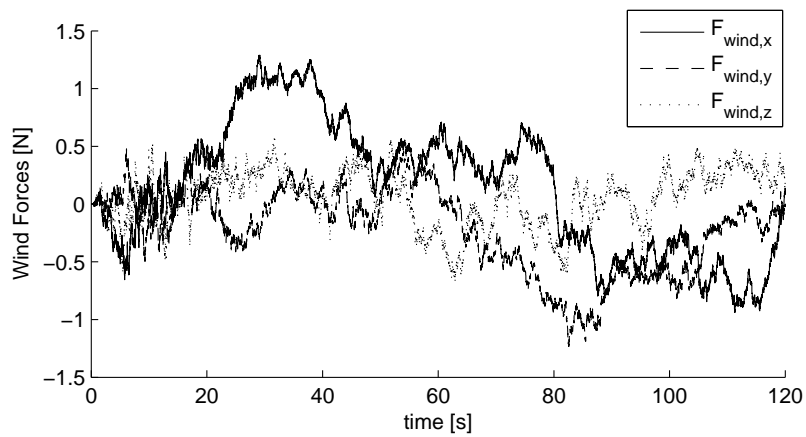


Figure 5.26: Wind forces acting as disturbance

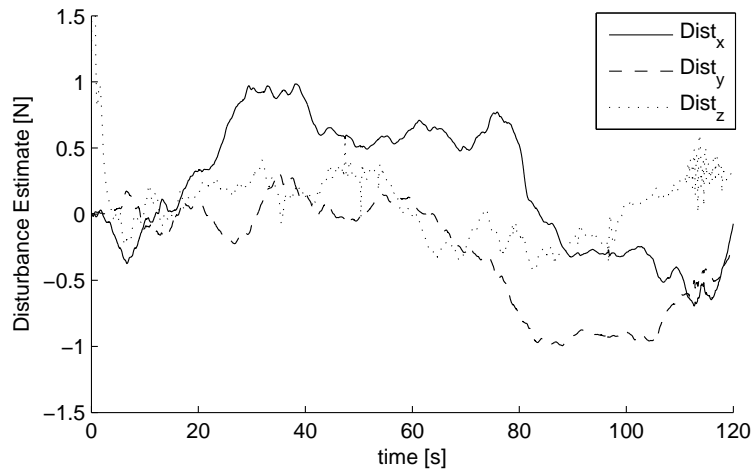


Figure 5.27: Disturbance Estimation

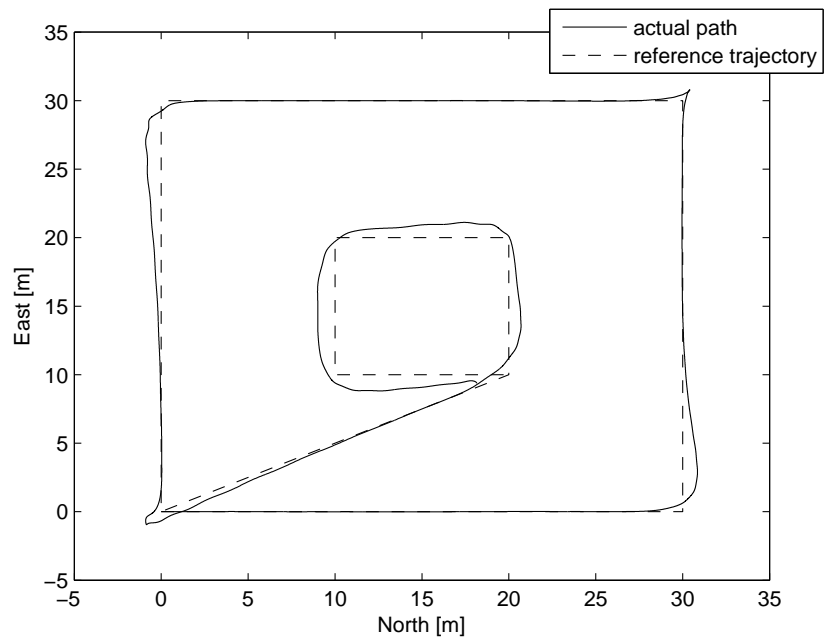


Figure 5.28: Square shaped trajectory tracking performance

5.2 Experimental Results

5.2.1 GPS Based Robust Hover

Proposed hovering controller is tested on the aerial vehicle SUAVI. Hovering controller is encoded in the onboard micro-controller and several flight tests have been performed under different weather conditions. Flight tests in open areas (helicopter field, campus, amphitheater) under average windy conditions are depicted in Figures 5.29, 5.30, 5.31 and 5.32. It is observed that actual flight performance of the vehicle is close to simulation results and the vehicle is able to hover in a robust manner. Note that the vehicle takes-off from a reference position on the ground and then keeps its position in the vicinity of that point quite successfully.



Figure 5.29: Outdoor hover test with SUAVI in helicopter field

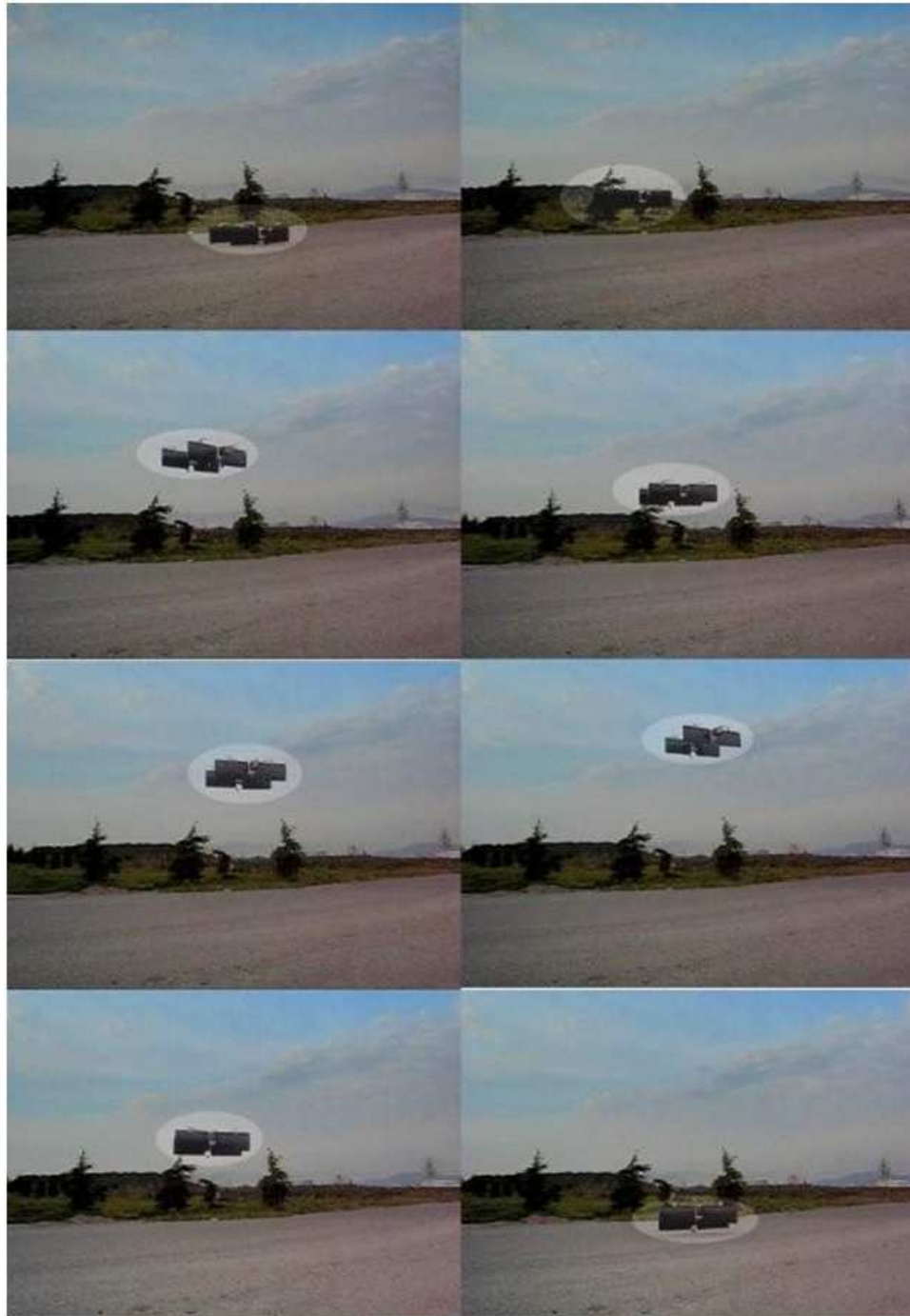


Figure 5.30: Outdoor hover test with SUAVI in university campus

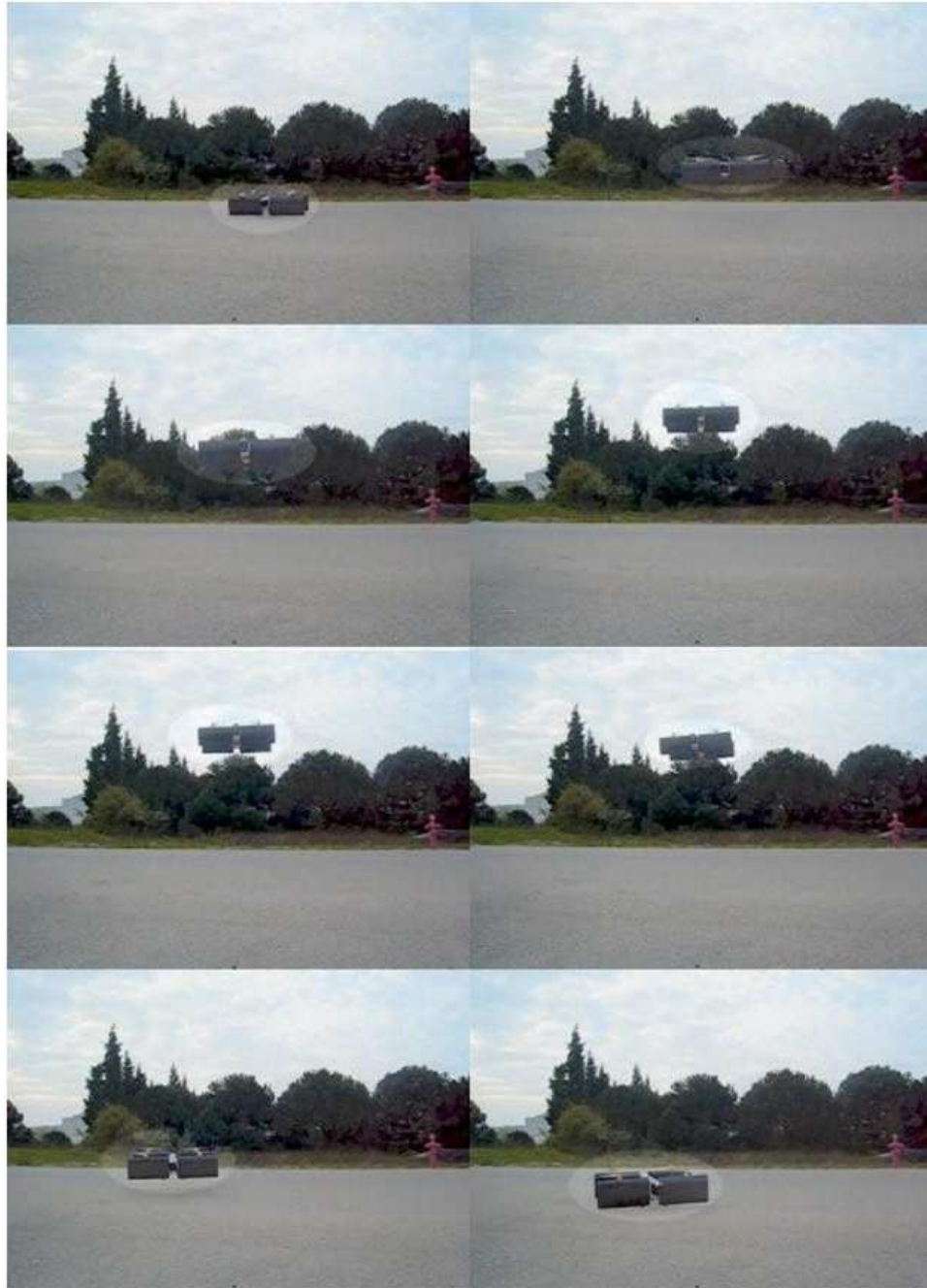


Figure 5.31: Outdoor hover test with SUAVI in university campus

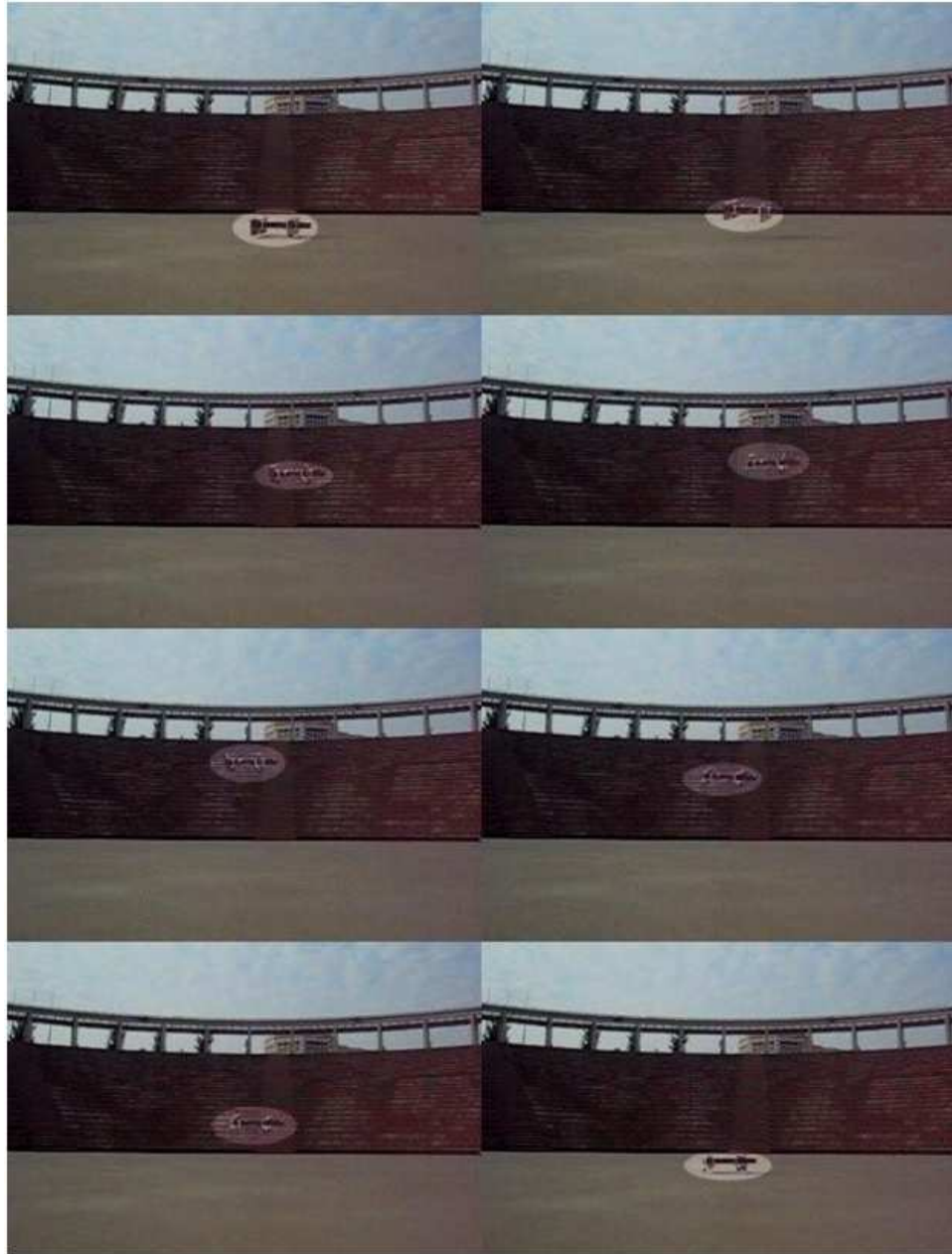


Figure 5.32: Outdoor hover test with SUAVI in amphitheater

Chapter V

6 Concluding Remarks and Future Works

The full mathematical model of the tilt-wing aerial vehicle SUAVI (Sabancı University Unmanned Aerial Vehicle) is derived using Newton-Euler formulation. Developed model includes aerodynamics effects such as wind and gusts. Both analog and digital filters are employed in order to obtain reliable sensor measurements. Extended Kalman filter for accurate estimation of attitude angles by preventing the drift in gyro integrals, Exponentially Weighted Moving Average (EWMA) filter and low pass filters with different cut-off frequencies are integrated to the model.

A high-level controller that is responsible for the control of the tilt-wing aerial vehicle is designed to supervise the low-level controllers for attitude stabilization in the context of hierarchical control architecture. Proposed robust hovering controller has enabled a quad tilt-wing aerial vehicle to hold in the vicinity of a given point under windy conditions. Hovering performance of the vehicle is also improved by utilizing a disturbance observer. Designed controllers are first verified with Matlab/Simulink simulations and then encoded in the onboard microcontroller. Simulation and experimental results are quite satisfactory.

Moreover, robust position controller for a tilt-wing quadrotor for waypoints tracking under external wind and aerodynamic disturbances are pre-

sented. Trajectory tracking performance of the vehicle is tested via simulations in Matlab/Simulink and the results obtained using this controller are quite promising.

Robust flight characteristics of the tilt-wing aerial vehicle under different circumstances is acquired from the tests in wind tunnel. Some of measurements obtained in wind tunnel tests are verified with the ones in the literature, some of them are new contributions to the literature.

Future works include implementation of the waypoint navigation algorithm on our tilt-wing aerial vehicle SUAVI and performing real flight tests. Position control of multiple UAVs is a challenging problem for the future. A group of UAVs can work in coordination to carry out complex tasks more efficiently.

Appendix A

Gumstix

As a high-level controller of aerial vehicle, a Gumstix® microcomputer ([76]) is utilized. The dimensions of Gumstix Overo Earth (see Fig. 6.1) is small (17 mm x 58 mm x 4.2 mm) and it is very light (6 gr). Even though the consumption of energy amount is very low, the processing power is high enough. It has a 600 MHz Texas Instruments OMAP (Open Multimedia Application Platform) 3053 processor and 256 DDR RAM.



Figure 6.1: Gumstix Overo Earth microcomputer

Moreover, an expansion board called Summit (see Fig. 6.2) is used in order to reach the signals easily. Similar to gumstix, the dimensions of expansion board is small (80 mm x 39 mm) and it is very light (16 gr). On this board, there is internal voltage regulator, DVI-D monitor outgoing, 3 USB connectors, voice input outgoing and a connector with 40 pins. There is also 2 serial port, 1 One-wire port, 6 PWM output, 1 I^2C port, 1 SPI port, 6 A/D input located on the connector.



Figure 6.2: Summit expansion board

IMU: Inertial Measurement Unit

For stabilization, control and attitude estimation purposes, SUAVI is equipped with Sparkfun V4 Inertial Measurement Unit (IMU) that consists of 3 axis gyroscopes from InvenSense, 3 axis accelerometers from FreeScale and 3 axis magnetometers from Honeywell (see Fig. 6.3).

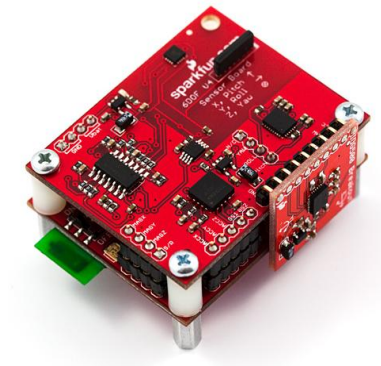


Figure 6.3: Sparkfun IMU V4

Control of the Sparkfun IMU is provided through a LPC2138 ARM7 processor. Sensor readings are available with 10 Bit precision from this processor over TTL communication at 115200 kbps [77]. Custom filters and sensor fusion algorithms are implementable inside this controller such that the Euler angles defining the attitude of the vehicle with reference to the ground are

output instead of raw sensor readings.

Ultrasonic Range Finder - Maxbotix LV-EZ4

Maxbotix LV-EZ4 sensor (see Fig. 6.4) provides very accurate altitude readings of 0 to 255 inches (0 to 6.45m) in 1 inch increments ([78]).

Features:

- 42 kHz Ultrasonic sensor
- Operates from 2.5-5.5 V
- Low 2mA supply current
- 20 Hz reading rate
- RS232 Serial Output - 9600bps
- Analog Output - 10mV/inch
- PWM Output - 147uS/inch
- Small, light weight module



Figure 6.4: Ultrasonic Range Finder - Maxbotix LV-EZ4

50 Channel D2523T Helical GPS Receiver

50 Channel D2523T Helical GPS Receiver (see Fig. 6.5) that is mounted on SUAVI provides reliable location and time information. More information about sensor can be found in data sheet [74].

Features:

- 50-channel
- 4 Hz position update rate
- ≤ 1 second time-to-first-fix for hot and aided starts
- High immunity to jamming
- PCB main board size 25 x 23 mm
- 3.3V supply voltage for low power consumption
- UART (TTL) interface
- Small, light weight module



Figure 6.5: 50 Channel D2523T Helical GPS Receiver

References

- [1] ASD Reports. *The Unmanned Aerial Vehicles (UAV) Market 2009-2019*. Visiongain, May 2009.
- [2] H. Eisenbeiss. A mini Unmanned Aerial Vehicle (UAV): System overview and image acquisition. *International Workshop on "Processing and Visualization Using High-Resolution Imagery*, 2004.
- [3] E. Altuğ. Vision based control of unmanned aerial vehicles with applications to an autonomous four rotor helicopter, Quadrotor. Master's thesis, University of Pennsylvania, 2003.
- [4] P. McKerrow. Modelling the Draganflyer four-rotor helicopter. In *Robotics and Automation, 2004. Proceedings. ICRA '04. 2004 IEEE International Conference on*, volume 4, pages 3596–3601 Vol.4, 26-May 1, 2004.
- [5] MQ-8B Fire Scout Vertical Unmanned Aircraft System, July 2009. [online] http://www.as.northropgrumman.com/products/mq8bfirescout_navy/assets/fs-fact-sheet.pdf.
- [6] Desert Hawk III Putting Capability in the Hands of the Warfighter, July 2009. [online] <http://www.lockheedmartin.com/data/assets/14502.pdf>.
- [7] Jang-Ho Lee, Byoung-Mun Min, and Eung-Tai Kim. Autopilot design of tilt-rotor uav using particle swarm optimization method. In *Control, Automation and Systems, 2007. ICCAS '07. International Conference on*, pages 1629 –1633, 17-20 2007.

- [8] QTW-UAS FS4, July 2009. [online] http://www.ghcraft.com/QTW/pdf/081001_QTW_FS4e.pdf.
- [9] Z. Sarris. Survey of UAV applicaitons in Civil Market. 2001.
- [10] Kenzo NONAMI. Prospect and recent research & development for civil use autonomous unmanned aircraft as uav and mav. *Journal of System Design and Dynamics*, 1(2):120–128, 2007.
- [11] J. Stoff. Historic Aircraft and Spacecraft in the Cradle of Aviation Museum. *Courier Dover Publications*, 2001.
- [12] I. Somers D. J. Fratello C. J. Nagy S. Schoenung R. J. Shaw M. Skoog Cox, T. H. and R. Warner. Earth observations and the role of UAVs: a capabilities assessment. *Courier Dover Publications*, 1.1:9–11, 2006.
- [13] BQM-34 Firebee 3-View. [online] <http://www.fas.org/irp/program/collect/Firebee-Sys-Desc.pdf>.
- [14] Predator/MQ-1 Predator Persistent ISR and Strike, July 2009. [online] http://www.ga-asi.com/products/aircraft/pdf/MQ-1_Predator.pdf.
- [15] Yamaha Autonomous-flight Unmanned Helicopter, July 2009. [online] <http://www.yamaha-motor.co.jp/global/news/2002/02/06/sky.html>.
- [16] RQ-4 Global Hawk High-Altitude, Long-Endurance Unmanned Aerial Reconnaissance System, July 2009. [online] http://www.as.northropgrumman.com/products/ghrq4b/assets/HALE_Factsheet.pdf.

- [17] Malazgirt, July 2009. [online] <http://www.baykarmakina.com/heliuav>.
- [18] V/STOL: The First Half-Century, Same Propulsion System for Hover and Forward Flight, July 2009. [online] <http://www.aiaa.org/tc/vstol/same.html>.
- [19] T. M. Gaffey P.B. Harendra, M. J. Joglekar and R. L. Marr. A Mathematical Model for Real-Time Flight Simulation of the Bell Model 301 Tilt Rotor Research Aircraft. *National Aeronautics and Space Administration Ames Research Center*, 1973.
- [20] M.A. Potsdam and M.J. Silva. Tilt rotor aeromechanics phenomena in low speed flight. In *Users Group Conference, 2004. Proceedings*, pages 151 – 157, 7-11 2004.
- [21] J.J. Dickeson, D. Miles, O. Cifdaloz, V.L. Wells, and A.A. Rodriguez. Robust l_p h gain-scheduled hover-to-cruise conversion for a tilt-wing rotorcraft in the presence of cg variations. In *American Control Conference, 2007. ACC '07*, pages 5266 –5271, 9-13 2007.
- [22] K. T. Öner, E. Çetinsoy, M. Ünel, M. F. Akşit, İ. Kandemir, and K. Gülez. Modeling and Position Control of a New Quad-rotor Unmanned Aerial Vehicle with Tilt-Wing Mechanism. In *International Conference on Control, Automation, Robotics and Vision*, volume 36, September 2008.
- [23] Earth Observations and the Role of UAVs: A Capabilities Assessment, 2009. [online] <http://www.articlearchives.com/defense-aerospace/defense-industry/military/2328012-1.html>.

- [24] Unmanned Aircraft Systems, July 2009. [online] http://www.uasresearch.org/UserFiles/File/183_Reference-Section_UAS_Civil-Commercial&Research&D-P.pdf.
- [25] Unmanned Aircraft Systems Roadmap 2005-2030, August 2005.
- [26] Haomiao Huang, G.M. Hoffmann, S.L. Waslander, and C.J. Tomlin. Aerodynamics and control of autonomous quadrotor helicopters in aggressive maneuvering. In *Robotics and Automation, 2009. ICRA '09. IEEE International Conference on*, pages 3277–3282, 12-17 2009.
- [27] Steven L. Waslander Gabriel M. Hoffmann, Haomiao Huang and Claire J. Tomlin. Quadrotor helicopter flight dynamics and control: Theory and experiment. In *Proceedings of the AIAA Guidance, Navigation and Control Conference and Exhibit*, August 2007.
- [28] J. Wendel N. Frietsch C. Schlaile G. F. Trommer O. Meister, R. Mönikes. Development of a GPS/INS/MAG navigation system and waypoint navigator for a VTOL UAV. *ISPIE Unmanned Systems Technology IX, Orlando, FL, USA*, 6561:6561, April 9-12 2007.
- [29] S. L Waslander G. M. Hoffmann and C. J. Tomlin. Quadrotor helicopter trajectory tracking control. In *2008 AIAA Guidance, Navigation and Control Conference and Exhibit*, August 2008.
- [30] T. Puls, M. Kemper, R. Kuke, and A. Hein. Gps-based position control and waypoint navigation system for quadcopters. In *Intelligent Robots and Systems, 2009. IROS 2009. IEEE/RSJ International Conference on*, pages 3374–3379, 10-15 2009.

- [31] Steven L. Waslander and Carlos Wang. Wind disturbance estimation and rejection for quadrotor position control. *In AIAA Infotech@Aerospace Conference and AIAA Unmanned...Unlimited Conference*, April 2009.
- [32] F. Kendoul, Yu Zhenyu, and K. Nonami. Embedded autopilot for accurate waypoint navigation and trajectory tracking: Application to miniature rotorcraft uavs. *In Robotics and Automation, 2009. ICRA '09. IEEE International Conference on*, pages 2884 –2890, 12-17 2009.
- [33] S. Grzonka, G. Grisetti, and W. Burgard. Towards a navigation system for autonomous indoor flying. *In Robotics and Automation, 2009. ICRA '09. IEEE International Conference on*, pages 2878 –2883, 12-17 2009.
- [34] O. Purwin J. Lee and R.D'Andrea. Design and control of a four-rotor autonomous flying vehicle. *Proceedings of IEEE International Conference on Robotics and Automation*, May 2006.
- [35] E. Mahony F. Russotto B. Herisse, T. Hamel. A nonlinear terrain-following controller for a VTOL Unmanned Aerial Vehicle using translational optical flow. *IEEE International Conference on Robotics and Automation*, May 2009.
- [36] M. Murata Y. Shimuzu. Flight Evaluation of GPS Precise Point Positioning for Helicopter Navigation. *SICE Annual Conference*,, September 2007.
- [37] B.B. Mohr and D.L. Fitzpatrick. A micro air vehicle navigation system. *In Position, Location, And Navigation Symposium, 2006 IEEE/ION*, pages 808 – 813, april 2006.

- [38] Ben Yun, Kemao Peng, and B.M. Chen. Enhancement of gps signals for automatic control of a uav helicopter system. In *Control and Automation, 2007. ICCA 2007. IEEE International Conference on*, pages 1185–1189, may 2007.
- [39] S.P. Soundararaj, A.K. Sujeeth, and A. Saxena. Autonomous indoor helicopter flight using a single onboard camera. In *Intelligent Robots and Systems, 2009. IROS 2009. IEEE/RSJ International Conference on*, pages 5307–5314, 10-15 2009.
- [40] S. Azrad, F. Kendoul, D. Perbrianti, and K. Nonami. Visual servoing of an autonomous micro air vehicle for ground object tracking. In *Intelligent Robots and Systems, 2009. IROS 2009. IEEE/RSJ International Conference on*, pages 5321–5326, 10-15 2009.
- [41] F. Kendoul and K. Nonami. A visual navigation system for autonomous flight of micro air vehicles. In *Intelligent Robots and Systems, 2009. IROS 2009. IEEE/RSJ International Conference on*, pages 3888–3893, 10-15 2009.
- [42] L. Tang Z. Yu. Experiment in 3D Vision Based Hovering Control of an Autonomous Helicopter. *Journal of System Design and Dynamics*, 1:120–128, 2007.
- [43] T. Kanade, O. Amidi, and Q. Ke. Real-time and 3d vision for autonomous small and micro air vehicles. In *Decision and Control, 2004. CDC. 43rd IEEE Conference on*, volume 2, pages 1655–1662 Vol.2, 14-17 2004.

- [44] O. Shakernia, R. Vidal, C.S. Sharp, Y. Ma, and S. Sastry. Multiple view motion estimation and control for landing an unmanned aerial vehicle. In *Robotics and Automation, 2002. Proceedings. ICRA '02. IEEE International Conference on*, volume 3, pages 2793 –2798, 2002.
- [45] S. Saripalli, J.F. Montgomery, and G.S. Sukhatme. Visually guided landing of an unmanned aerial vehicle. *Robotics and Automation, IEEE Transactions on*, 19(3):371 – 380, june 2003.
- [46] Kong Wai Weng and M.S.B. Abidin. Design and control of a quad-rotor flying robot for aerial surveillance. In *Research and Development, 2006. SCORed 2006. 4th Student Conference on*, pages 173 –177, 27-28 2006.
- [47] A. Hably and N. Marchand. Global stabilization of a four rotor helicopter with bounded inputs. In *Intelligent Robots and Systems, 2007. IROS 2007. IEEE/RSJ International Conference on*, pages 129 –134, oct. 2007.
- [48] S. Leven, J.-C. Zufferey, and D. Floreano. A minimalist control strategy for small uavs. In *Intelligent Robots and Systems, 2009. IROS 2009. IEEE/RSJ International Conference on*, pages 2873 –2878, 10-15 2009.
- [49] M.G. Earl and R. D’Andrea. Real-time attitude estimation techniques applied to a four rotor helicopter. In *Decision and Control, 2004. CDC. 43rd IEEE Conference on*, volume 4, pages 3956 – 3961 Vol.4, 14-17 2004.
- [50] DongBin Lee, T.C. Burg, Bin Xian, and D.M. Dawson. Output feedback tracking control of an underactuated quad-rotor uav. In *American Control Conference, 2007. ACC '07*, pages 1775 –1780, 9-13 2007.

- [51] A. Ramirez-Serrano C. Nicol, C.J.B. Macnab. Robust Neural Network Control of a Quadrotor Helicopter. *Canadian Conference on Electrical and Computer Engineering*, 2008.
- [52] T. Cheviron, A. Chriette, and F. Plestan. Generic nonlinear model of reduced scale uavs. In *Robotics and Automation, 2009. ICRA '09. IEEE International Conference on*, pages 3271 –3276, 12-17 2009.
- [53] T. Madani and A. Benallegue. Backstepping control with exact 2-sliding mode estimation for a quadrotor unmanned aerial vehicle. In *Intelligent Robots and Systems, 2007. IROS 2007. IEEE/RSJ International Conference on*, pages 141 –146, oct. 2007.
- [54] S.L. Waslander, G.M. Hoffmann, Jung Soon Jang, and C.J. Tomlin. Multi-agent quadrotor testbed control design: integral sliding mode vs. reinforcement learning. In *Intelligent Robots and Systems, 2005. (IROS 2005). 2005 IEEE/RSJ International Conference on*, pages 3712 – 3717, 2-6 2005.
- [55] Haomiao Huang, G.M. Hoffmann, S.L. Waslander, and C.J. Tomlin. Aerodynamics and control of autonomous quadrotor helicopters in aggressive maneuvering. In *Robotics and Automation, 2009. ICRA '09. IEEE International Conference on*, pages 3277 –3282, 12-17 2009.
- [56] D. Kubo K. Muraoka, N. Okada. Quad Tilt Wing VTOL UAV: Aerodynamic Characteristics and Prototype Flight Test. In *2009 AIAA*, April 2009.

- [57] C.J.B. Macnab C. Coza. A New Robust Adaptive-Fuzzy Control Method Applied to Quadrotor Helicopter Stabilization. *North American Fuzzy Information Processing Society*, 2006.
- [58] Suzuki, S. and Zhijia, R. and Horita, Y. and Nonami,K. and Kimura, G. and Bando, T. and Hirabayashi, D. and Furuya, M. and Yasuda, K. Attitude Control of Quad Rotors QTW-UAV with Tilt Wing Mechanism. *Transactions of the Japan Society of Mechanical Engineers. C*, 73(731):2012–2019, July 2007.
- [59] R. Hill Z. Omar, C. Bill. The Application of Fuzzy Logic on Transition Manoeuvre Control of a New Ducted-Fan VTOL UAV Configuration. *Innovative Computing, Information and Control*, 2007.
- [60] C. Yoo-Y. Kim S. Koo Y. Kang, B. Park. Flight Test Results of Automatic Tilt Control for Small Scaled Tilt Rotor Aircraft. *International Conference on Control, Automation and Systems*, October 2008.
- [61] K. T. Öner, E. Çetinsoy, M. Ünel, M. F. Akşit, İ. Kandemir, and K. Gülez. Yeni Bir İnsansız Hava Aracının (SUAVİ) Mekanik ve Aerodinamik Tasarımı. In *TOK'08: Otomatik Kontrol Ulusal Toplantısı, İstanbul Teknik Üniversitesi*, volume 36, November 2008.
- [62] K. T. Öner. Modeling and Control of a New Unmanned Aerial Vehicle (SUAVİ) with Tilt-Wing Mechanism. Master's thesis, Sabanci University, 2009.
- [63] T. Bresciani. Modeling Identification and Control of a Quadrotor Helicopter. Master's thesis, Lund University, 2008.

- [64] K. T. Öner, E. Çetinsoy, E. Sırımoglu, C. Hançer, M. Ünel, M. F. Akşit, K. Gülez, and İ. Kandemir. Mathematical Modeling and Vertical Flight Control of a Tilt-Wing UAV. In *Turkish Journal of Electrical Engineering and Computer Sciences*, 2009.
- [65] I. H. Abbott and A. E. von. Doenhoff. *Theory of Wing Sections*. Dover Publications Inc., 1959.
- [66] R. E. Sheldahl and P. C. Klimas. Aerodynamic Characteristics of Seven Symmetrical Airfoil Sections Through 180 Degree Angle of Attack For Use in Aerodynamic Analysis of Vertical Axis Wind Turbines. July 1981. [online] <http://prod.sandia.gov/techlib/access-control.cgi/1980/802114.pdf>.
- [67] Jen M. Davoren Thomas Moor, Jorg Raisch. Admissibility Criteria for a Hierarchical Design of Hybrid Control Systems. *IFAC Conference on Analysis and Design of Hybrid Systems*, 2003.
- [68] Thomas Moor Jorg Raisch. Hierarchical Hybrid Control of a Multiproduct Batch Plant. *Lecture Notes in Control and Information Sciences*, 2005.
- [69] Y. Suh. Attitude Estimation Using Low Cost Accelerometer and Gyroscope. *Proceedings of the 71h Korea-Russia International Symposium*, pages 423–427, 2003.
- [70] P. Zhang, J. Gu, E.E. Milios, and P. Huynh. Navigation with imu/gps/digital compass with unscented kalman filter. In *Mechatronics and Automation, 2005 IEEE International Conference*, volume 3, pages 1497–1502 Vol. 3, 2005.

- [71] D. Pomorski P. Vanheeghe F. Caron, E. Dufflos. GPS/IMU data fusion using multisensor Kalman filtering: introduction of contextual aspects. *Information Fusion* 7, pages 221–230, 2006.
- [72] R. E. Kalman. A New Approach to Linear Filtering and Prediction Problems. *Transactions of the ASME, Journal of Basic Engineering*, (82 (Series D)):35–45, 1960.
- [73] K. Ohnishi and T. Murakami. Advanced motion control in robotics. In *Industrial Electronics Society, 1989. IECON '89., 15th Annual Conference of IEEE*, pages 356 –359 vol.2, 6-10 1989.
- [74] The Global Positioning System (GPS). [online] <http://www.gps.gov/systems/gps/>.
- [75] K. Kondak, M. Bernard, N. Meyer, and G. Hommel. Autonomously flying vtol-robots: Modeling and control. In *Robotics and Automation, 2007 IEEE International Conference on*, pages 736 –741, 10-14 2007.
- [76] Gumstix Overo Earth, July 20010. [online] <http://focus.ti.com/lit/ds/symlink/omap3503.pdf>.
- [77] IMU 6 Degrees of Freedom v4 Data Sheet, July 2010. [online] <http://www.sparkfun.com/datasheets/Sensors/DataSheet-6DOF-v4-Rev1.pdf>.
- [78] Ultrasonic Range Finder - Maxbotix LV-EZ4, July 2010. [online] <http://www.maxbotix.com/uploads/LV-MaxSonar-EZ4-Datasheet.pdf>.